DOI: 10.14750/ME.2023.032

UNIVERSITY OF MISKOLC
FACULTY OF MECHANICAL ENGINEERING AND INFORMATICS

NUMERICAL AND EXPERIMENTAL INVESTIGATION ON THE USE OF AN IMPACT DAMPER BORING BAR

PHD THESIS

Prepared by

Wallyson Thomas Alves da Silva
Technologist in Industrial Mechatronics (BSc),
Mechanical Engineering (Material Science and Manufacturing) (MSc)

ISTVÁN SÁLYI DOCTORAL SCHOOL OF MECHANICAL ENGINEERING SCIENCES
TOPIC FIELD OF DESIGN OF MACHINES AND STRUCTURES
TOPIC GROUP OF DESIGN OF MACHINE TOOLS

Head of Doctoral School

Prof. Dr. Gabriella Vadászné Bognár
DSc, Full Professor

Head of Topic Group

Dr. György Hegedűs
Associate Professor

Scientific Supervisors

Dr. Attila Szilágyi†
Dr. László Péter Kiss
Associate Professor

Miskolc
2023

DOI: 10.14750/ME.2023.032

CONTENTS

DOI: 10.14750/ME.2023.032

SUPERVISOR'S RECOMMENDATION

Wallyson began his PhD studies at the István Sályi Doctoral School of Mechanical Engineering Sciences in September 2019 under the supervision of Dr. Attila Szilágyi. Following the sudden passing of Attila, Wallyson came under my supervision in March 2022. As a result of almost 4 years of hard work, this young talent is now edging closer to a conclusion. It is my pleasure to recommend this PhD thesis to the Reader.

Wallyson is really versatile, proving his abilities in both experimental and theoretical investigations he has carried out about the dynamic behaviour of impact damper (ID) boring bars. The overall performance of the manufacturing process on parts made of hardened materials is, without doubt, a very important aspect. Let us just think about the significance of the resulting surface roughness, circularity or the tool lifespan. Compared to standard tools, these properties can be improved when using the proposed impact damper bar. Such novel boring bar also perform better for long overhangs to make deep holes. It is an application that is always critical in terms of stability. In the hollow ID bar, there are spheres which offer a high level of damping through a series of impacts. It is also important to properly choose and model the clamping system itself as this condition as well affects the mechanical behaviour. The established and evaluated mechanical models within this thesis provide an insight into the reasons for the favourable properties of impact damper bars. The theoretical findings are confirmed by a vast number of experiments. The research work gives some important answers and surely leaves room for further investigations into a topic of current interest.

A total of 300 credits were earned by Wallyson during his post-graduate training. He has taken active part in departmental research, education activities, and international collaborations. So far, he has (co-)authored 30 scientific works, including multiple papers published in well-reputed international journals. He has attended 16 conference events. His publication activity clearly overachieves the requirements. Thinking of him as a person, above all, he has a very positive attitude. He is always cheerful, even when facing the difficulties, he had to during the past years. He does not get stuck at the problem, instead he sees the opportunity and seeks the solution. Knowing his approach and persistence he has put into his thesis work; he absolutely merits the praise. I sincerely wish him a fruitful future career.

Miskolc, 24 March 2023

Supervisor L. P. Kiss

DOI: 10.14750/ME.2023.032

LIST OF SYMBOLS AND ABBREVIATIONS

GREEK LETTERS

α clearance angle

β_{f1} non-dimensional natural frequency of the first vibration mode with free support.

β_{w1} non-dimensional natural frequency of the first vibration mode with the Winkler foundation.

γ rake angle

$\gamma(t)$ time component of the displacement

δ logarithmic attenuation ratio

δ_n relative deformation distance between the bodies (indentation)

$\dot{\delta}_n$ relative velocity of the collision between the bodies

$\dot{\delta}_n^{(-)}$ initial contact velocity (immediately before the impact)

ε nose angle

ζ_i Lehr damping

ζ_{iS} Lehr damping of the standard boring bar

ζ_{iID} Lehr damping of the ID boring bar

ζ_{ipID} Lehr damping in an ID boring bar after the parametric study

η hysteresis factor of the ID boring bar

$\dot{\theta}_e$ rotation of the ball

κ_r tool cutting edge angle

λ rake angle

μ coefficient of friction

ρ specific density

τ_d damped period

$\Phi_i(z)$ *i-th* mode shape

DOI: 10.14750/ME.2023.032

$\tilde{\Phi}_i(z)$ non-normalized mode shape

χ hysteresis damping factor

χ_r entering angle

ω circular frequency excitation of boring bar

ω_i natural circular frequency of the i^{th} vibration mode

ω_c chatter circular frequency of the tool

ω_1 first natural circular frequency

ω_2 second natural circular frequency

ω_{di} damped circular eigenfrequency

Ω frequency factor

LATIN LETTERS

D coefficient matrix

D boring bar diameter

DIN Deutsches Institut für Normung

e coefficient of restitution

f feed rate

FFT Fast Fourier Transformation

FRF Frequency Response Function

HRC Hardness Rockwell C

i number of segments

IRF impulse response function

ISO International Standardization Organization

k stiffness of the Winkler foundation

L total length of the boring bars

L/D Length to diameter ratio

N number of sampling points

q distributed surface loading intensity

r ball radius

R cavity radius

S Spindle speed

DOI: 10.14750/ME.2023.032

s clearance gap between the ball's surface and cavity wall

t time

w vertical deflection of the contact surface

SUBSCRIPTS

A_x area of the cross-section

$a_{\lim}$ critical depth of cut

$\mathbf{a_i}$ column vector

a_p depth of cut

c_n viscous damping coefficient

c_{ID} damping coefficient of the ID boring bar

c_f damping factor between the ball and the cavity

E_t Young's modulus of the tool

E_b Young's modulus of the ball

E Young modulus of the boring bar

E_* effective Young modulus

E_s Young modulus of the ball material

F_{ID} normal force in the impact damper

F_c damping component

F_n normal force

F_t tangential force

F_{cn} normal contact force

F_{cnj} normal contact force

F_{ctj} tangential contact force

F_{cy} tangential contact force in Y direction

F_{cx} radial contact force in X direction

F_{x0} excitation force amplitude in X direction

F_{y0} excitation force amplitudes in Y direction

DOI: 10.14750/ME.2023.032

F_{exc} experimental excitation force

F_0 excitation force of the numerical simulation

$f(x,t)$ transverse load per unit length

f_{m1} first natural frequency

f_{m2} second natural frequency

f_{exp} experimental natural frequencies

f_m theoretical natural frequencies

$\left|G(i\omega)\right|_{\text{standard}}$ peak value of the frequency response

$\left|G(i\omega)\right|_{ID}$ peak value of the frequency response

Gap_0 clearance gap of the numerical simulation

$H(j\omega)$ transfer function of the boring bar

h_{ioa} accelerance amplitude

h_{ioc} compliance FRF amplitude

I_x moment of inertia of the cross-section to X

k_a lobes

k_n contact stiffness

k_{ID} contact stiffness between the ball and the cavity

k_{do} dynamic stiffness of the boring bar

$(k_s)_i$ experimental static stiffness

K_f specific cutting coefficient

L_1 tool overhang

L_2 immovable clamping bushing length

m_i mass of body i

m_j mass of mass j

$q_i(t)$ generalized displacement

$\dot{q}_i$ generalized velocity

$q_{xi}(t)$ modal coordinates in X direction

DOI: 10.14750/ME.2023.032

$q_{yi}(t)$ modal coordinates in *Y* direction

R_* effective radius

r_s cavity radius

r_b ball radius

r_ε nose radius of the insert

R_a arithmetic means deviation

R_z total height of the profile

$u(z,t)$ displacement of the ID boring bar in *X* direction

$v(z,t)$ displacement of the ID boring bar in *Y* direction

v Poisson ratio of the boring bar

v_s Poisson ratio of the ball material

v_c cutting speed

v_{te} tangential velocity of the ball

v_{tc} tangential velocity of the cavity

$v_C(t)$ displacement of the spectrum

$v_i(z,t)$ deflection of the boring bar

$V_i(z_i)$ shape function of the transverse motion

X_{rms} RMS value of the displacements

X_i equidistant sampling displacements

z_1 first beam segment free-free end

z_2 second beam segment with Winkler foundation

DOI: 10.14750/ME.2023.032

LIST OF FIGURES

DOI: 10.14750/ME.2023.032

DOI: 10.14750/ME.2023.032

DOI: 10.14750/ME.2023.032

1. INTRODUCTION

Low amplitude vibration of the metal-cutting process is important to make sure the efficiency of the process with good quality and tight tolerances of the workpiece. In the opposite case, when the vibration amplitude increases, self-excited vibration takes place and the metal-cutting process starts to be unstable, as illustrated in Figure 1 [1].

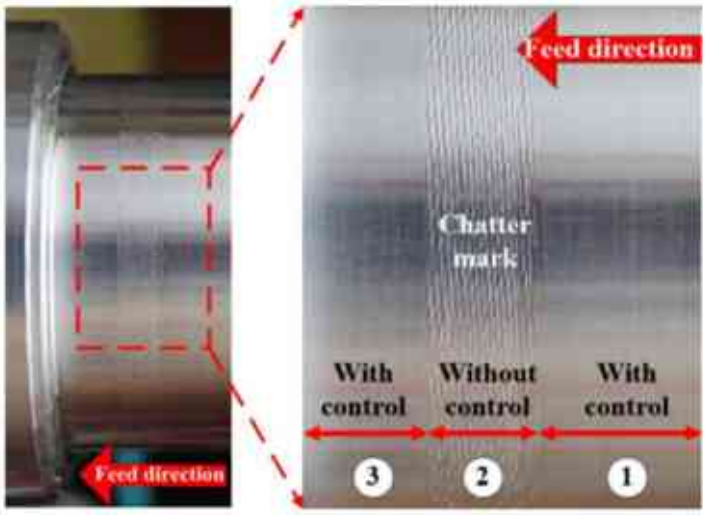

Figure 1. Chatter marks in the workpiece surface in the turning process [2]

The self-excited vibration, commonly defined as chatter occurs from their own system and attracts energy to start and grow from the interaction of the workpiece and the tool in the cutting process [3],[4]. This type of vibration causes instability in the cutting system and is the most undesirable and less controlled among the other types of vibrations like the free and forced ones. For that reason, it has become a great interest in academic and industrial research [1],[5],[6].

The stability goes around the cutting parameters, the material of the workpiece, the machine tool components, and the tool configuration. Among those parameters that affect the stability of the cutting process, the tool configuration is the weak link, it is because the chip formation that leads to the performance of the process needs a stable cutting tool and clamping system for the tool and the workpiece before setting up the other parameters.

It means that the production starts with the selection of a rigid enough machine. Then the workpiece and the tools pre-selected are assembled into the machine, and after the tool offset the cutting parameters are programmed. Finally, the cutting process can run to the desired operation.

It is difficult to establish the stability of the cutting system when we have a critical scenario as follows:

DOI: 10.14750/ME.2023.032

- Internal tuning operation – the diameter of the tool is limited by the pre-drilled hole and the chip evacuation gap.
- Long overhangs – the stiffness of the tool decrease because the ratio of the limited diameter and the long length out of the clamping system let the tool become unstable during the cutting operation.
- Hardened material – The stability diagram becomes even harder to set when the specific cutting pressure of the material is high. It is because the cutting temperatures and the cutting forces are the highest for the metal-cutting process.

An alternative to obtaining a more stable process lies in using vibration control by passive dampers, which aim to increase the damping of the system and thus dissipate the vibrations generated during the machining process [7].

Passive dampers can have different configurations, like viscoelastic dampers and tuned mass dampers (TMD), which are well implemented in industry to suppress the vibration amplitude [8], [9]. However, the application of these dampers is limited by the properties of viscoelastic dampers, which are limited to the frequency and temperature in a small range around their resonance frequency. Then, to solve this limitation, there are mechanisms to dissipate vibration energy by using granular materials, which are known as impact dampers or granular dampers [10]. Just a few authors like [11] - [14] suggest impact damper tools to suppress the vibration in the cutting process for all three complex scenarios.

In this way, to cover completely the three main problems to avoid the chatter regime, this work suggests understanding the dynamic behaviour of a new type of impact damper (ID) boring bar which proved to be efficient for the three exposed scenarios, according to many authors [11], [13], [15], [16]. The results are theoretically investigated and validated experimentally. For that reason, a mathematical model is proposed to let us understand the damping capacity of the ID bar compared to the standard tool. With that, it is possible to plot the limits of the stability lobe diagram (SLD) simulated numerically for the given tools to increase the depth of cut in the internal turning operation of hardened materials for long overhangs.

1.1 Objectives

The metal cutting industry employs damping techniques to avoid and suppress the vibration of the cutting process. These techniques include active, passive, and hybrid methods. The Silent Tool, a commercially available tool, has been in use for more than 50 years and has been extensively investigated in studies [15] - [27]. In contrast, the ID boring bar, an efficient tool that was recently invented [11], has relatively few studies published in the field. This is mainly due to the complexity of its damping mechanism. There are some notable differences between the TMD and ID bar that should be mentioned. For example, the TMD boring bar requires pre-adjustment to avoid the chatter regime, while the ID bar does not. The TMD boring bar has limitations in terms of natural frequency range and overhangs and is recommended only for relatively long overhangs. The Silent Tool has a complex design and is much more expensive than the ID boring bar. The ID boring bar has a simple construction and can be derived from conventional tools by drilling a hole and filling it with several balls.

DOI: 10.14750/ME.2023.032

One of the difficulties in setting up the ID tools is determining the clearance gap to achieve the best damping ratio of the tool, resulting in the highest overhang possible, lower tool deflection, and less vibration amplitude at the tip of the tool. The general objective of this PhD thesis is to contribute to the understanding of the use of an impact damper boring bar for turning the longest possible hole in hardened material. The focus is on the dynamic behaviour of the ID boring bar and its damping effect on the stability of the cutting process to avoid undesirable chatter regimes.

The specific objectives are:

1) To analyze the dynamical properties of standard and impact damper boring bars using impact tests and numerical investigations. The analysis aimed to propose a new approach to study the dependence of the bar's natural frequencies, damping, static stiffness, and mode shapes on different overhangs commonly used in the industry, with L/D ratios ranging from 3 to 9. Additionally, the research aimed to verify the impact of overhang on the stability of internal turning operations on hardened materials.

2) To model and analyze the dynamic response of the boring bar as an Euler-Bernoulli beam partially on Winkler foundation. By providing a theoretical framework to describe the dynamic behaviour of the clamping system effect, this study aims to enhance the understanding and control of the Winkler foundation modulus of the system.

3) To set up a mechanical model for the boring bar, perform numerical calculations for the ID tool with different numbers of balls, excitation forces, and clearance gaps, and determine the optimal configuration for achieving the highest damping capacity for different overhangs. The study also aims to validate the theoretical results with experimental results and provide a comprehensive understanding of the impact damper tool and its damping mechanism, which exhibits chaotic behaviour.

4) To test and investigate experimentally the stability of the impact damper tool in the internal turning operation of hardened material in long overhangs, and compare the roughness, roundness, and displacement parameters to a standard boring bar. By demonstrating the practical advantages of the impact damper tool in the metal cutting industry and providing practical guidance for its optimal use in real cutting operations, this study aims to enhance the use of the tool in practical applications.

1.2 Thesis outline

After addressing the engineering problem, this work will show relevant studies to better understand how the ID boring bar affects the stability of metal cutting, the properties of the tool, and the clamping system. The review of the literature will show the current works to avoid the chatter by implementing damping techniques to improve the cutting operation letting it more stable by using active, passive, and hybrid dampers. For that, the achievements on the ID boring bar will be described in detail, together with the applied mathematical models.

The methodology and decisions used to solve the dynamic problem of the ID boring bar are formulated mathematically and investigated experimentally. Then the results of the dynamical behaviour of the ID boring bar compared to the standard tool are studied in free and forced vibrations. In free vibration, the analytical mathematical model of the system are proposed and numerically calculated to define the natural frequencies of the tool and the corresponding mode

DOI: 10.14750/ME.2023.032

shapes. Furthermore, experimentally the dynamic properties of the tools will be tested: natural frequency, damping ratio, and the static stiffness of the tool. Secondly, the forced vibration equation of motion will be set up and analyzed with a series of numerical computations to understand the behaviour of the balls inside the cavity and the damping capacity of the tool for different forces, clearance gaps and overhangs.

Finally, after the parametric study, many experiments were performed to validate the results in terms of stability, roughness, cylindricity and vibration measurements. In brief, the new scientific results will be stated to emphasize the novelty of the thesis by including the relevant references used in this work.

DOI: 10.14750/ME.2023.032

2. LITERATURE REVIEW

This section will discuss the literature related to the stability of the metal cutting system that can be established in terms of enhancing the tool's performance. For that, the occurrence of chatter will be analyzed in the internal turning operation, especially when the tool is in long overhangs. The literature review will investigate the main techniques to suppress vibration during the internal cutting operation in long overhangs by suggesting clamping system configurations and anti-vibration tools to help the cutting be stable. It was with the intention that the literature review highlighted the following topics: stability of the metal cutting, tool main properties, boring bar with long overhangs, damping techniques, passive dampers and modelling of ID boring bars, by describing the most important characteristics and peculiarities of each topic developed through the world in different ages.

2.1 The stability of metal cutting

The turning process of hardened materials is used in the shopfloor, because it can replace the finishing operation of hardened workpieces, which is between 42 - 68 HRc in grinding of bearings, automotive transmissions, gears, shafts, small holes of injector nozzles for gasoline motors and other automotive components [28], [29].

For some years, the turning processes of hardened materials have been increasingly used because of many advantages related to the grinding process and it can cause low roughness, less than *2.5* micron R_a and tight dimensional tolerances [30]. It is just possible because of the development of new materials for tools of high hardness, like ceramic and CBN, no coolant is needed, machine tools are more rigid and modern tools [31].

The tools should have enough stiffness to resist higher forces during the turning operation of hardened materials it is because the cutting forces are higher than no-hardened materials. It is because the Young modulus, the microstructure, the yield strength, and the hardness are high, which results in high forces and temperatures because of the shearing of the hardened material [32] - [35]. It is proved by Strafford and Audy [36] who investigated the relation of hardness and cutting forces during the turning of AISI 4340 (57 HRc) and alumina tools. The results suggested that the increase of *48%* in hardness, grows the cutting forces between *30* and *80%* [36].

Another problem to solve for the cutting of hardened materials is the tools for internal turning operation for deep holes, which require the use of tools with a high length over the diameter (*L/D*) ratio used to machine aircraft components, automotive equipment, pipes and plumbing. The boring bar for long overhangs has low stiffness and is sensitive to vibration. In this case, the radial deflection of the tool also increases making an irregular distribution of the chip thickness over the cutting edge, and the precision of the hole. It causes cyclic variation of the chip thickness that corresponds to the force intensity, which results in regenerative vibration called chatter, which is

DOI: 10.14750/ME.2023.032

transferred from the cutting edge to the clamping system. This topic is widely discussed in many papers and textbooks throughout the years [37], [38], [39].

It is important to remember that the stability of the internal turning operation increases proportionally to the tool diameter, which is limited by the hole diameter, the chip evacuation, and the radial movements of the tool. In this context, it is important to keep in mind that the clamping system must be as stiffer as possible, with a correct bushing attached to the machine turret and alignment with the tool [40].

The variation of the cutting force in the radial direction induces oscillation in the tool tip, which weakens the stiffness of the machine-workpiece-tool-clamping system. This can cause the real roughness profile of the workpiece to differ significantly from the ideal roughness profile, especially under unstable cutting conditions such as chatter. Chatter generates vibrations in the cutting tool, which creates an oscillating profile on the workpiece surface. This is superimposed on the theoretical profile calculated by the cutting kinematics, resulting in an average roughness that is the combination of both profiles [41].

It is important to note that the instability of the machine-tool-workpiece system is the primary factor influencing surface quality, not the cutting conditions. Therefore, higher stiffness leads to lower roughness. In conclusion, optimizing the system's stiffness, cutting parameters, tool geometry, and workpiece material is critical to achieving a stable cutting process and improving surface finish. Techniques such as vibration damping, tool path optimization, and adaptive control can also be utilized to reduce the effects of chatter and improve surface finish [42].

In this sense, to achieve efficiency in the internal turning of hardened materials in deep holes, the final cutting operation has to be done with a low depth of cut for the dimensional deviations to be reduced, because of the low cutting forces. The vibration should be minimized by making the tool stiffer, the feed rate low level, high cutting speed, no cutting fluid, inserts of CBN (Cubic Boron Nitrate) or ceramic, negative geometry of the inserts, rake angle of *90* degrees, small tip radius and sharp cutting edge. It results in good surface quality and adequate surface integrity of the material [33]. Furthermore, by using damping elements integrated into the machine tools (rigid clamping systems), the dynamic behaviour of the tool can have its instability reduced [43] – [45].

Thomas et al. [46] verified the stability of the internal turning operation over CBN tool life in long overhangs. In brief, when the boring bar is within its stable regime, the vibration amplitude of the tool is higher at the beginning of the insert lifespan than at the end, while the roughness values of the workpiece remained similar. However, in an unstable regime in boring bar operation in hardened materials with continuous cutting, the flank wear of the tool insert is mainly caused by the abrasion of CBN particles originating from it [47].

In any machining process where there is transmitted energy and the clamping has low stiffness, high vibration amplitudes can appear on the machine, on the workpiece and on the tool. It can be observed three categories of vibrations: free, forced and self-excited vibrations, where the last two are machining vibrations [48].

The self-excited vibrations, also known as chatter, are commonly present in the machine tool system. It happens because of the variation of the cutting conditions, under specific process parameters. These variations cause disturbance in the cutting system, appearing with excitation frequencies close to the natural frequency of the cutting system, thus let to appear undesirable vibrations [49]. Besides, it can be characterized by excessive vibration between the tool and the

DOI: 10.14750/ME.2023.032

workpiece, causing noise and low surface quality. Another effect is to decrease the machine life and premature wear of the insert, which harms the reliability and the safety of the cutting operation [50].

Basically, there are three forms of chatter: self-excited vibration, regenerative vibration, and coupling mode.

The first one is the self-excited vibration that is caused by the dependence of the force variation and the cutting speed. The excitation frequencies are close to the natural frequency of the tool and the workpiece [50]. In that case, the vibration amplitude is inversely proportional to the product of the workpiece stiffness and of the damping ratio of the machine-tool-clamping system. Furthermore, this amplitude can be produced for the cutting process (friction, thermodynamics problems, or even the clamping system of the tool and the workpiece) [51].

The second form of chatter is the regenerative vibration, typical in turning operations, where one imperfection on the surface caused by one complete rotation of the turning workpiece can make a new imperfection on the next rotation. In that case, the excitation frequency is not constant nor directly proportional to the cutting speed [48]. This kind of vibration is found when there are irregular surfaces to be machining, because of the variation of the cutting forces, damaging the cutting operations [50].

The third form of chatter is associated with the coupling mode, when the cutting forces acting in one direction cause movements in another direction or vice-versa. The results of that are simultaneous vibrations in two coupled directions. Physically, it can be caused by a series of sources, such as friction in the lead and rake angle [50].

In the machining process, the regenerative vibration is frequently detected. However, the three different ones are independent and can take place simultaneously, making the analysis and identification challenging [51], [52].

Regenerative vibration may excite one of the structural vibration modes of the machine-tool system and, consequently, occurs a relative displacement between the tool and the workpiece. This changes the chip thickness generating a wavy surface that will be modulated during the next rotation. It will change the cutting forces and again generate vibrations [1], [3].

Siddhpura and Paurobally [53] investigated in chatter regime, i.e., the relative movement between the tool and the workpiece in the turning process with only a single degree of freedom (SDoF) model. When there is no phase difference the system remains free of self-excited vibrations, with constant chip thickness and cutting force. However, when there is a phase difference, the chip thickness becomes irregular and the cutting force is no longer constant, resulting in regenerative vibrations. The authors showed that the chatter phenomenon is not related to an external energy source, but to the dynamics of the cutting process itself. For the authors, the main parameter that contributes to causing self-excited vibration is the depth of cut, due to the thickness of the chip, which increases with the increase of the depth of cut. Chatter starts when the chip thickness exceeds a certain limit, which increases in intensity if the chip thickness continues to increase.

In practice, chatter appears above a certain depth of cut and produces high amplitudes of vibration, which lead to problems such as high roughness and tool premature breakage [54].

In [55], the vibration signal was measured by attaching an accelerometer to a boring bar during the internal turning of long holes over different cutting parameters. Initially, in a stable cutting

DOI: 10.14750/ME.2023.032

process, the amplitude of the acceleration is at least one magnitude smaller than in the chatter regime. It is observed that the acceleration amplitude increases sharply when the chatter occurs, because of the increase in the cutting speed, in that case. During the transformation process from stable to unstable, there is a period where the vibration amplitude does not have a significant increment, while the vibration is in the transition stage. The vibration needs to be identified exactly in that period, for that does not have the appearance of chatter.

Bhaskaran [56] conducted post-processing on the acceleration signal to obtain Frequency Response Functions (FRF). According to the author, during the stable cutting regime, the cutting is uniform and regular, which commonly results in more frequency peaks. In contrast, in the unstable regime, the vibration amplitude is defined for only a couple of frequency peaks due to the irregular cutting conditions. The author observed that during stable cutting, there are no frequency differences in vibration amplitude. In such cases, the clamping system's setup is sufficiently stiff, and the surface quality is good. However, under the same clamping conditions and cutting parameters, the present chatter exhibits a peak value of *472.6* Hz with an acceleration amplitude of *0.08* m/s^2, which is isolated from the other frequency peaks. This vibration peak is around *100* times higher than the stable cutting, making the chatter marks more spacious and harming the workpiece surface roughness.

That instability was caused by the lack of stiffness on the boring bar during the cutting process. Identifying chatter's trend is essential to detect the vibration based on relevant characteristics of the vibration signal during the transition mode. Two types of vibrations should be considered: the increment of the vibration amplitude in the time domain and, in the frequency domain, the energy concentration of vibration dissipates for the tool in a range of frequencies [55].

According to [3], [7], [57], the stability of the cutting system not only depends on the dynamic properties of the tool such as mass, damping ratio, and stiffness but also on the delay in the variation of the chip thickness.

In terms of process parameters, the edge between the stable cutting, without chatter, and unstable cutting, with chatter can be seen based on the depth of cut (a_p) in the function of spindle speed (*rpm*) [5], [58].

A high number of papers set up mathematical models in the vibration of internal turning operation to determine the stability lobe diagram (SLD) in the modelling of the cutting process [59] – [61]. It can be used to find the specific combination of machining parameters that results in the maximum material removal rate without chatter. The cutting speed and depth of cut determine the boundaries between stable and unstable cutting conditions, which are represented by these characteristic lobes. This method makes it possible to predict unstable regions for certain cutting parameters even before machining, which ensures that the machining system as a whole can be fully mapped [58], [62].

Plotting a stability lobe diagram (SLD) requires prior information about, the frequency response function (FRF) of the cutting system which is the combination of tool, clamping system, machine tool, and workpiece material. Modelling the process to identify the SLD is not an easy task, since the structures have several degrees of freedom. In addition, multiple cutting edges, variations in cutting forces, variations in the chip thickness, stiffness of the clamping system, and damping ratio of the tool make the experimental and theoretical analysis complex [5], [62]. Among that

DOI: 10.14750/ME.2023.032

parameters, this thesis is about to discuss the modelling of the SLD for a standard and an ID tool in different overhangs in the internal turning operation of hardened materials.

Generally, machine tool operators select conservative machining parameters to avoid chatter, and in some cases, additional manual operations are required to remove chatter marks left on the workpiece. This common practice often results in a decrease in productivity [5], [62].

2.1.1 Methods to avoid chatter in internal turning operation

Among the strategies to mitigate chatter available in the literature, we can divide them into four main approaches [58]:

- Ensure the dynamic stability of the process by selecting the parameters of the cutting process.
- Generate disturbances in the regenerative phenomenon using tools with variable pitches geometries, or even varying the spindle speed.
- Increase the stiffness of the components of the cutting system, aiming to avoid resonant frequencies.
- Maximize the damping of the cutting process using active or passive techniques.

It is important to highlight the main procedures to suppress the vibrations, such as increasing the stiffness, decreasing the cutting force, and increasing the dynamic stiffness. Then, to increase the static stiffness is necessary to increase the tool diameter and shorten the overhang. This alternative is many times limited, because the dimension of the hole is a restriction to the dimension of the tool, such as the space to evacuate the chip and the radial movement of the tool inside the hole [63].

It is important to mention that the tool length and its relation to the tool diameter have a direct impact on the tool deflection, but it does not affect the force intensity. And the geometry of the tool and the cutting parameters affect directly the cutting forces [28].

Much research aims to develop more stable tools that allow working with longer overhangs. More stable tools (chatter resistant) permit machining in deep holes, and therefore fewer passes or operations are needed, also resulting in higher productivity. These tools also combine better roughness with more intense machining regimes and have lower tool wear due to reduced vibration amplitudes [51], [64].

2.1.2 Damping techniques

A great effort has been performed in machining engineering to obtain good workpiece surface roughness [65], which can be achieved by keeping the cutting stable in internal turning operations with long overhangs. The stability of the cutting essentially depends on the damping capacity of the tool.

One way to decrease tool vibration is the use of dampers in the tool. They dissipate part of the energy generated by the vibration movement, increasing the range of the process stability [66] - [68].

DOI: 10.14750/ME.2023.032

Therefore, it is very important to use an internal turning tool with some kind of damping effect, mainly when the turning operation is made in deep holes. There are different vibration dampers used in machining operations. They are divided into three categories: active, passive and hybrid dampers [69], [70].

Active dampers are those in which the attenuator mechanism is controlled based on the system information, measured continuously throughout the process. Passive dampers do not have controls that allow real-time adjustments, but their construction is simpler when compared to active dampers and, therefore, cheaper [69], [70]. When it is used to reduce vibration in machining, it must provide a high level of damping with a relatively low loss of static stiffness [71]. Several works proved their effectiveness via modelling [72] - [74] and damping rate tests [75] - [77].

Several times, however, the passive dampers demand the construction of a mass-spring system in the toolbar, which must work at the frequency the bar. Moreover in [69] it was showed that it is difficult to exactly determine the damping coefficient for several situations and also to keep the dampers tuned in the desired frequency, once the space is limited, mainly for internal turning toolbars.

Various passive damping strategies are discussed in review paper [7] to suppress chatter, such as:

- Damper Vibration Absorber (DVA) - consists of an additional mass-spring system connected to the bar, which needs to be set up in order to be tuned with the natural frequency of the structure [78]. According to the literature, this kind of damper works efficiently up to a toolbar *L/D* ratio of *15* [79].

- Tunable Vibration Absorber (TVA) or Tuned Mass Damper (TMD) with viscous elastic material - they are easy to apply in any kind of structure. An example of this toolbar is the one called Silent Tool by the manufacturer. It consists of an interchangeable head and a body made of heavy metal, supported by elements of rubber and oil [43], [80], [81].

- Friction Damper - it consists of several disks placed inside a cavity of the toolbar. Each disk rubs to another disk and also to the cavity wall in such a way as to dissipate vibration energy [82], [83].

- Impact damper - the most usual of these dampers is the Particle Impact Damper (PID), which consists of hundreds of small particles (metallic, ceramic of little sizes) placed inside either the toolbar cavity or the workpiece wall using a reservoir stuck to it. These particles impact against the wall of the toolbar cavity while it vibrates and dissipates vibration energy [84]. The behaviour of this kind of damper is non-linear, which implies some difficulties to control damping parameters like static stiffness (the bar loses some rigidity due to the cavity made in it), the restitution coefficient between the bar and the particles and the gap between the particles and the cavity wall [85]. On the other hand, it can provide high levels of damping along with a large range of frequencies [20], [45].

Applications with a passive damping mechanism in internal turning operation were used by Sørby [26] who simulates the behaviour of the TMD boring bar compared to the standard boring bar. He considers using carbide elements, rubber elements, and viscous damping fluid (magnetorheological fluid) in the TMD boring bar. After he compared the results of the FRF with and without the passive damper. As was expected with the TMD absorber by mounting the secondary mass close to the tooltip of the tool he could increase the stiffness, decrease the vibration

DOI: 10.14750/ME.2023.032

amplitude, increase the depth of cut and reach an *L/D* ratio up to *18* without the system being unstable.

Silent Tool is the trademark of a tool holder with a passive damper, developed by Sandvik [43], available for turning, milling and drilling operations. As shown in Figure 2, the absorber consists of a heavy mass (carbide) supported by o-rings rubber, that is located inside the tool as close as possible to the tooltip and wrapped in oil. It is considered as a tool that uses a dynamic absorber to reduce the vibrations generated during the machining process, analogous to the TVA/TMD previously described.

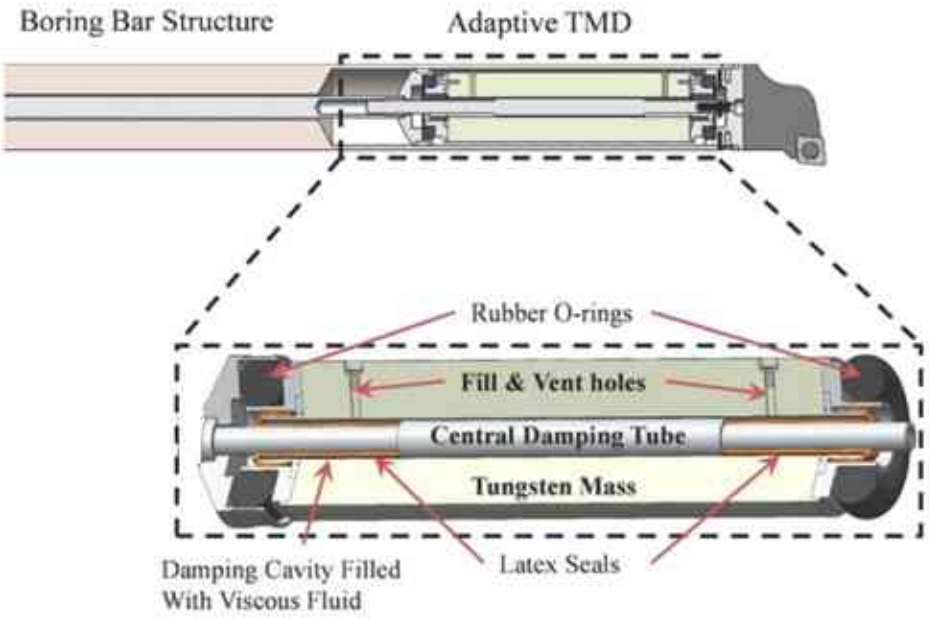

Figure 2. Main components of a Tuned Mass Damper (TMD) boring bar [17]

Sandvik showed in [43] that by using a damping device, it is possible to increase cutting parameters and achieve operation with tighter tolerances, good surface finish, and higher material removal rates, which can reduce the manufacturing cost of the workpiece. This tool holder is indicated for operations that require the use of long overhangs, applications that require an excellent surface finish, or high productivity.

A number of techniques are proposed by [86] to use active or passive dampers attached to the boring bar to avoid or minimize vibrations. Another way to attenuate internal turning vibrations is to reduce the cutting forces by changing the machining parameters (decreasing the depth of cut, cutting speed, and feed rate). These changes reduce productivity dramatically.

Thomas [20] suggests that the use of dampers in machining operations is an effective way to reduce tool vibration and improve workpiece surface roughness, especially when working on long or deep holes. However, it also presents some limitations and challenges in using passive dampers, which include the need to construct a mass-spring system and to tune it to the desirable frequency, difficulty in determining the damping coefficient, and limited space for internal turning tool bars. The author also presents some alternatives to reduce chatter, including reducing cutting forces by adjusting machining parameters, such as depth of cut, cutting speed, and feed rate, and using active dampers that can adjust the attenuator mechanism based on the system information measured

DOI: 10.14750/ME.2023.032

continuously throughout the process. Additionally, the author describes several types of passive dampers that can be used, including Damper Vibration Absorber (DVA), Tuned Mass Damper (TMD) with viscous elastic material, Friction Damper, and Impact damper.

For example, Alammari et al. [87] reduced the chatter to *38%* by increasing the boring bar stiffness. It was possible because the authors fill the cavity located on the tooltip with balls and magnetorheological fluid.

In order to increase the damping ratio of the tool and consequently the depth of cut and the stable regime of the SLD Yuvaraju et al. [88] could enhance experimentally the dynamic properties of the tool holder by using hybrid nanocomposite coatings (nano-SiC/GFRE) on the surface of the boring bar. While Tarng et al. [89] used an actuator acting as TVA to control vibration amplitudes close to chatter in turning operations. The results showed that chatter can be controlled efficiently with the use of this type of damper properly tuned to the natural frequency of the tool.

Peterka et al. [15] analyzed the impact of different tools configurations on the roundness and roughness of the workpiece. They concluded that Silent Tool which use the TMD passive damping mechanism can reach a higher range of overhangs compared to standard and carbide bars in stable conditions. Therefore, the Silent Tool could keep a small vibration amplitude and acceptable values of micro and macro geometric for an internal turning operation of deep holes in hardened materials.

2.1.3 Impact Dampers for vibration control in machining Processes

Another technique used to increase the damping ratio of the tool is using impact dampers. They are made up of one or more bodies in free movement. They can be composed of a free mass inside the cavity with a clearance gap. There is also a particle impact damper, which consists of a container containing thousands of small metallic or ceramic particles or powders. These particles dissipate energy by friction and impact when the container vibrates. The behaviour is highly nonlinear, resulting in difficulties in controlling the absorption parameters - such as the stiffness and coefficient of restitution of the bar, and the clearance gap between particles and cavity - each time the amount of mass in the system changes [85]. On the other hand, it can provide high levels of damping over a wide frequency range [45].

While viscoelastic materials dissipate elastic energy to treat damping, particle absorbers focus on dissipating kinetic energy by the balls in a combination of collision, friction and deformation to achieve damping. High-density metal particles such as copper, lead and tungsten carbide are the most satisfactory damping-improving materials [90].

The cavity diameter of the boring bar is fixed, meaning that the size of the ball that can be used is limited by this dimension. As the diameter of the ball increases within the studied frequency range, the tool overhang also increases. It is important to note that the natural frequency range between stable overhang positions also increases as the ball diameter increases. This factor must be considered when selecting the appropriate ball size. In order to achieve better results, it is recommended to have a greater ball mass and a smaller clearance gap between the ball and the cavity wall. This leads to a lower velocity of the impact of the ball against the wall. With the largest ball diameter used, it was possible to use boring bars with *L/D* ratios up to *8* while still achieving good surface quality holes [20].

DOI: 10.14750/ME.2023.032

In the work of Ema and Marui [91], an auxiliary mass with free movement inside a cavity, located externally at the free end of a turning bar, was used and presented an effective control of the vibration when the clearance gap is adjusted. The authors indicated that, in practice, it is desirable to apply the absorber to act on the tip of the turning bar and that with the absorber it is possible to machine deeper holes.

Sims et al. [45] used particle dampers to eliminate chatter during the milling process. The authors concluded that the application of these absorbers on the tested workpiece significantly increased the stability, increasing the depth of cut limited by the cutting process.

The performance of a turning bar partially filled with metallic balls to attenuate vibrations during the internal turning process has been analyzed by authors such as Biju and Shunmugam [92], Sathishkumar et al. [93], Suyama et al. [52], Diniz et al. [13] and Thomas et al. [11], [94]. In all of these mentioned works, the balls provided a reduction in tool vibration and the roughness of the parts.

Biju and Shunmugam [92] evaluated the damping capacity of different ball sizes and volume fractions from experiments using impact and shaker tests. Then they tested the absorber during internal turning, whose results indicated that the balls promoted an improvement in the circularity and surface finish of the workpiece.

As previously discussed, when addressing the impact absorber, the material of the balls and the clearance gap between the cavity and the balls directly influence the performance of the absorber. Ramesh and Alwarsamy [95] apud Paul et al. [96] indicated that, in the impact damper, materials with high-density lead to a greater reduction in tool vibration.

Sathishkumar et al. [93] used small particles of different diameters and materials such as steel, copper, brass, lead and silver, to fill the tool cavity. With this, the authors sought to analyze the influence of the size, density and hardness of the particles on the surface roughness of the workpiece. The authors concluded that smaller, denser and harder particles are favourable to damping, promoting better surface roughness.

The work by Suyama et al. [52] presents a comparison of *SAE 4340* hardened steel internal turning with three different tool holders: steel, carbide and steel with balls to absorb vibration. Steel balls of *0.5* to *1* mm in diameter were used, filling the cavity with *20%* of the volume, which was produced by an axial hole, following the centerline of the tool. Tests performed by Suyama et al. [52] indicated that the *20* mm diameter steel tool holder with balls was more efficient than the conventional steel tool holder, achieving stable cutting up to *80* mm overhangs. However, the performance of the carbide tool holder (*20* mm in diameter) was better, achieving stable cuts up to *95* mm overhangs. The authors concluded that the use of an impact damper boring bar can be a simple and inexpensive alternative to carbide tool holders. This occurs when the required overhang exceeds the maximum value of a conventional tool holder and it is lower than the limited overhang for a stable cutting of a carbide tool holder. Suyama et al. [52] presented results based on the use of a tool holder with specially mounted balls, considering parameters such as the material and diameter of the balls, the packing ratio volume percentage of the cavity, and the presence or absence of airflow inside the cavity. It is well-established that alterations in absorber parameters can lead to significant changes in the responses obtained from it.

Increasing the efficiency of hardened steel internal turning has been studied in two ways by Silva [28]. The first was the use of a clamping device in the turret using *Easy Fix* bushing. The second

DOI: 10.14750/ME.2023.032

was to compare the performance of a solid bar and a bar with a passive damper in internal turning with the *Easy Fix* clamping system. The test results presented in the paper showed that the *Easy Fix* clamping allows turning holes for approximately *32%* longer than using conventional bushing. In addition, the bar with the tested absorber allowed the machining of longer holes than the standard boring bar, by which the best results were obtained when using larger balls. At the same time, it is related to greater mass with less clearance gap, since the diameter of the cavity is constant. With the best boring bar configuration used, it was possible to increase the tool overhang by almost two times (from *L/D = 4.4* to *L/D = 8*) obtaining an efficiency of *82%* when compared to the standard boring bar, keeping the workpiece with the same roughness and tool lifespan.

It was shown in [96] the impact dampers increase the damping ratio of the turning tool, which provides a reduction in cutting force, tool wear and surface roughness during the machining of hardened AISI4340 steels.

The big difference between the works by Thomas et al.[11], Diniz et al. [13] and Silva et al. [28] are in the parameters adopted for the balls: instead of using a large number of small balls to fill the cavity of the tool holder. The authors used balls with a diameter very close to the diameter of the cavity. Excellent results are presented on this topic in their papers.

The work by Suyama et al. [52] evaluated the use of the absorber in the internal turning of *SAE 4340* hardened steel. However, Thomas et al. [11] proposed a configuration for the absorber different from that used so far: a hole of *8.32* mm in the axial direction of a *16* mm tool diameter, with steel balls with diameters slightly smaller than the cavity hole (*5*, *6.5* and *8* mm) were added. Among the configurations tested, Thomas et al. [11] verified that the impact damper bar with balls of diameter *8* mm presented the best result, allowing overhangs up to *128* mm (*L/D = 8*), maintaining good levels of roughness to the workpiece. The authors concluded that the best results are found when associating balls with greater mass and smaller clearance gaps between ball and cavity [11], [52].

In a similar work, Thomas et al. [11] and Thomas et al. [94] showed through experimental tests that the use of impact damper bars enables turning workpieces with deep holes, without impairing the surface roughness and tool life. The authors also verified that the tool life of both bars (without and with absorber) is not different when the tool overhangs are at the stability regime. However, this limit is much higher for the impact damper bar than for the standard bar, indicating that the impact bar can be used in longer holes without damaging the tool life.

Generally, systems with impact absorbers use the kinetic energy of the vibrating structure to promote impacts. However, the use of an extra source of energy to promote more impact has also been studied recently. Aguiar et al. [97] used compressed air flows to impose a greater amount of small ball collisions inside the cavity of a boring bar during the internal turning operation of hardened steels. In this case, the authors used small balls partially filling the cavity of the tool holder, indicating that compressed air flows can favour impacts, increasing the efficiency of the absorber.

2.1.4 Modelling of impact damper boring bar

The dynamics of vibro-impact have brought great benefits in recent years, mainly in the vibration control of structures and machines [98]. Paget's work [99] to attenuate the vibration of the turbine blade, entitled Mechanical Damping by Impact, from 1930, was the pioneer in this study. From

DOI: 10.14750/ME.2023.032

then on, several works were published exploring contact dynamics and their application in systems to decrease the vibrational amplitude. Then came the impact vibration absorbers, known in the literature as impact dampers [100]. In this work, the name impact damper is given to distinguish the different types of these absorbers.

Basically, impact absorbers are devices made up of one or more solid particles that move freely confined in a certain pre-established unit. They are applied to a structure that presents undesirable vibrations so that this vibration can make collisions between particle-particle and particle-structure. The various collisions and friction between the bodies reduce the energy of the structure, resulting in lower vibration amplitude [100].

These dampers in vibrating systems aim to dissipate part of the kinetic energy, providing a decrease in the amplitude of vibration. Successive collisions induce the exchange of linear momentum between the involved masses, causing changes in the dynamic responses and decreasing the vibration of the system [101], [102]. They are simple, cheap devices, insensitive to degradation and temperature and do not require external energy, being able to provide effective damping over a range of accelerations and frequencies in environments where some traditional devices may fail [103]. Other advantages of using the impact absorber compared to other devices are low cost, simplicity, robustness and the capacity of damping at different accelerations and frequencies, being used in television towers, turbine blades, shafts, and plates, among others [104].

Impact absorbers can be divided into different types depending on the adopted configuration [10]. In general, they can be classified according to the number of particles and the number of units, where the particles are inserted. Impact dampers are absorbers that contain a single ball allocated in a unit. The main structure will have the vibration reduced by the linear momentum transfer from the unit to impact damping mass. When there are several units and one ball is allocated to each, the absorber is called a multi-unit impact damper. Using a larger number of balls, the absorbers start to use the name particle damper and multi-unit particle damper, if they are made up of one or several units, respectively [105].

Over the years, these absorbers have been studied analytically, numerically and experimentally by several researchers, such as in the works of Masri [101], Bapat and Sankar [106], Friend and Kinra [107], Blazejczyk-Okolewska [108], Cheng and Wang [109], Duncan et al. [104], Cheng and Xu [110], Albuquerque [100], and Kovacs [67] among many others.

Through the various experiments carried out over the years, and also with the advent of numerical simulations, the researchers noticed that, despite the apparent simplicity of the absorber, its performance could be greatly modified by varying some essential parameters, such as the clearance gap and the mass ratio (ratio between the masses of the particle(s) and the main system) [111].

Masri's paper [101] is one of the most highly regarded works, cited by many researchers in the area. His work presented an analytical solution in a steady-state process with an impact damper, comparing the obtained responses with experimental results. Yasuda and Toyoda [112] analyzed the relationship between the internal clearance gap and the damping rate for several mass ratios in a system subjected to free vibration and verified that this relationship is linear. Bapat and Sankar [106] showed that large clearance gaps produce low damping. This is due to the small number of impacts that occur on the cavity wall of the primary unit. Thus, considering that all other parameters are kept constant, there is a specific gap that provides maximum damping to the system. Li and Darby [113] noticed the non-linear tendency of the clearance gap for multiparticle dampers,

DOI: 10.14750/ME.2023.032

similar to what occurs for a single ball damper colliding against a wall coated with softer material, it was called a buffered impact damper. These authors concluded in their tests that the presence of these materials increased the absorber performance.

Bapat and Sankar [114] studied the effect of Coulomb friction applied to systems with a multi-unit impact damper. According to these authors, the performance of the multi-unit impact damper affected by friction is generally detrimental compared to frictionless, being more pronounced when the resonant frequency is extremely low.

The capacity of energy dissipation by the impact absorber is directly related to the force amplitude, frequency of vibration, the mass of the particles, stiffness and structural damping ratio, clearance gap, the natural frequency of the system, initial displacement, gravitational acceleration and coefficient of restitution [104], [112].

Some studies also address the application of impact absorbers in systems with multi-degree-of-freedom (multi-DoF), such as Li and Darby [113], Nigm and Shabana [115] and Li and Darby [116].

Regardless of the type of absorber, numerical simulation is a very important tool for the representation and/or prediction of phenomena/experimental responses. Simulations are usually performed from formulations based on the dynamics of rigid or flexible bodies. However, other formulations are also found in the literature, such as the one used by Liu et al. [117], who used an equivalent viscous damping model to represent the nonlinearity of the system, based on experimental results. According to Lu et al. [118], although these equivalent models or empirical studies have made important contributions to the subject, they are essentially phenomenological and the results are difficult to extrapolate beyond their respective experimental conditions.

The study conducted by Albuquerque [100] analyzed the mathematical modeling of an impact-induced vibration absorber applied to beams with and without rotation. The results showed that the addition of balls to beams is highly effective in reducing vibration amplitude, but not always does a large quantity of balls provide greater damping. The mathematical model used was satisfactory in representing the experimental conditions imposed on the experimental setups and was sensitive to parameter variations such as cavity radius and coefficient of restitution. The experimental results showed that balls are capable of promoting a reduction in vibration even when the vibrating structure has angular motion around its axial axis, but rotation tends to decrease the absorber's efficiency at very high rotations. The key point of the mathematical model used was the nonlinear contact model of Flores et al. [119], which demonstrated its viability for representing the proposed experimental cases.

A methodology that brought great benefits to the study of the dynamics of systems with bulk and granular material is the Discrete Element Method (DEM), developed by Cundall and Strack [120]. DEM is a numerical modelling method for the computational simulation of interactions between particles [121], being successfully applied in the simulation and prediction of the performance of many applications involving granular materials [123], [124]. With DEM, particle interactions are modelled, using equations of motion and contact laws to establish the relationship between force and deformation [125], [126]. This technique is often applied to studies related to soil mechanics, for example.

DEM is an alternative to the typical approach adopted in simulating the mechanical behaviour of bulk and granular materials, in which it is assumed that the soil behaves as a continuous material

DOI: 10.14750/ME.2023.032

and the relative movements and rotations of the particles within the material are often not considered. This is because accounting for particle rotation would significantly increase the computational complexity of the simulation. Additionally, in many applications, particle rotation is not expected to have a significant impact on the overall mechanical behaviour of the material. Therefore, neglecting particle rotation in DEM simulations is often a reasonable simplification, allowing for more efficient and practical simulations of granular materials [121].

The work of Lu et al. [118] numerically investigates through the DEM the performance of impact absorbers (vertical and horizontal) connected to a primary system (1GDL and MGDL) under different dynamic loads (free vibration, stationary random excitation, as well as non-stationary random excitation), in order to find efficient ways to better characterize the behaviour of this absorber.

Within DEM different contact models can be used in numerical simulation. In general, the model to represent the contacts in the normal direction is characterized by an association of a spring-damper system. The simplest model that can be applied to the contact model in the normal direction is the elastic linear model (based on the work of Cundall and Strack [120]), in which the contact force F_n is proportional to the deformation between the bodies δ_n :

$$F_n = k_n \delta_n \tag{1}$$

here k_n is the contact stiffness.

According to O'Sullivan [121] the value of k_n cannot be easily related to the material properties of the particles, however, it is possible to calibrate the model by adjusting the value of k_n to match the response observed in the laboratory.

To avoid using a stiffness parameter that has no direct relationship with the mechanical properties of the bodies, the model can be based on Hertz's theory for elastic contacts. The Hertzian contact model includes non-linear formulations [121], [122].

In the elastic contact model, both linear and nonlinear, the energy is conserved. In inelastic collisions, the energy is not conserved and the lost energy must be considered. Walton and Braun [127] used different stiffnesses to represent the collision phases. However, the most common is to consider in the contact force equation a portion that represents a viscous damping with coefficient c_n, as Kelvin-Voigt model:

$$F_n = k_n \delta_n + c_n \dot{\delta}_n \tag{2}$$

The damping parameter c_n is associated with the energy dissipation that occurs during the collision process. Therefore, it is a parameter that is related to the coefficient of restitution. As discussed by Cleary [128] and O'Sullivan [121], for a given coefficient of restitution e, the value of c_n for contact between two bodies of masses m_i and m_j is calculated from the following expression:

$$c_n = 2\frac{-\ln(e)}{\sqrt{\pi^2 + \ln(e)^2}}\sqrt{\frac{m_i m_j}{m_i + m_j} k_n} \tag{3}$$

DOI: 10.14750/ME.2023.032

The damping portion includes energy dissipation due to no-linear viscoelastic deformation at the contact point, depending on the impact velocity and deformation. Delaney et al. [129] proposed the use of a non-linear formula for the contact force:

$$F_n = k_n \delta_n^{1.5} + c_n^* \dot{\delta}_n \delta_n^{0.5} \tag{4}$$

Although the linear and nonlinear models seem to be very similar for applications in the modelling of DEM, the behaviour of the particles obtained by the two models can be very different and is strongly dependent on the values chosen for the contact parameters [130].

In the Hertz model for the normal force, the surface of the particle is assumed to be completely smooth. Theoretically, friction cannot develop between two perfectly smooth particles. However, sliding friction is included in almost all DEM codes, where it is assumed to have arisen due to the interlocking of asperities on particle surfaces [121].

Also according to O'Sullivan [121], the terms "shear forces" and "tangential forces" are often and interchangeably used to refer to the component force acting along the contact surfaces, i.e., orthogonal to the normal contact.

The simplest alternative to consider a tangential force F_t acting at the particle contact point is to use the Coulomb friction model. Thus, the tangential force assumes a value proportional to the normal force developed during the collision: $|F_t| \leq \mu F_n$, where μ is the coefficient of friction. When $|F_t| < \mu F_n$, the movement is in the "stick" phase and while $|F_t| = \mu F_n$ the bodies slip between them and the tangential force acts in the opposite direction to the slip and is equal to the product μF_n.

Considering the contact of two rigid bodies, the simplest way to model the contact is through a spring-damper combination in parallel. According to Nagurka and Huang [131], the literature had not yet related mass, stiffness and damping to properties related to impacts, such as coefficient of restitution and contact time. Then, the authors developed this connection for a case of a ball bouncing on a rigid surface. The formulation presented in the work by Nagurka and Huang uses the contact time and coefficient of restitution data to estimate the stiffness and viscous damping parameters of the contact.

Other impact problems are also studied in multibody systems, through the implementation of the contact force model in a similar way to that applied in the DEM. Contact force models have gained significant importance for application in multibody systems with contacts, due to their simplicity and computational efficiency [119].

The linear spring-damper model (Kelvin-Voigt) presents a weakness, the fact that the contact force is not zero at zero deformation due to the existence of the non-zero damping component. This problem is unrealistic because, when contact begins, the elastic force and damping components must be zero [119], [132].

According to Lu et al. [133], several researchers have proposed various contact models to represent the normal and tangential contacts, however, the linear contact model in the normal direction and the Coulomb friction model in the tangential direction are widely adopted in simulation studies nowadays.

DOI: 10.14750/ME.2023.032

Based on Hertz's theory, some nonlinear contact models were developed, such as those presented in the works of Hunt and Crossley [134], Lankarani and Nikravesh [135] and Flores et al. [119], among others. These models have been used to simulate the impact between two approaching bodies with relative speed. These nonlinear contact force models are proportional to the stiffness of the contact and a dissipative viscous element. In general, the models proposed by the authors differ by the calculated damping component, more precisely by the χ factor:

$$F_n = k_n \delta_n^n + \chi \dot{\delta}_n \delta_n^n \tag{5}$$

where χ is the hysteresis damping factor.

In the model proposed by Hunt and Crossley [134], it is assumed that the loss of energy during contact is associated with the damping of the material of the bodies in contact, which would dissipate energy in the form of heat. The damping factor for the Hunt and Crossley model is:

$$\chi = \frac{3k_n(1-e)}{2\dot{\delta}_n^{(-)}} \tag{6}$$

where e is the coefficient of restitution and $\dot{\delta}_n^{(-)}$ is the initial contact velocity.

Lankarani and Nikravesh [135] also proposed their model based on the Hertz contact theory incorporated with a hysteresis damping factor for application in multibody systems. It is a model very similar to Hunt and Crossley's [134] and was obtained by equating the kinetic energy lost from the system on impact with the work of the contact force. The damping factor of the Lankarani and Nikravesh model is:

$$\chi = \frac{3k_n(1-e^2)}{4\dot{\delta}_n^{(-)}} \tag{7}$$

Flores et al. [119] point out that the models presented by Hunt and Crossley [134] and Lankarani and Nikravesh [135] are more suitable for impacts that have a high coefficient of restitution, close to 1. Flores et al. [119] presented its mathematical model, whose damping factor is

$$\chi = \frac{8k_n(1-e)}{5e\dot{\delta}_n^{(-)}} \tag{8}$$

Hu and Guo [136] compared the different nonlinear models proposed by well-known authors since each of these authors proposes its own damping factor. According to Hu and Guo [136], the models proposed by Lankarani and Nikravesh and Hunt and Crossley are indicated for impacts with a high coefficient of restitution, while the model by Flores et al. [119] is appropriate for impacts with any coefficient of restitution. Besides the comparisons, Hu and Guo [136] also proposed their own damping factor model and showed that it can be used for any contact. The damping factor proposed by Hu and Guo is given by:

$$\chi = \frac{3k_n(1-e)}{2e\dot{\delta}_n^{(-)}} \tag{9}$$

Analyzing the traditional modeling in impact absorbers, the formulation based on the conservation of linear momentum is generally applied to rigid bodies, but not to deformable bodies. A linear spring-damper contact model is most appropriate for describing the contacts between rigid and deformable structures. However, in this case, the contact time is a necessary input parameter to

DOI: 10.14750/ME.2023.032

estimate the stiffness and damping coefficients. It is very difficult to obtain the contact time experimentally, especially when the bodies in contact are deformable. Therefore, the application of non-linear models for the mathematical formulation of these absorbers is acceptable, since it is independent of the contact time, despite still being dependent on the coefficient of restitution as an input parameter.

In my thesis work, I decided to use the non-linear viscoelastic model proposed by Flores [119], Filipe and Nicoletti [137] instead of the linear spring-damper model (Kelvin-Voigt). The Flores and Filipe and Nicoletti model is based on the analysis and development of three main issues, including the dissipated energy associated with the coefficient of restitution, the stored elastic energy, and the dissipated energy due to internal damping. This model can be used for contact problems involving materials with low or moderate values of coefficient of restitution, which allows for a high amount of energy dissipation. Furthermore, the resulting contact force model is suitable for inclusion into the equations of motion of a multibody system and contributes to their stable numerical resolution.

On the other hand, the linear spring-damper model (Kelvin-Voigt) presents a weakness in that the contact force is not zero at zero deformation due to the existence of the non-zero damping component. This problem is unrealistic because, when contact begins, the elastic force and damping components must be zero. In contrast, the viscous part in the Flores and Nicoletti model is proportional to the contact pressure, making it a more realistic option for my thesis work. Therefore, I believe that the Flores and Nicoletti model is the best choice for my thesis work [41], [119], [132].

2.2 Clamping systems

Boring bar vibrations are usually related to the lower-order bending modes, while the dynamic properties of a boring bar installed in a lathe are directly influenced by the boundary conditions, i.e. the clamping of the bar. Following the literature review, it seems that little work has been done to investigate the influence of the clamping properties on the dynamics of a clamped boring bar. Thus, it is important to study this influence to gain a further understanding of the dynamic behaviour of clamped boring bars in the metal-cutting process [138], [139].

In addition to the influence of the *L/D* ratio, it is also necessary to pay attention to the clamping of the tool in the machine tool turret. This clamping must also be as rigid as possible. In this way, configuring a bar that has a length/diameter ratio (*L/D*) sufficient to keep the cut stable and, thus, to produce a smooth machined part is fundamental [140].

To implement such a scheme successfully, the dynamic properties of the system (boring bar and the clamping structure) must be known, as well as the nature of the disturbing vibrations. Few experimental studies have been carried out on mechanisms explaining tool vibration during turning operations [141] - [143] and on the dynamic properties of boring [144] - [146].

Thomas et al. [147] tested two different clamping systems to mount the boring bar in the internal turning operation of hardened materials for different overhangs. It is proved by them that when the *Easy Fix* bushing enclosure the boring bar the clamping system allows to increase the overhang by *32%* since it has higher stiffness than the conventional clamping. Besides, the *Easy Fix* could decrease the vibration amplitude of the tool and also the roughness of the workpiece, which permits an increase in the stable regime of the boring bar for similar overhangs.

DOI: 10.14750/ME.2023.032

Furthermore, various analytical models/analytical methods relating both to the boring bar and to the cutting process have been continuously developed, assuming various conditions. For example, Zhang and Kapoor [144] developed a model derived from a two-degrees-of-freedom model of a clamped boring bar and four cutting force components. In addition, Rao et. al. [148] included a variety of chip cross-sectional areas in their model, whilst Kuster et al. [145] developed a computer simulation based on a three-dimensional model of regenerative chatter. Walter et al. [146] developed a model of the chuck-workpiece connection where the workpiece is considered to be weak, using the Finite Element Method (FEM) and experimental studies of a ring-shaped weak workpiece; this model focuses on the influence of clamping forces when using jaw chucks.

Chatter or regenerative vibrations may occur because of the lack of stiffness of the clamping system. Keep the clamping system strictly rigid, the occurrence of chatter in internal turning will directly depend on the dynamic stability of the tool. The dynamic stability of the tool is due to the dynamic interaction of the *L/D* ratio and the rigidity clamping system in the turret [149].

We can also say that long internal turning tools, which have long, slender shanks, often lead to chatter vibration because of their extremely low damping capabilities [75].

The literature review explores the significance of tool stiffness, vibration reduction, and surface quality in internal turning operations. It discusses the use of dampers, both passive and impact dampers, and emphasizes their effectiveness in reducing vibration and chatter during machining. Various types of impact dampers are covered in the review, and the importance of material selection and clearance gap in influencing their performance is highlighted. Using an impact damper boring bar is considered a simple and inexpensive alternative to standard tool holders. Additionally, the review delves into the dynamics of vibro-impact and the application of impact absorbers in multi-degree-of-freedom systems. It also discusses the importance of clamping properties on the dynamics of the clamped boring bar, emphasizing the significance of the *L/D* ratio and rigid clamping of the tool in the turret for stable cutting and smooth machining.

Overall, the literature review offers valuable insights for enhancing the dynamic behaviour of an impact damper boring bar and reducing vibration and chatter during internal turning operations.

DOI: 10.14750/ME.2023.032

3. METHODOLOGY OF STUDY

The most important goal of this work is to achieve the highest overhang possible of the boring bar to turn deep holes. Then it is necessary to define the most suitable clamping system for the boring bar in the machine turret. Furthermore, it is necessary to set up the impact damper configuration such as the clearance gap, the cavity dimensions and the number of balls inside the cavity. Both are done based on the results discussed in the literature of Chapter 2. Firstly, a mathematical model of that specific clamping is proposed for the first time in order to predict the dynamic properties of the tool in different overhangs. Secondly, considering the results obtained in the first step, a mathematical model for the impact damper will be set up in order to predict the damping ratio of the tool during the internal turning operation over different initial conditions, i.e., excitation force and clearance gap values. With these results, it is possible to determine the stability limits of the standard and the ID tool for the turning operation under a controlled set of cutting parameters. For that reason, the final step is to validate experimentally the values obtained theoretically under real cutting conditions and determine the highest overhang possible in a stable condition.

3.1 Mathematical model setup for the internal turning system

It is crucial to understand the damping mechanism of the ID systems to be able to control it. One of the difficulties of setting up the ID, for example, is to determine the clearance gap to achieve the best damping ratio of the tool and, consequently, the highest overhang and lowest tool displacement amplitude and greatest eigenfrequencies to create the most favourable conditions for boring.

This study seeks to contribute to a better understanding of the dynamic behaviour of the ID tool in different overhangs and the damping effect on the stability of the cutting process. Numerical computations will be carried out to find its best performances, i.e., the highest damping for different overhangs, compared to the standard boring bar. However, some assumptions will necessarily be made to perform the computations and describe the dynamical model of the boring bar.

3.1.1 Mathematical model set up for the clamping system

A new method is presented in this thesis to determine the foundation modulus under different clamping conditions with a boring bar, which is obtained through the Winkler theory. To check the convergence and accuracy of the present method, the results of the free vibration beam system partially resting on elastic foundation are presented. The damping effects and variations of the stiffness in the space domain are neglected.

The considerations start with the contact phenomena with a normal contact problem, where two bodies are pressed together inducing perpendicular contact forces at their contact surfaces. A

DOI: 10.14750/ME.2023.032

prominent example is the boring bar clamped by a bushing in a lathe's turret [140], [150]. The geotechnical engineering analogy is used to model the clamping system. Many researchers have worked to develop techniques to evaluate the modulus of subgrade reaction, that can be used to obtain the Winkler foundation modulus [151], [152]. Then the geometry and dimensions of the foundation are assigned to be the most important effective parameters on the subgrade reaction [153], [154].

Biot [151] calculated empirically the k_s stiffness of the soil, based on his correlation of the continuum elastic theory and the Winkler model where the maximum moments in the beam are equated. On similar grounds, Vesic [152] improved Biot's formula by matching the maximum displacements of the beam in both models. The discrepancy between the Winkler-based method and the measurement or numerical analysis may be ascribed to the underestimation of tunnel-ground stiffness using Vesic's expression and overestimation with the Biot method [155]. Interpreting the results of contact pressure is a little more complex. With a Winkler model, the relations of Biot and Vesic lead to different values of contact pressures with Biot's method always being superior to Vesic's values. The calculated results from Biot's and Vesic's methods are quite different from each other when parameters are changed such as the material or the tool geometry. The differences bring great uncertainty to the calculations of the foundation capacity and deformation in the clamping system with a boring bar [156]. Consequently, an improvement to these methods is essential in order to make it convenient for this thesis application. The values obtained from the Winkler model have reliable values compared to those studies. The difference is derived from ignoring the damping coefficients in the Winkler model [157].

The foundation model was first formulated by Winkler [158]. He suggested that the model should include a distributed springy support, similar to a mattress, that restrains the beam's motion. This foundation model can either extend throughout the entire beam or can be limited to a certain section of it. When the foundation is subjected to a partially distributed surface loading, whose density is q, the springs will not be affected beyond the loaded area. However, in reality, the foundation undergoes surface deformation. As a result, this theoretical model lacks continuity in the intermediate support. By comparing the behaviour of the theoretical model and the actual foundation, it becomes apparent that there is a significant difference. The load-deflection equation for this case is written as [159]

$$q = kv \tag{10}$$

where k is the spring constant and is often referred to the foundation modulus, and v is the vertical deflection of the contact surface. It can be observed that Eq. (10) is exactly satisfied by an elastic plate floating on the surface of a liquid and carrying some load that causes it to deflect. The pressure distribution under such a plate will be equivalent to the force of buoyancy, with k being the specific weight of the liquid. With this analogy in view, the first solution for the bending of plates on a Winkler-type foundation was presented by Hertz [160], [159].

The boring bar is modelled as a cantilever Euler–Bernoulli beam of two spans, with one segment supported by a clamping mechanism that can be considered a Winkler foundation type, while the other is free. The stiffness of the clamping mechanism significantly impacts the natural frequencies of the boring bar and its mode shapes as well. When the clamping mechanism is very stiff (with large values of k), it can become a fixed support. This implies that it provides a high level of stability and rigidity to the boring bar, and consequently, the amplitude of the mode shapes in the

DOI: 10.14750/ME.2023.032

Winkler supported span reduces significantly. As a result, this condition leads to higher natural frequencies, which can prevent resonance and chatter during internal turning operations. [161].

On the other hand, when the stiffness of the clamping mechanism decreases, the mode shapes become more extended into the turret of the CNC machine, and the natural frequencies decrease. This reduction in natural frequency can be beneficial in reducing the risk of resonance and chatter during internal turning operations. However, if the stiffness is too low, the boring bar may become too flexible, leading to excessive deflection and vibration. Therefore, the stiffness of the clamping mechanism needs to be carefully selected and optimized based on the operating conditions and requirements of the internal turning operation.

To obtain the natural frequencies and associated mode shapes of the vibrating system, we used an analytical approach, directly solving the differential equation of motion of the continuous beam without any additional assumptions. This approach resulted in exact solutions, without the need for the high degree of freedom and lengthy running time associated with FEM approaches used by Albuquerque [100] and Wu et al. [162]. Overall, the analytical approach used in this work proved to be a faster and more efficient alternative to FEM, delivering accurate solutions without requiring extensive computational resources.

The stiffness of the clamping mechanism is carefully selected and optimized in this work based on natural frequency of the boring bar obtained in the impact test. The optimization involves selecting a stiffness that is high enough to provide adequate support to the boring bar but not so high that it leads to excessive natural frequencies. By carefully selecting the stiffness, the boring bar proved to operate smoothly and efficiently without experiencing resonance and chatter.

The thesis use the trial and error method to determine the Winkler foundation stiffness in order to better represent the real clamping conditions. In addition, the method considers the Young modulus, specific density, the boring bar and dimensions of the clamping system. Once the experimental eigenfrequencies are obtained by the hammer test in the longest overhang, the algorithm programmed in *SciLab* automatically updates the model. Approximating the eigenfrequencies calculated from the numerical model to the experimentally obtained ones as closely as possible.

The calculation procedure in this thesis, it is quite nontrivial since the determinant of the coefficient matrix is not only an exceedingly large transcendental expression but oscillates wildly as a function of k, taking values in the range -10^{-80} to 10^{+80}. However, calculating the roots of the determinant was not feasible using the usual hardware floating point arithmetic of a typical computer, which can handle only roughly *15* to *16* significant digits. Attempts to do so in hardware floating-point either produced no result (no convergence) or produced junk. Therefore, the calculations were performed using *SciLab's* software floating point arithmetic with *15* significant digits, and it was verified that a further increase in the number of significant digits did not appreciably affect the results.

In addition, the Euler-Bernoulli equations are used instead of the Timoshenko model since the internal tool analyzed is slender and not thick, and continuous beams are considered, eliminating the need for discretization. The theoretical model developed requires experimentation to determine unknown parameter values that appear in the model equations[163].

DOI: 10.14750/ME.2023.032

3.1.2 Mathematical model set up for the ID boring bar

The purpose of setting up a model for the ID boring bar is to better understand the behaviour of the impact damper mechanism and analyze the impact absorber in real machining operations. Thus, the numerical and experimental results can be qualitatively compared with the results obtained during the numerical simulations. Due to these considerations, it was decided to establish the following relevant modelling strategies and parameters:

(i) To analyze the kinematics (and later the kinetics) of a ball inside the cavity, it has three DoF, in addition to two (*X, Y*) translational degrees of freedom, the balls can rotate around the *Z*-axis.

(ii) The normal and tangential vectors of the contact points in each ball are used to represent the directions of the contact force during numerical computations. At the initial instant of the collision, the contact points represented on the ball and the cavity are coincident and the deformation is assumed to be zero.

(iii) During the collision, it is chosen to use the normal-tangential reference for the representation of the contact deformation and the relative velocity, in order to determine the normal contact force and the frictional force.

(iv) Contact between the balls will occur whenever the relative position of the balls (r_i) is greater than or equal to the difference in the radii of the cavity (R) and the ball (r). In this case, the bodies will be exerted by the contact force, as illustrated in Figure 3.

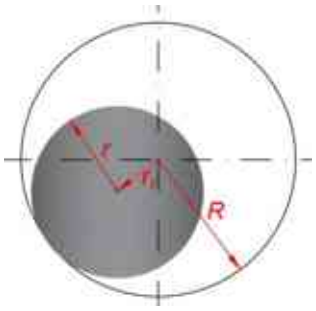

Figure 3. Relative position of the balls (r_i)

(v) To identify the occurrence of contact, the relative position between the bodies is checked continuously. While the collision does not occur, only gravitational force acts on the ball, which moves freely. With respect to the cavity, an external force representing the cutting process is the source of the excitation. The reaction forces related to its stiffness and damping are also acted on it. The impact between the cavity and the ball is characterized by the compression and restitution phases. During the impact time, the contact forces act on the bodies, modelled in this work as a non-linear spring-damper pair, in which the spring represents the stiffness of the contact and the damper is where the dissipation of energy happens. Besides, the Coulomb frictional force in each collision is also considered. While the normal and tangential contact forces F_{cnj} and F_{ctj} are responsible for the translational movement of the ball, the friction force F_{ctj} modifies its rotational movement. Figure 4 shows the free-body diagrams of the bodies during the collision.

DOI: 10.14750/ME.2023.032

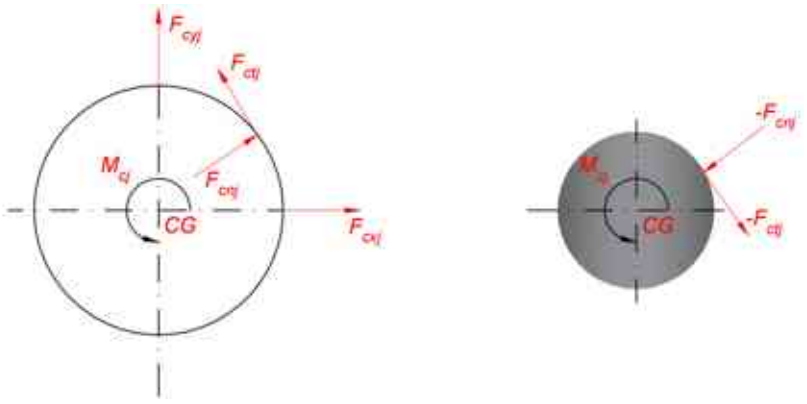

(a) (b)

Figure 4. Free body diagram of (a) the cavity and (b) the ball j

(vi) To model the contact, we utilized a non-linear spring model based on Hertz Theory. This model relates the product of the contact stiffness (k_{ID}) by the relative deformation between the bodies ($\delta_n^{1.5}$). Specifically in this model, only elastic collisions are considered, that is, energy dissipation is not taken into account. Thus, we write the force developed in the non-linear spring as:

$$F_{ID} = k_{ID}\delta_n^{1.5} \tag{11}$$

For this study, we utilized the dissipative model proposed by Flores et al. [119]. This model relates the damping component (F_c) to the product of a damping factor (c_f) and the relative deformation raised to the power of 1.5 ($\delta_n^{1.5}$), as well as the relative velocity of the collision ($\dot{\delta}_n$). Therefore, the expression for the damping component is:

$$\begin{aligned} F_c &= c_f \delta_n^{1.5} \dot{\delta}_n \\ c_f &= \frac{8(1-e)}{(5e\dot{\delta}_n^{(-)})k_{ID}} \end{aligned} \tag{12}$$

where e is the coefficient of restitution and $\dot{\delta}_n^{(-)}$ is the relative velocity immediately before the impact.

The normal contact force F_{cnj} is written as the sum of the F_{ID} and F_c components, and can be expressed as follows:

$$F_{cnj} = F_{ID} + F_c \tag{13}$$

Assuming that k_{ID} and c_f represent the contact stiffness and damping factor between the ball and the cavity, respectively, and that contact only occurs in the normal direction, we have the model to represent the contact force in the normal direction F_{cn} expressed as:

$$F_{cnj} = k_{ID}\delta_n^{1.5} + \frac{8(1-e)}{(5e\dot{\delta}_n^{(-)})k_{ID}}\delta_n^{1.5}\dot{\delta}_n \tag{14}$$

DOI: 10.14750/ME.2023.032

(viii) The magnitude of the tangential component of the contact force F_{ctj} is represented by the Coulomb frictional force that may exist during the collision. The direction of F_{ctj} depends on the direction of the relative tangential velocity between the ball and the cavity at the contact point, and it is given as:

$$F_{ctj} = \mu F_{cnj} sign(v_{tc} - v_{te}) \tag{15}$$

where: $v_{te} = \dot{\theta}_e r$ is the tangential velocity of the ball due to its rotation, v_{tc} is the tangential velocity of the cavity at the contact point and μ is the coefficient of friction.

(ix) The system's equations of motion are established from the free-body diagram of the balls using the Newton-Euler formulation. There are two translational and one rotational equations. The angular acceleration of the ball can be calculated from the moment of the tangential force (about the CG of the ball) or by the tangential acceleration, depending on the type of movement that the ball performs on the surface: rolling, sliding or both.

(x) The negative values of the contact forces are acting in the cavity at the same time.

(xi) Numerical computations of the equations of motion are performed by the Runge-Kutta method, using the *ode* integrator from *SciLab*. Careful adjustment between the time increment is necessary, due to the short impact time between the contacting bodies.

In the course of the machining process, the interaction of the tool and the workpiece, the boring bar is excited dynamically, i.e., the bar is forced to vibrate. The focus of this study is to investigate the damping characteristic of the ID boring bars under different conditions of overhangs, multiple numbers of balls, constant clearance gap and constant force magnitude. It is a contribution of this work to propose an analytical model for the ID boring bars and numerically analyze the ID tool with multiple balls over different harmonic excitation forces and clearance gaps.

3.2 Experimental set-up and procedures

Simulating, analyzing, and modeling an impact-damped boring bar as a vibratory system is a part of this work. It aims to investigate and compare the behaviour of internal turning processes when using a standard bar versus an impact-damped boring bar, using a boring bar with the largest possible length to diameter (*L/D*) ratio in a system with an *Easy Fix* bushing, as well as to improve absorption parameters of that impact-damped boring bar.

In this way, experiments are performed where the overhang is set to a given value, and internal turning is performed while measuring tool vibration. After cutting, surface roughness is measured on the turned surface. The procedure is repeated by increasing the tool overhang and following the same steps (turning, vibration measurement, and roughness measurement) until the cutting becomes unstable, which is determined by a sudden increase in vibration and roughness. Each experiment is performed twice, and cutting conditions are established beforehand.

This subsection elaborates on the equipment, materials, tools, machines, and devices used in the experiments of this work. The experiments aim to identify the dynamic properties of the turning bar to achieve the best tool performance in terms of maximum overhang achieved by comparing two different bar configurations: the solid bar and the anti-vibration bar (a cavity bar with steel balls to damp vibrations).

DOI: 10.14750/ME.2023.032

Table 1 describes the main data of the tools used in this work: the data were kindly supplied by Ltd. Sandvik Coromant (Sandviken, Sweden). Table 1 shows that all of the tool holders have common parameters, which can also be verified by checking their codes. These parameters include a tool cutting edge angle of $\kappa r = 95°$, zero degrees orthogonal rake angle, −8.397° inclination angle, and $-5°$ tool lead angle. At the tip of the standard and ID tool, CBN inserts—code *CCGW09T308S01020F 7015* (class *ISO H10*). Both inserts have similar characteristics: with *50%* CBN and ceramic phase of $Al_2O_3 + TiCN$ (Sandvik *CC 650*), insert grain size *0.3–2.0* μm with rectangular geometry with hole for clamping, nose radius $r_\varepsilon = 0.8$ mm, chamfer *0.1* mm × *20°*, entering angle $\chi_r = 95°$, rake angle $\gamma = +6°$, rake angle $\lambda = -6°$, nose angle $\varepsilon = 80°$, and clearance angle $\alpha = 7°$ [164]. It has lower toughness than inserts with a higher CBN content, but is still sufficient to maintain cutting-edge integrity. The advantage of this CBN class over the class with the highest CBN content is its greater chemical stability with iron.

Table 1. Main data of the tools with a constant diameter of 16 mm

Name	Code	Material
Insert for standard and ID bars	*CCGW09T308S01020F 7015* (class *ISO H10*)	CBN
Bushing	*132L-4016105-B*	Steel
standard and ID bar	*A16R SCLCR 09-R*	Steel

The experiments were performed in a *DMG CTX alpha 500* CNC turning center with *40* CV of power and a maximum of *5000* rpm in the main spindle. The tests were carried out with a clamp attached to the turret, commonly known as *Easy Fix* clamp housing. In order not to compromise the clamping rigidity, the length of the boring bar inside the turret was equal to or greater than 4 times the diameter of the bar [43], [165].The boring bars had a diameter (*D*) of *16* mm and a total length (*L*) of *270* mm where L_1, in Figure 5(a) indicates the tool overhang. The boring bar has a specific density (ρ) of *7860* kg/m^3, area of the cross-section (*A*) of 1.64×10^{-4} m^2 and inertia of the cross-section (*I*) of 2.84×10^{-9} m^4, a Poisson ratio of *0.33* and Young's modulus of the tool (E_t) equal to 2.0×10^{11} N/m^2 were used. In a specific case, the ID boring bar (custom design of the author himself) was manufactured with a cavity of dimensions *Ø 8.33* mm × *180* mm and filled with steel balls of *Ø 8* mm, a mass of *0.0021071* kg, and a Poisson ratio of 0.33, and Young's modulus of the ball (E_b) equals 2.0×10^{11} N/m^2, resulting in a clearance gap (*s*) between the ball's surface and cavity wall of *0.33* mm. The *Ø 8.33* mm hole was drilled with a long carbide drill bit into the *Ø 6.00* mm hole, which was originally used for internal cooling, as illustrated in Figure 5(b).

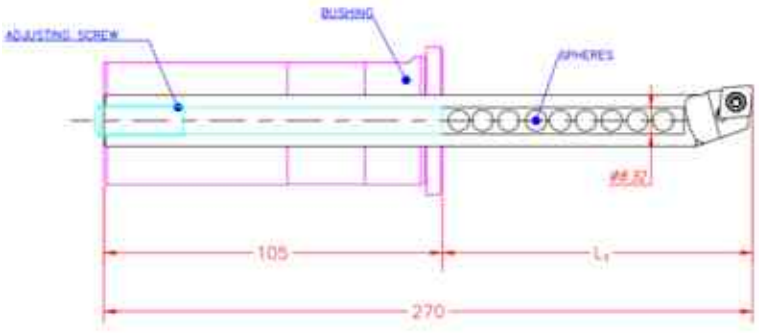

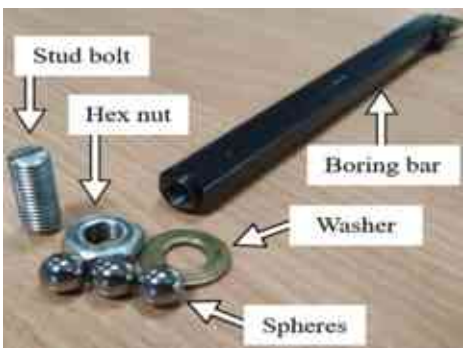

DOI: 10.14750/ME.2023.032

(a) (b)

Figure 5. (a) Drawing of the Impact Damper boring bar and the bushing dimensions and (b) Impact Damper boring bar components manufactured in the laboratory

The workpiece is *DIN EN 1.2842 (ISO 90MnCrV8),* and is made of steel. The shape of the workpiece was a cylinder. The material presents reasonable machinability. Its hardness after quenching changed from *54 to 59* HRC. During turning operations, we did not use cooling fluids, and the cutting parameters are as follows: depth of cut $a_p = 0.1$ mm, feed rate $f = 0.14$ mm, and cutting speed $v_c = 360$ mmin^{-1}.

The roughness measurement was carried out according to a measurement schedule: number of measurements in one location—*5* times; number of measurement points—*3*; displacement of measurement points on the component—equidistant points (*120*°). The laboratory's temperature was *20* °C. The equipment used was a profilometer *SURFCOM 1900SD2*. Its resolution was equal to *0.04* µm in all measurement axes [166]. The treatment of the roughness profile was according to the *ISO 4288:1996* parameters [167]. The parameters of roughness were measured: the arithmetic means deviation of the profile (R_a) and the total height of the profile (R_z).

In addition to the roughness measurements, we performed circularity measurements. These measurements were carried out on the *CenterMAX* coordinate measuring machine with a *VAST XTR* head from the company *Zeiss*. The measurement velocity was *15* mm/s in *5000* points. The accuracy of the measurement is provided as follows: *1.5 + L/250* at *26 °C*.

From the measurements of vibration, we used the IRF (impulse response function) and FRF (frequency response function) of the tool holders. These functions were obtained for different overhangs and were used in hammer impact tests. The acceleration of the boring bars was measured at *20* mm before the tip of the tool during the cutting process with a triaxial piezoelectric accelerometer positioned in the *X* direction of the tool where the roughness is more affected. The measured vibration time was *4* s, and the sampling rate was *12,800* Hz. The signal of the accelerometer was filtered below *4500* Hz and a minimum resolution of *1* Hz. Boring bar overhangs corresponding to a *L/D* greater than *3* were experimentally evaluated, as smaller ratios do not yield interesting results for this research study, as it has also been evaluated in [168], [43].

The boring bars was analyzed with different overhangs (*L/D*) as follows: *3; 4; 5; 6; 7; 8;* and *9*. With a digital caliper it was guaranteed the same position of the boring bar inside the clamping house. The manufacturer's catalogues recommended a maximum *L/D* ratio for a standard boring bar, equal to *4* [43]. However, it is an underestimation of the critical *L/D* ratio, as the dynamics of machine tools and clamping or the selection of cutting conditions and workpiece material also partly contribute to the dynamics of the cutting process. Therefore, it was chosen a limit overhang of *9* for all bars tested.

Next, we define specific terms that are important for deciding the evaluation of the experiments:

- Stable cut: The vibrations present acceleration signals that are inferior to *100* m/s^2. At the same time, the roughness of the machined surface is less than *0.8* µm.
- Unstable cut: The vibrations present acceleration signals of more than *100* m/s^2; at the same time, the roughness of the machined surface was more than *0.8* µm.

Figure 6 shows the dimensions of the specimen.

DOI: 10.14750/ME.2023.032

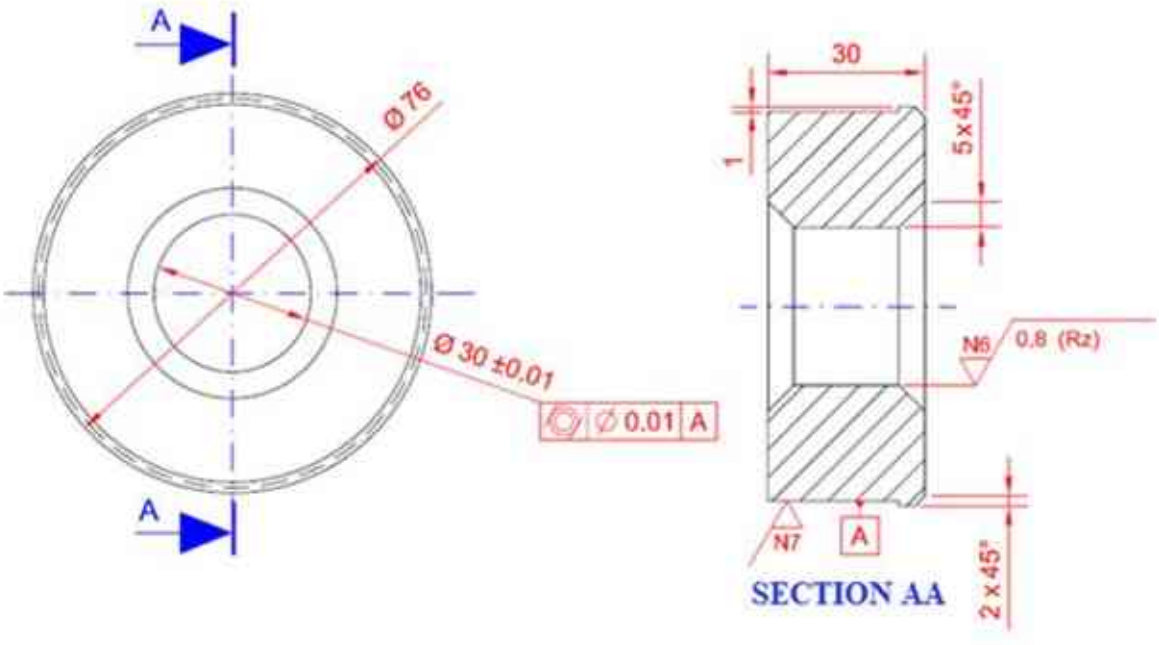

Figure 6. The specimen dimensions

Figure 7 represents the setup and the layout of the main measurement equipment and lathe parts used during the experiments. Impact tests were executed by hammering the tooltip in a transverse direction (perpendicular to the insert rake angle), since it is mostly responsible for the regenerative effect causing chatter during the cutting process. After that, the accelerometer transfers the signal to the computer (with the modal analysis software *RT photon – Brüel & Kjær*) and this signal is captured by the data acquisition module. Owing to the geometrical dimensions of the clamping-boring bar structure with the corresponding cross sections, just transverse direction was measured during the impact test in different overhang configurations, also confirming the hypotheses outlined in [52], [38] which couples with the majority of experimental measurements. Experiments along the transverse direction will be discussed in the following. It is because the most rigid direction of the tool is in the axial direction which does not interfere with the bending moment.

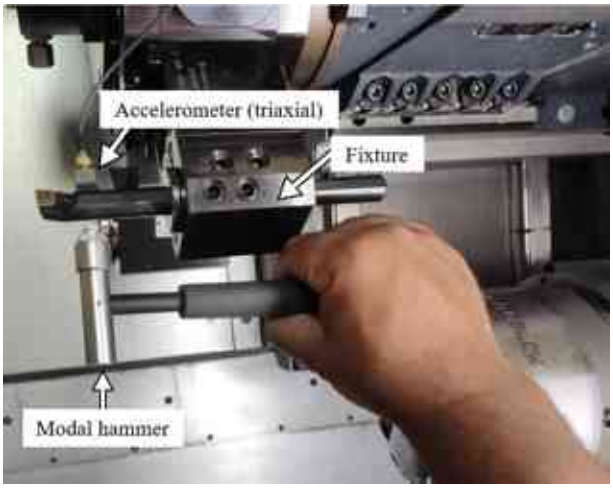

(a)

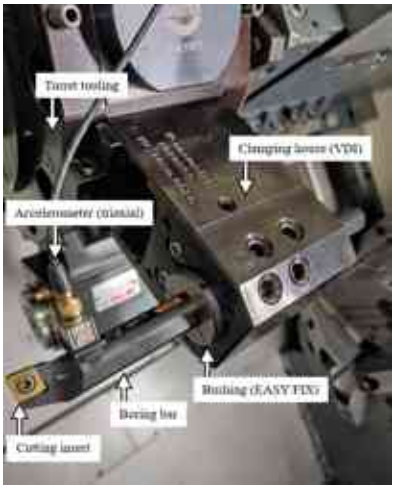

(b)

DOI: 10.14750/ME.2023.032

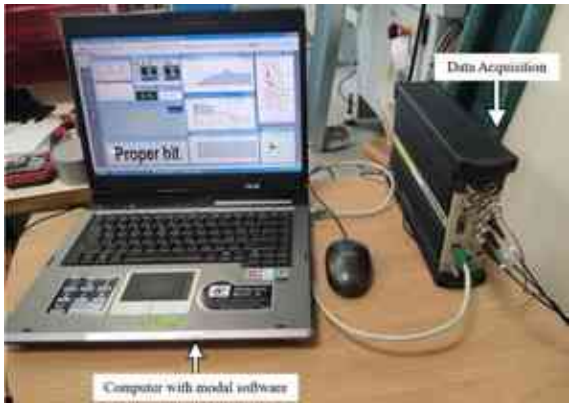

(c)

(d)

Figure 7. The measurement equipment: (a) modal hammer and accelerometer; (b) boring bar and lathe parts used during the experiments; (c) data a aquisition system; (d) clamping system of the workpice

DOI: 10.14750/ME.2023.032

4. RESULTS AND DISCUSSIONS

The chapter describes several analyses and experiments conducted on standard and impact-damped boring bars for internal turning operations. The first analysis uses the Euler-Bernoulli beam supported with Winkler foundation model to determine the the first dominant eigenfrequencies, damping, static stiffness, and eigenmodes of the boring bar for different overhangs (free vibration analysis). The second analysis investigates the damping characteristics of the impact-damped tool using a Hertzian contact model and numerical computations under various conditions (forced vibration analysis). The third analysis measures the vibration amplitudes of the standard and impact-damped boring bars during the internal cutting operation to determine stable and unstable limits for different overhangs.

4.1 Free vibration analysis of a standard boring bar in different overhangs

In this section, we present a new analysis of standard boring bars using the Euler-Bernoulli beam model to determine the eigenfrequencies and eigenmodes. Our analysis takes into account the dependence of the bar's natural frequencies, damping, static stiffness, and eigenmodes on the overhang. To achieve this, we propose a model that treats the boring bar as a multi-span beam with Winkler foundation support, and the deflection of the boring bar is expressed as a piecewise-defined function. We also compare modal parameters and FRFs for different overhangs. Additionally, we describe the process of determining damping through hammer tests and accelerometer signals.

4.1.1 Mathematical model of the standard bar in different overhangs

We present a complete and self-contained analysis of standard boring bar vibrational frequencies and mode shapes based on the classic Euler–Bernoulli beam model. Our approach is novel, as the vibration of boring bars with a Winkler foundation is not a well-explored area. Besides, the analysis of the dependence of the bar’s natural frequencies, damping ratio, static stiffness and mode shapes on the overhang appears to be new.

Figure 8 shows a schematic drawing of a boring bar with an overall length of $L = L_1 + L_2$. The boring bar is held in place by an immovable clamping bushing, also known as *Easy Fix*, which is set a distance L_2 apart from the overhang of length L_1. The overhang holds the cutting tip, which is composed of a rigid screw and insert. All elements in the drawing are considered to be one rigid structural element.

DOI: 10.14750/ME.2023.032

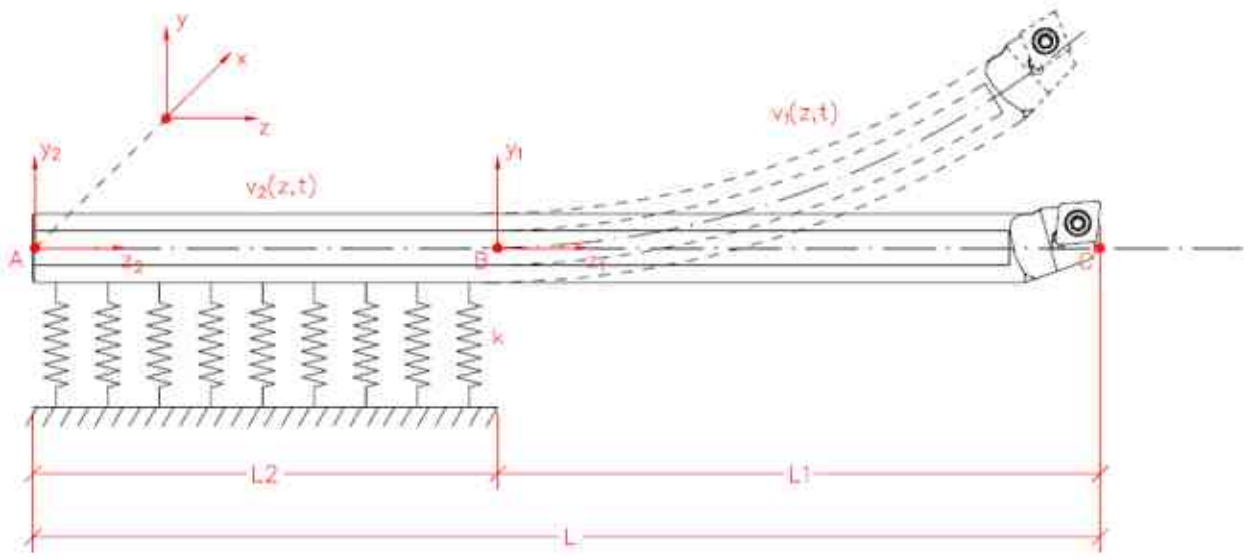

Figure 8. Mechanical model for a standard boring bar partially resting on a Winkler foundation

The proposed boring bar model is treated as a multi-span beam where one or more intermediate supports are considered. It is because the natural frequencies of uniform multi-span beams can be expressed in the same form as the natural frequencies of single-span beams. In this way, we express the deflection of the boring bar as a multi-span beam, $v_i(z,t)$ as a piecewise-defined function:

$$v(z,t) = \begin{cases} v_1(z_1,t) & if \quad L_2 \le z_1 \le L_1 \\ v_2(z_2,t) & if \quad 0 \le z_2 \le L_2 \end{cases} \tag{16}$$

Similarly to many authors [169]- [176], we used the Euler–Bernoulli beam equation to describe the transverse displacements $v_i(z,t)$ at time t of a boring bar of length L aligned in the interval $0 \le z \le L_1 + L_2$ in the Cartesian zy plane: where $f(x,t)$ is the transverse load per unit length acting on the boring bar. In the rest of this study, we take $f(x,t) = 0$ since we deal mainly with the bar's natural frequencies. When it is about the free span, the governing equation of motion is:

$$EI_x \frac{\partial^4 v_1(z_1,t)}{\partial z_1^4} + \rho A_x \frac{\partial^2 v_1(z_1,t)}{\partial t^2} = 0 \qquad L_2 \le z_1 \le L_1 \tag{17}$$

while for the boring bar part, supported by Winkler foundation, the related formula is [177]-[181]:

$$EI_x \frac{\partial^4 v_2(z_2,t)}{\partial z_2^4} + \rho A_x \frac{\partial^2 v_2(z_2,t)}{\partial t^2} + k(z_2) v_2(z_2,t) = 0 \qquad 0 \le z_2 \le L_2 \tag{18}$$

Here, A_x is the beam's cross-sectional area, I_x is the cross-sectional moment of inertia of the beam, ρ is the mass density (i.e., mass per unit volume of the beam), and E is the Young's modulus. All of these are assumed to be constant. k is the stiffness of the foundation, allowing for the stiffness to vary with z in general arbitrarily, but in our calculations, we are specifically interested in the cases where $k(z_2)$ is piecewise constant.

DOI: 10.14750/ME.2023.032

The general solution of each of these fourth-order equations comes with four undefined coefficients. Therefore, the solution of the overall system involves *8* unknown coefficients. The physics of the problem supply *8* boundary and continuity conditions which may be applied to determine the 8 unknowns. Those conditions are:

- Both ends of the beam are free in points *A ($z_2 = 0$)* and *C ($z_1 = L_1$)* of Figure 8, thus:

$$\text{(point C)} \quad v_1''(L_1,t)=0, \quad v_1'''(L_1,t)=0, \tag{19}$$

$$\text{(point A)} \quad v_2''(0,t)=0, \quad v_2'''(0,t)=0. \tag{20}$$

- At the *B* junction of the two segments the displacement, rotation, bending moment and shear force should be continuous:

$$v_1(0,t)=v_2(L_2,t), \quad v_1'(0,t)=v_2'(L_2,t), \quad v_1''(0,t)=v_2''(L_2,t), \quad v_1'''(0,t)=v_2'''(L_2,t). \tag{21}$$

where

- $v_1'(L_i,t), v_2'(L_i,t)$ represents the first derivative of v_1, v_2 with respect to the corresponding segment $L_i, i=1,2$ at time (t);

- $v_1''(L_i,t), v_2''(L_i,t)$ represents the second derivative of v_1, v_2 with respect to the corresponding segment $L_i, i=1,2$ at time (t);

- $v_1'''(L_i,t), v_2'''(L_i,t)$ represents the third derivative of v_1, v_2 with respect to the corresponding segment $L_i, i=1,2$ and time (t).

The boundary conditions (19) set the bending moment and shear force at the endpoint $z_1 = L_1$ to zero, implying that the end is free. The boundary conditions (20) do the same for the endpoint $z_2 = 0$.

Solutions of partial differential equations (17) and (18) can be obtained by the separation of variables [172]:

$$v_i(z_i,t)=V_i(z_i)\gamma(t). \tag{22}$$

Here $\gamma(t)$ represents the time component of the displacement, $V_i(z_i)$ is the shape function of the transverse motion and *i* represents the number of segments into which the beam was divided.

Substituting (22) into (17) and (18) yields independent ordinary differential equations for the time and spatial domains. Solving them separately as given in [172] and then substituting back to (22) the solution of equations (17) is as given:

$$\begin{aligned} v_1(z_1,t) &= V_1(z_1)\gamma(t) \\ v_1(z_1,t) &= \left[A_1\sin(\beta_{f1}z_1) + A_2\cos(\beta_{f1}z_1) + A_3\sinh(\beta_{f1}z_1) + A_4\cosh(\beta_{f1}z_1)\right](C_1\cos\omega t + C_2\sin\omega t) \end{aligned} \tag{23}$$

by defining $\beta_{f1}=\sqrt[4]{\frac{\rho A_x\omega_i^2}{EI_x}}$ as the non-dimensional natural frequency of the first vibration mode with free support and ω as the circular frequency excitation.

DOI: 10.14750/ME.2023.032

Solving (18) requires more effort since the expression for the general solution depends on the sign of $(k-\rho A_x\omega_i^2)$. For that reason, the analysis branches out into the case, when $\omega_i^2 < \frac{k}{\rho A_x}$:

$$v_2(z_2,t) = V_2(z_2)\gamma(t) =$$
$$v_2(z_2,t) = \left[B_1 e^{-\beta_{w1}z_2}\sin(\beta_{w1}z_2) + B_2 e^{-\beta_{w1}z_2}\cos(\beta_{w1}z_2) + B_3 e^{\beta_{w1}z_2}\sin(\beta_{w1}z_2) + B_4 e^{\beta_{w1}z_2}\cos(\beta_{w1}z_2)\right] \quad (24)$$
$$(C_1\cos\omega t + C_2\sin\omega t)$$

by defining $\beta_{w1} = \sqrt[4]{\frac{k-\rho A_x\omega_i^2}{4EI_x}}$ as the non-dimensional natural frequency of the first vibration mode with the Winkler foundation. z_1

The sign change of the parenthesized coefficient $(\omega_i^2 - k)$ has a profound effect on the form of general solution of the equation.

Plugging the expressions from the solution fragments (23) and (24) into the boundary and interface conditions (19) - (21), and applying (17) and (18), we arrive at eight homogeneous linear equations that related the eight coefficients. We express the equations in the form of a compact matrix as

$$\mathbf{D}(\omega_i)\mathbf{a_i} = \mathbf{0} \quad (25)$$

Account taken of the boundary conditions, the following system of 8 homogeneous linear algebraic equations in the 8 unknown coefficients can be obtained from the following matrix:

$$\begin{bmatrix}
-1 & 0 & 1 & 0 & 0 & 0 & 0 & 0 \\
1 & 1 & 1 & -1 & 0 & 0 & 0 & 0 \\
\theta^-\sin\theta & \theta^-\cos\theta & \theta^+\sin\theta & \theta^+\cos\theta & 0 & -1 & 0 & -1 \\
-\beta\alpha_1^- & -\beta\alpha_2^- & \beta\alpha_1^+ & \beta\alpha_2^+ & -1 & 0 & -1 & 0 \\
-2\beta^2\theta^-\cos\theta & 2\beta^2\theta^-\sin\theta & 2\beta^2\theta^+\cos\theta & 2\beta^2\theta^-\sin\theta & 0 & 1 & 0 & -1 \\
2\beta^3\alpha_2^- & -2\beta^3\alpha_1^- & 2\beta^3\alpha_2^+ & -2\beta^3\alpha_1^+ & 1 & 0 & -1 & 0 \\
0 & 0 & 0 & 0 & -\sin\theta^* & -\cos\theta^* & \sinh\theta^* & \cosh\theta^* \\
0 & 0 & 0 & 0 & -\cos\theta^* & \sin\theta^* & \cosh\theta^* & \sinh\theta^*
\end{bmatrix}
\begin{Bmatrix} B_1 \\ B_2 \\ B_3 \\ B_4 \\ A_1 \\ A_2 \\ A_3 \\ A_4 \end{Bmatrix} =
\begin{Bmatrix} 0 \\ 0 \\ 0 \\ 0 \\ 0 \\ 0 \\ 0 \\ 0 \end{Bmatrix}$$

To facilitate the analytical investigation, the following non-dimensional ratios are added:

$$\theta^* = \beta_1 L_1 \quad \theta = \beta_2 L_2 \quad \beta = \frac{\beta_2}{\beta_1} \quad \theta^+ = e^{\theta} \quad \theta^- = e^{-\theta}$$
$$\alpha_1^+ = \theta^+(\sin\theta + \cos\theta) \quad \alpha_1^- = \theta^-(\sin\theta - \cos\theta) \quad \alpha_2^+ = \theta^+(\cos\theta + \sin\theta) \quad \alpha_2^- = \theta^-(\cos\theta + \sin\theta)$$

where the elements of the coefficient matrix $\mathbf{D}(\omega_i)$ and $\mathbf{a_i}$ is the column vector of length 8 with components: *A1, ..., A4, B1,..., B4*.

$$\mathbf{a_i^T} = \{A_1, A_2, A_3, A_4, B_1, B_2, B_3, B_4\} \quad (26)$$

The system will have a non-trivial solution, which is the exact characteristic equation of the boring bar provided that the determinant of its coefficient matrix must be zero.

$$\det\left[\mathbf{D}(\omega_i)\right] = 0 \quad (27)$$

DOI: 10.14750/ME.2023.032

The positive real roots of this equation are the exact non-dimensional natural frequencies of the boring bar resting partially in Winkler foundation. Moreover, in order to obtain numerical values of the circular eigenfrequencies of the boring bar, e.g., the bisection method can be applied to (27). It is important to mention that the roots depend on the choice of the span length L_1. The computations are performed in *SciLab* software floating point arithmetic with double precision.

In the following, using the concept of modal analysis, the deflection $v_i(z,t)$ of the boring bar can be expressed by using eigenfunction expansion as [170]:

$$v_i(z,t) \cong \sum_{i=1}^{2} \Phi_i(z) q_i(t), \qquad i = 1,2 \tag{28}$$

where $\Phi_i(z)$ are the spatial coordinates necessary to set up the mode shape function and $q_i(t)$ is the generalized displacement which describes the modal motion.

The mode shapes $\Phi_i(z)$ were normalized with respect to the mass of the boring bar [172], [182]-[184]:

$$\Phi_i(z) = \frac{\tilde{\Phi}_i(z)}{\sqrt{\rho A_x \int_0^{L_1+L_2} \tilde{\Phi}_i^2(z)dz}} \tag{29}$$

where $\tilde{\Phi}_i(z)$ is the non-normalized mode shape,

$$\tilde{\Phi}_i(z) = \begin{cases} V_1(z_1) & if \quad L_2 \le z \le L_1 \\ V_2(z_2) & if \quad 0 \le z \le L_2 \end{cases} \tag{30}$$

The integral in (29) is computed numerically using the trapezoidal rule.

4.1.2 Numerical calculations of a two-span Winkler-supported boring bar

Modal parameters and FRFs for different overhangs are compared subsequently. In this section, the eigenfrequencies and eigenfunctions of the boring bar are calculated in *SciLab*, to show the accuracy and efficiency of the present work, by finding the roots of the characteristic equation presented in the matrix of Section 4.1.1. There is a clamped bushing (*Easy Fix*) fastening along the length L_2, which is modelled by Winkler-foundation. If the distributed force is exerted on the *Easy Fix* bushing uniformly along the length L_2, the Winkler foundation's stiffness is obtained as $k = 4.25 \times 10^{10}$ N/m. This stiffness value is proposed in accordance with the empirical measurements, in a way that it was tuned to the natural frequencies of the experimental results given in Table 2.

The length of the elastic foundation, the cross-sectional area, the inertia of the cross-section, the density and the Young modulus are given, respectively: $L_2 = 0.105$ m, $A_x = 1.64 \times 10^{-4}$ m², $I_x = 2.84 \times 10^{-9}$ m^4, $\rho = 7860$ kg/m^3 and $E = 2.0 \times 10^{11}$ N/m². Besides, the value of L_1 changes for different overhangs when the length-to-diameter (L/D) ratio of the tool is between 3 and 9 for a tool with $D = 0.016$ m of cross-section diameter, it is because these L/D intervals are easily available commercially [182].

DOI: 10.14750/ME.2023.032

Now the intention is to vary the overhang ratio and investigate the dependence of the bar's natural frequencies on that ratio. With the aid of the mathematical machinery that we have developed in the preceding subsection, this can be accomplished with only a minimal amount of extra effort.

The mode shape corresponding to each ω_i through the singular value decomposition of **D** as described in the previous subsection was determined. Figure 9 shows the mode shapes corresponding to ω_1 and ω_2 for a wide range of overhangs, which varies between *L/D = 3 ... 9*. We have avoided plotting the higher frequency modes in the interest of reducing clutter [185].

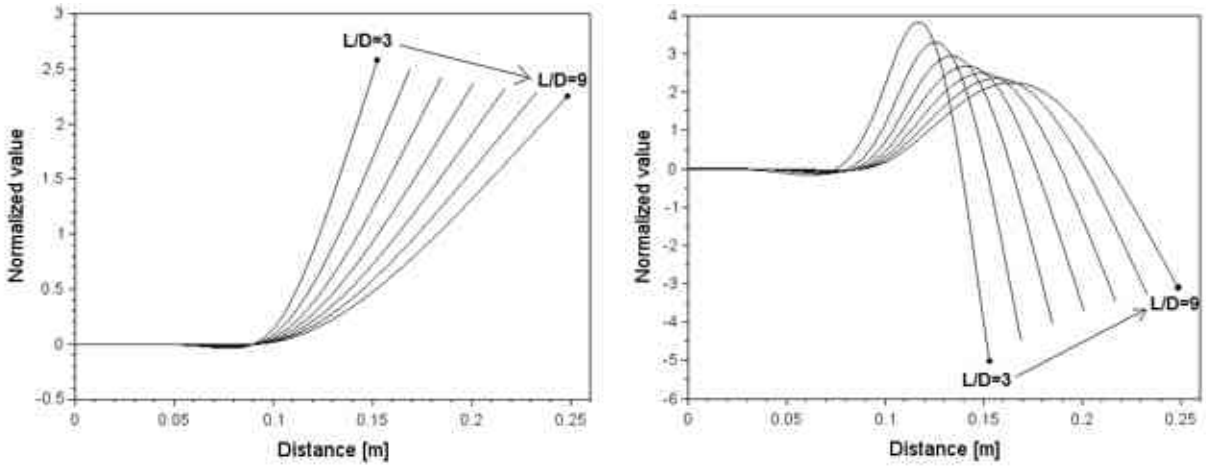

(a) (b)

Figure 9. Normalized mode shapes for the standard boring bar in (a) the first and (b) second mode for overhangs between L/D 3 and 9

Figure 9 presents a series of mode shapes that illustrate the first and second modes of vibration of the boring bar. The mode shapes represent different lengths of the tool, which correspond to different natural frequencies, as shown in Table 2. The normalized values differ along the axis *X* as long as the dimension L_1 has the values changed. As the length of the boring bar increases, the mode shapes become flatter and the curvature of the mode shape decreases its normalized value, which results in a horizontal translation of the curvatures. This is because a longer overhang ($L/D \geq 5$) results in a lower natural frequency and static stiffness, which are unfavourable in terms of manufacturing quality. Conversely, a shorter overhang ($L/D \leq 5$) has a higher natural frequency and static stiffness, resulting in more significant deviation from the axis *X* along dimension L_1.

Table 2. Eigenfrequencies for the standard boring bar in the first (f_{m1}) and second (f_{m2}) modes for overhangs between L/D 3 and 9

L/D	***3***	***4***	***5***	***6***	***7***	***8***	***9***
f_{m1} [Hz]	*2914.2*	*1863.9*	*1292.5*	*948.3*	*725.1*	*572.3*	*463.1*
f_{m2} [Hz]	*16449.7*	*11094.5*	*7866.9*	*5835.6*	*4489.6*	*3556.6*	*2884.9*

4.1.3 Transient responses of a standard boring bar with different overhangs

In engineering practice, the structural modal parameters are identified as natural frequency, damping ratio and static stiffness by the Impulse Response Function (IRF) and Frequency

DOI: 10.14750/ME.2023.032

Response Function (FRF), respectively. Applying the concept of modal analysis, the dominant eigenfrequencies and eigenmodes are considered as it is given in (28). Utilizing the orthogonality of the eigenfuctions Φ_i the partial differential equations of motion (16) and (17) can be simplified to a decoupled system of ordinary differential equations expressed by generalized displacements q_i. Since in real problems, the damping is always present, the system is extended conveniently with viscous damping terms [186], [187].

The decoupled equations are written as:

$$\ddot{q}_i + 2\zeta_i \omega_i \dot{q}_i + \omega_i^2 q_i = 0, \qquad (i = 1,2) \tag{31}$$

The boring bar can be regarded as a damped single-degree-of-freedom system whose vibration response represents the real solution for the generalized displacement expressed as:

$$q_i(t) = e^{-\zeta\omega_i t}(C_1 \cos\omega_{di} t + C_2 \sin\omega_{di} t) \tag{32}$$

By defining $\omega_{di} = \omega_i\sqrt{1-\zeta_i^2}$, where the constants $C_1(q_{i0};\dot{q}_{i0})$, $C_2(q_{i0};\dot{q}_{i0})$ depend on the initial conditions. Hence, for a unit impulse of i^{th} mode, the modal Impulse Response Function (IRF) is given as:

$$q_i(t) = e^{-\zeta\omega_i t}(q_{io}\cos\omega_{di} t + \frac{\dot{q}_{io} + \zeta q_{io}}{\omega_{di}}\sin\omega_{di} t) \tag{33}$$

Substituting (33) into (31) the displacement $v_C(t, L_1 + L_2)$ at the tip of the tool can be obtained. This describes a vibratory motion with diminishing amplitude and time intervals τ_d which separate two successive points $v_C(t)$, $v_C(t+\tau_d)$, is $\tau_d = 2\pi/\omega_i$. Then, the logarithmic attenuation ratio δ_i, $\delta_i = \zeta_i\omega_i\tau_d$, which represents the rate at which the amplitude of motion decays is [66], [188]:

$$\delta_i = \ln\frac{v_C(t)}{v_C(t+\tau_d)}, \quad \text{or} \quad \delta_i = \frac{1}{n}\ln\left(\frac{v_C(t)}{v_C(t+n\tau_d)}\right) \tag{34}$$

where τ_d is the damped period which is measurable and *n* is the number of intervals to determine more precisely the damping coefficient.

The dependence of the logarithmic decrement (δ_i) of the system and the damping ratio (ζ_i), is expressed as follows [189]:

$$\zeta_i = \frac{1}{\sqrt{1+(2\pi/\delta_i)^2}} \tag{35}$$

4.1.4 Determination of the damping ratio of a standard boring bar

The damping of the tool is usually determined by a hammer test. The impact hammer induces transient vibration of the tool, which can be simulated by modal analysis assuming that the first two eigenmodes dominate the solution [189].

DOI: 10.14750/ME.2023.032

In the hammer test, an accelerometer provides the signal of the accelerations. The determination of Lehr damping is based on displacement signals obtained during the tests in Section 3.2. The acceleration can be integrated two times with respect to time then using (34) and (35).

The acceleration signal of the hammer test was captured by sampling rate *12,800* Hz. The numerical integration was performed by trapezoid rule. An example of the IRF of the acceleration *(a)* for the experimental result in *L/D = 7* is shown in Figure 10. The corresponding velocity and displacement are shown in Figure 11 and Figure 12, respectively.

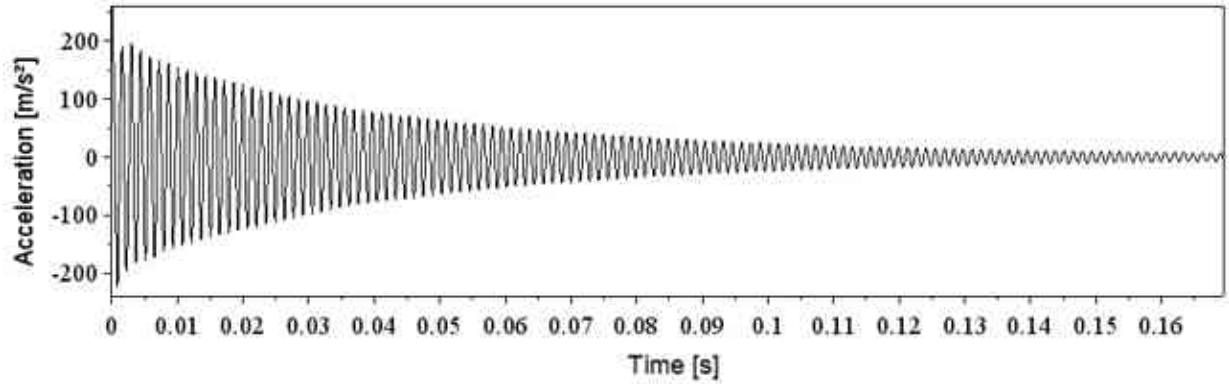

Figure 10. IRF curve of the acceleration for the standard boring bar L/D = 7

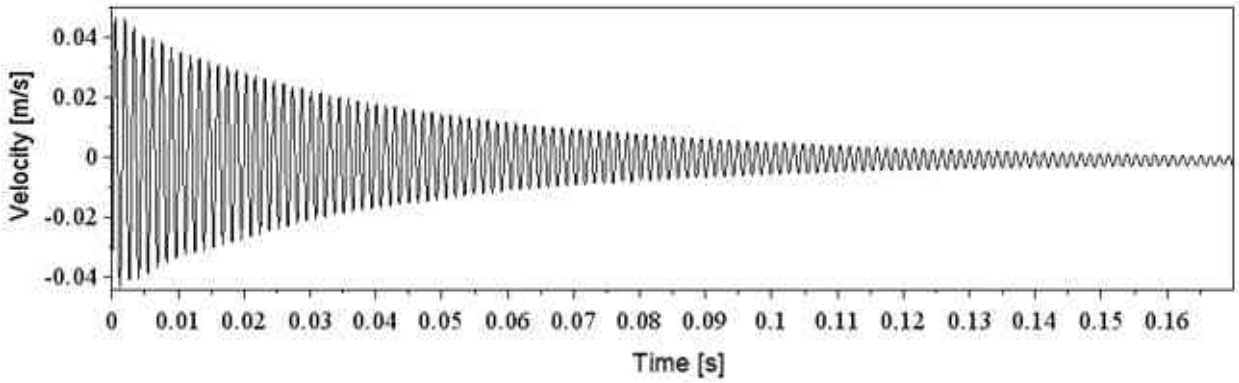

Figure 11. IRF curve of the velocity for the standard boring bar L/D = 7

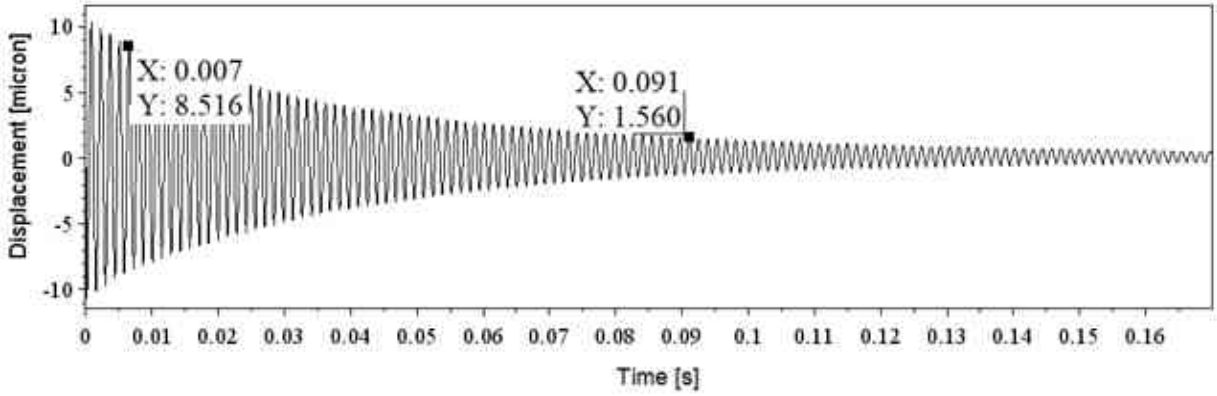

Figure 12. IRF curve of the displacement for the standard boring bar L/D = 7

Applying formulae (34)-(35) for the data given in Figure 12, the logarithmic decrement is:

DOI: 10.14750/ME.2023.032

$$\delta_7 = \frac{1}{60}\ln\left(\frac{8.516}{1.556}\right) = 0.02833$$

and the damping ratio for the boring bar is:

$$\zeta_7 = \frac{1}{\sqrt{1+\left(2\pi / 0.02833\right)^2}} = 0.0045$$

Table 3 summarizes the Lehr damping parameters for different overhangs. Interestingly, there is a trend, i.e., the greater the overhang the smaller the damping.

Table 3. Experimental Lehr damping of the standard tool in different overhangs for the first mode

L/D	***3***	***4***	***5***	***6***	***7***	***8***	***9***
δ_i	*0.1580*	*0.1260*	*0.0650*	*0.0347*	*0.02833*	*0.0210*	*0.0220*
ζ_i	*0.025*	*0.020*	*0.010*	*0.0055*	*0.0045*	*0.0033*	*0.0035*

4.1.5 Determination of the natural frequencies of a standard boring bar

This subsection describes the post-processing of the capture accelerations of the boring bar for different overhangs. FRF analysis is performed to determine two parameters: natural frequencies and also dynamic stiffnesses.

The selected frequencies shown in Table 4 were based on the experimental tests and the proposed model which were correlated and presented when the tool assumed overhang ratios between *L/D* 3 and 9. Only the one dominant peak characterized the first flexural mode of the tool and the machine components such as the turret and the lathe structure can be attributed to the minor peaks.

It is thus clear in Table 4 that, with knowledge of the parameters listed in Chapter 2, the natural frequency is inversely proportional to the reference length L_1. Within this context, longer overhangs result in lower natural frequencies making the boring bar more flexible and vulnerable to undesired vibrations.

The experimental measurements were compared with the Euler-Bernoulli proposed model. It is noted that, the Winkler foundation's stiffness obtained as $k = 1.0 \times 10^{11}$ N/m was adjusted to the highest overhang until the first mode theoretical natural frequency tuned to the measured natural frequency.

For long overhangs (L/D ≥ 5) the identified maximum absolute error is *2.80%*. The analytical model proposed exhibits some slight differences with experimental results, particularly in short overhangs, but proved to be sufficiently accurate in long overhangs [149].

In short overhangs, the shear deformation of the beam can no longer be ignored, and the Euler-Bernoulli model becomes less accurate. As a result, the numerical calculations from the model may deviate from the experimental measurements, leading to higher error. Conversely, for long overhangs, the thickness of the beam is relatively small compared to its length, and the assumption of negligible shear deformation holds more accurately. Therefore, the Euler-Bernoulli model can

DOI: 10.14750/ME.2023.032

better predict the behavior of the beam, resulting in a smaller absolute error between the numerical calculations and experimental measurements.

Furthermore, the intrinsically unpredictable behavior of most damped mechanical systems also contributes to the higher error in short overhangs, making it difficult to further improve the model. The analysis of the signal loses accuracy when the sampling rate approaches the eigenfrequency. This may explain the greater errors observed in short overhangs compared to long overhangs.

Table 4. Comparison of the lowest experimental (f_{exp}) and theoretical (f_m) natural frequencies for different overhangs for a standard boring bar

L/D	***3***	***4***	***5***	***6***	***7***	***8***	***9***
f_{exp} [Hz]	*3677.3*	*2281.2*	*1348.4*	*985.9*	*751.5*	*609.3*	*482.0*
f_m [Hz]	*3247.6*	*2029.2*	*1386.2*	*1006.4*	*763.6*	*599.1*	*482.6*
Error [%]	*11.69*	*11.05*	*2.80*	*2.08*	*1.61*	*1.67*	*0.12*

Using the Fast Fourier Transformation (FFT) it is possible to plot Figure 13 by transforming the time-domain variables (IRF) in their equivalent frequency-domain (FRF) expressions [190]–[195].

Figure 13 depicts the frequency response function (FRF) as acquired by a piezoelectric accelerometer in response to hitting the boring tool in different overhangs with a hammer. The multiple curves show the growth of the natural frequency as long as the *L/D* is decreased from *9* to *3*. According to [28], when replacing the natural frequency parameter (ordinate axis) with the tool deflection parameter, it was noticed that the lower the stiffness of the bar, represented by large *L/D* ratio values, the larger its deflection will be, and vice versa. Consequently, in Table 5, the values show that long overhangs decrease the dynamic stiffness of the tool, directly affect the acceleration amplitude of the tool and, consequently, influence the roughness of the workpiece and let the cutting process lose the necessary stability to avoid chatter.

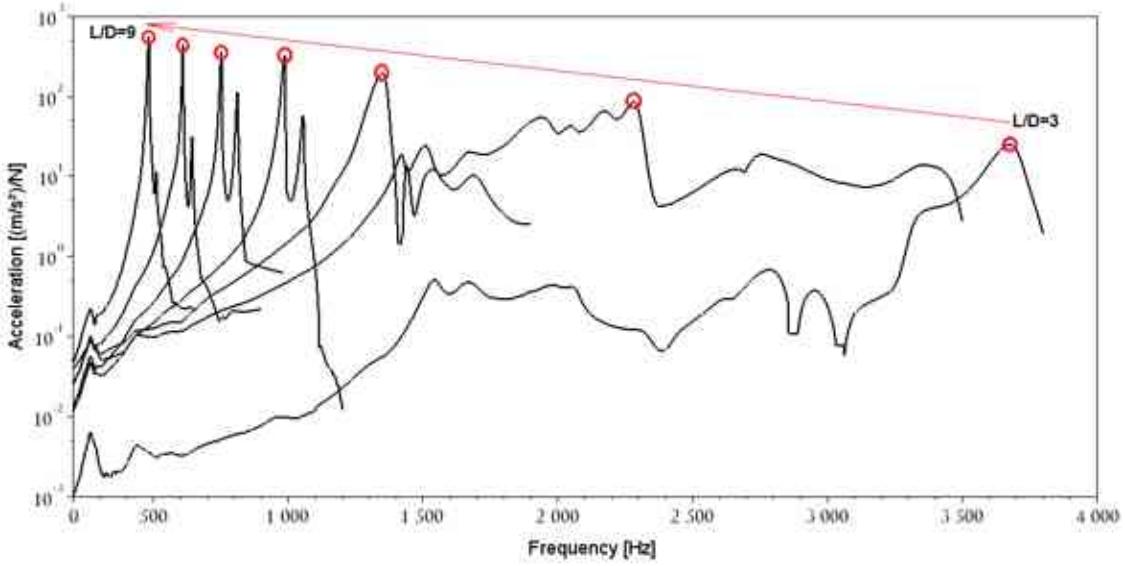

Figure 13. Natural frequency spectrum for the standard boring bar in different overhangs

DOI: 10.14750/ME.2023.032

The highest resonant peak at the first bending mode is identified from the multi-span beam model with Winkler foundation, while other peaks are negligible. Then, to plot Figure 13, equation (36) [196], [197] was applied considering the accelerance amplitude (h_{ioa}) and eigenfrequency (ω_i) of the i^{th} and o^{th} vibration mode and certain overhang, respectively, to obtain the compliance FRF amplitude (h_{ioc}) in order to understand the interaction between the reacceptance amplitude at the main resonant peak and the tool overhang:

$$h_{ioc} = \frac{h_{ioa}}{\left(2\pi\omega_i\right)^2}; \quad k_{do} = \frac{1}{2h_{ioc}} \tag{36}$$

where k_{do} is the dynamic stiffness of the tool in the corresponding overhang related through (37). According to [33] the experimental static stiffness $\left(k_s\right)_i$ can be calculated as follows:

$$\left(k_s\right)_i = \frac{k_{do}}{\zeta_i} \tag{37}$$

Table 5, equations (36) and (37) demonstrate the possibility of estimating the experimental static stiffness of the tool. As the *L/D* ratio increases, the static stiffness decreases, which makes the tool more vulnerable to deflections when long overhangs are compared to short ones. This low static stiffness can also make the tool more susceptible to vibration.

Table 5. Experimental static stiffness with different overhangs

L/D	***3***	***4***	***5***	***6***	***7***	***8***	***9***
$(k_s)_i \times 10^6$ [N/m]	*423.47*	*59.68*	*18.23*	*10.63*	*6.93*	*4.94*	*2.34*

4.2 Forced vibration analysis of the ID boring bar in different overhangs

The section discusses the damping characteristics of an impact-damped tool used in an ID boring bar. The Hertzian contact model is used to analyze the impacts between the balls and the tool. The section aims to investigate the dynamics of the ID tool and find its best performance in terms of highest damping for different overhangs. Numerical computations are used to investigate the forced vibrations of the tools under different circumstances, such as overhangs, clearance gaps, excitation forces, and excitation frequencies. The section presents a map graph that shows the smallest average peak amplitudes within a gap interval, which indicates that the tool used in the experiments is within this range.

4.2.1 Mathematical model of the ID boring bar in different overhangs

In the course of the machining process, the interaction of the tool and the workpiece the boring bar is excited dynamically, i.e., the bar is forced to vibrate. The focus of this section is to investigate the damping characteristics of the impact-damped tool under different conditions of overhangs, number of balls, clearance gaps and force magnitudes. This work is about modelling and understanding the behaviour of an impact damper applied in a standard boring bar.

DOI: 10.14750/ME.2023.032

The known Hertzian contact model is used to treat the impacts between the balls and the tool. The mathematical model is efficient to provide the contact force and very sensitive to the variation of the clearance gap.

Describing the dynamic boring bar model, the following assumptions have been made [161]:

(i) The instantaneous boring force is proportional to the instantaneous uncut chip area of cross-section, under dynamic boring conditions. This constant force is neglected in the model.

(ii) The effect of the radius of curvature of the work on the chip geometry is also negligible.

(iii) The geometrical orientation of the resultant cutting force under dynamic cutting conditions is the same as that in steady-state conditions.

(iv) The change in the uncut chip cross-sectional area by the tool nose radius is negligible.

(v) The elastic, plastic and viscous model of the support at the cutting edge of the tool is being neglected due to the complexity of the chip formation process. In other words, the friction force and normal reaction calculated by [198] were also neglected.

(vi) Perpendicular radial and tangential dynamical excitation forces are exerted on the tip of the tool as shown in Figure 14.

(vii) The torsion and axial vibration of the tool are neglected, only its deflection in directions *X* and *Y* are considered.

(viii) The cutting tool model of internal turning operation is shown in Figure 14 with the components of cutting forces in radial and tangential directions. Since the cutting force has got horizontal and vertical components, the bending deflections of the tool are considered in directions *X* and *Y*. The cutting force in axial direction will not be considered. In this sense, the rigidity of the bar is much higher along the feed or axial direction than in the tangential and radial bending directions. Similarly, the bar exhibits higher stiffness in torsion than in bending. Therefore, the bending vibrations caused by the tangential force F_{cy} and radial force F_{cx} are considered in the analysis [199].

Then excitation force is expressed in vector form as follows:

$$\mathbf{F}_0 = \mathbf{F}_{cx} + \mathbf{F}_{cy} \tag{38}$$

To simplify the computations, the time-dependence of the excitation forces can be expressed by harmonic functions [200], [201];

$$\begin{aligned} F_{cx} &= F_{x0}\sin(\omega_f t) \\ F_{cy} &= F_{y0}\sin(\omega_f t) \end{aligned} \tag{39}$$

where F_{x0} and F_{y0} are the force amplitudes, while ω_f is the frequency excitation of the machine spindle.

DOI: 10.14750/ME.2023.032

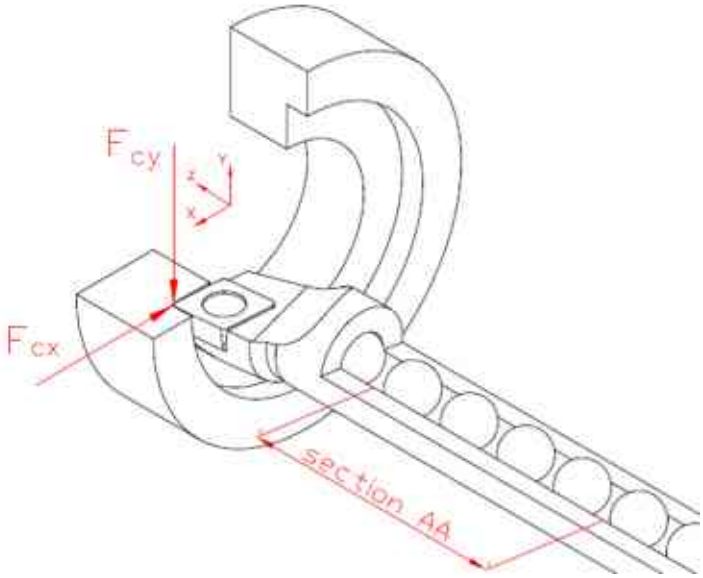

Figure 14. Forces at the tip of the tool in radial and tangential directions

The interaction of the balls and the wall of the tool cavity is being considered with nonlinear viscoelastic contact model displayed in Figure 15.

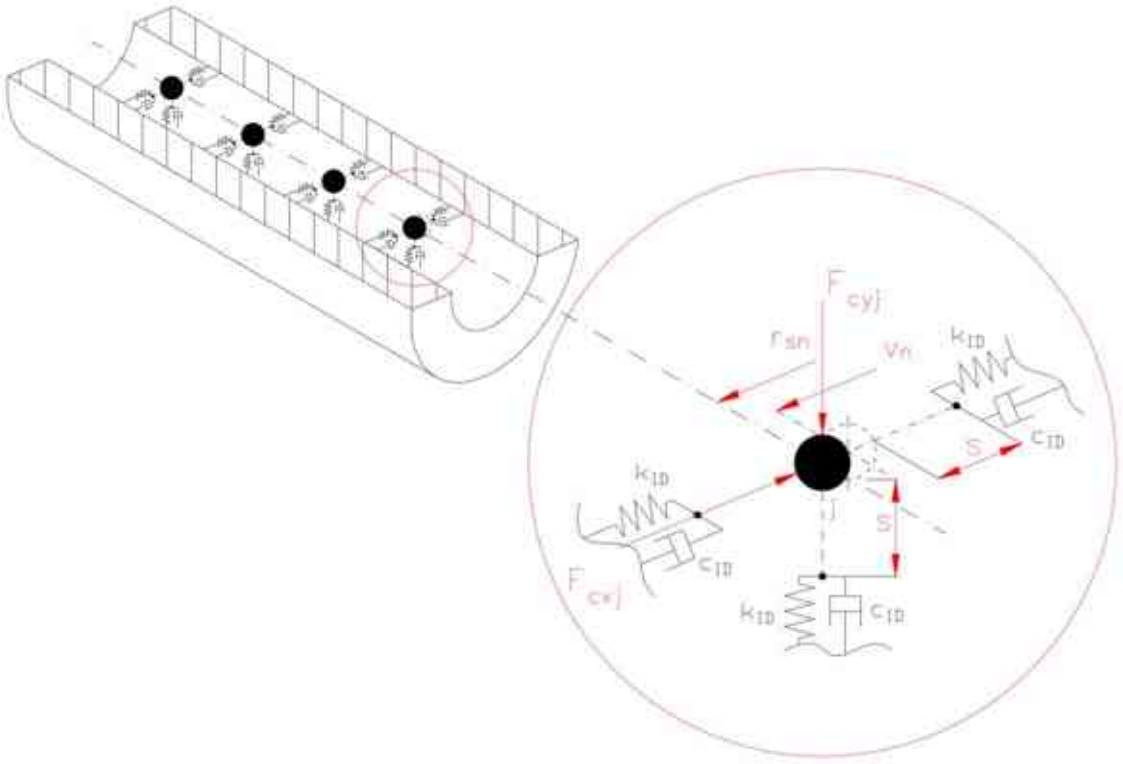

Figure 15. Contact model of the balls and the tool

The model of Figure 16 illustrates the ID boring bar. In this way, the contact force is considered only between the cavity wall and the ball surface, where viscoelastic deformation is assumed. In this sense, Hertz's theory for contact is introduced to provide contact force between the ball and

DOI: 10.14750/ME.2023.032

the cavity wall [137]. The contact model proposed by Lankarani-Nikravesh [135] extends the Hertzian elastic contact force with a velocity-dependent term, which is given as:

$$F_{cnj} = k_{ID}\delta_n^{1.5} + c_{ID}\dot{\delta}_n \tag{40}$$

where δ_n indentation (deformation distance between bodies)

The damping coefficient c_{ID} in which the represented hysteresis factor η was proposed by [134] and can be calculated as:

$$c_{ID} = \eta\delta_n^{1.5} \tag{41}$$

Using the same procedure adopted by [202], which is based on the energy balance with the application of the fundamental laws of conservation of momentum, [119] proposed the following relationship for the hysteresis factor η, the same as to ID tools given by [188]:

$$\eta = \chi\frac{k_{ID}}{\dot{\delta}_n^{(-)}} = \frac{8(1-e)}{5e}\frac{k_{ID}}{\dot{\delta}_n^{(-)}} \tag{42}$$

where $\dot{\delta}_n^{(-)}$ initial impact velocity

The contact stiffness, based on Hertz theory, is related to the material properties of contact bodies (Young modulus and the Poisson ratio of the boring bar (E_t, v_t); Young modulus and the Poisson ratio of the ball (E_s, v_s)) and the surface curvature radius of the bodies (radius of the cavity (r_b) and radius of the ball (r_s)). The normal contact stiffness of the ball and the cylindrical surfaces in a general direction **n** according to [137] and [203] is written as follows:

$$\begin{aligned} k_{ID} &= \frac{4}{3}E_* R_*^2\left(\frac{h_n}{R_*}\right)^{1.5} \quad if \quad v_n - r_{sn} \geq s \\ k_{ID} &= 0 \quad if \quad -s < (v_n - r_{sn}) < s \\ k_{ID} &= \frac{4}{3}E_* R_*^2\left(\frac{h_n}{R_*}\right)^{1.5} \quad if \quad v_n - r_{sn} \leq -s \end{aligned} \tag{43}$$

where

$$\begin{aligned} \frac{1}{E_*} &= \frac{(1-v_t^2)}{E_t} + \frac{(1-v_s^2)}{E_s} \\ \frac{1}{R_*} &= \frac{1}{r_b} + \frac{1}{r_s} \\ h_n &= |v_n - r_{sn}| \end{aligned} \tag{44}$$

The tangential contact forces are obtained by Coulomb friction. The normal and tangential force components can be expressed as shown below:

DOI: 10.14750/ME.2023.032

$$
\begin{aligned}
&F_{ctj} = \pm \mu F_{cnj} \\
&\mathbf{F}_{cj} = F_{ctj}\mathbf{t}_j + F_{cnj}\mathbf{n}_j \\
&j = 1,...,nb
\end{aligned}
\tag{45}
$$

where the sign depends on the relative tangential velocity between the contacting bodies. The contact force vectors can be expressed in *X* and *Y* directions:

$$
\mathbf{F}_{cj} = F_{ctj}\mathbf{t}_j + F_{cnj}\mathbf{n}_j = F_{cxj}\mathbf{i} + F_{cxj}\mathbf{j} \qquad j = 1,...,nb \tag{46}
$$

The equations of motion of the ball j, which can be in contact with the cavity, are given as

$$
\begin{aligned}
&M_{cj}\ddot{x}_j = F_{cxj} \\
&M_{cj}\ddot{y}_j = F_{cyj} - M_{cj}\mathbf{g} \\
&J_m\ddot{\Phi} = r_s F_{ctj}
\end{aligned}
\tag{47}
$$

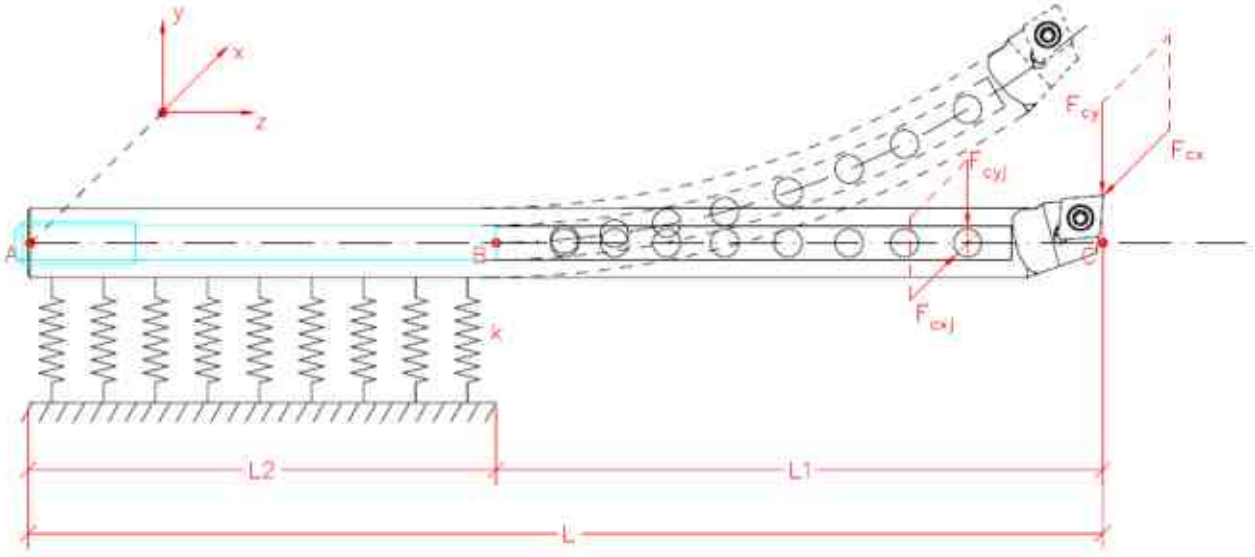

Figure 16. Mechanical model for an impact damper boring bar in Winkler foundation

The radial and tangential displacements $u(z,t)$ and $v(z,t)$, as functions of time *t* and axial coordinate *z*, can be expressed as a linear combination of eigenfunctions for ID according to

$$
\begin{aligned}
&u(z,t) = \sum_{i=1}^{nf} \Phi_i(z)\, q_{xi}(t) \\
&v(z,t) = \sum_{i=1}^{nf} \Phi_i(z)\, q_{yi}(t) \\
&i = 1,2
\end{aligned}
\tag{48}
$$

where $q_{xi}(t)$ and $q_{yi}(t)$ are the modal coordinates and $\Phi_i(z)$ is the i^{th} mode shape.

The equations of motion of the bar are based on (31) extending them with the contact forces (between the balls and the cavity wall of the boring bar) and the external excitation forces:

DOI: 10.14750/ME.2023.032

$$\begin{aligned}\ddot{q}_{xi}+2\zeta_i\omega_i\dot{q}_{xi}+\omega_i^2 q_{xi}&=\Phi_i(z)F_{x0}\sin\left(\omega_f\, t\right)-\sum_{j=1}^{nb}\Phi_i(z)F_{cxj}\\ \ddot{q}_{yi}+2\zeta_{\,i}\omega_i\dot{q}_{yi}+\omega_i^2 q_{yi}&=\Phi_i(z)F_{y0}\sin\left(\omega_f\, t\right)-\sum_{j=1}^{nb}\Phi_i(z)F_{cyj}\end{aligned} \tag{49}$$

A computer code has been developed under *SciLab* software and in Fortran programming language on the basis of the equations (38)-(49).

4.2.2 Numerical computation of two-span Winkler-supported boring bars with different overhangs with and without impact damper

This section will analyse the forced vibrations of the standard and ID tools. The aim of the numerical computations is to understand the dynamics of the ID tool, and to find its best performances, i.e., highest damping for different overhangs.

As it was assumed in Section 4.2.1 the cutting process is not modelled here only the forced vibration of the tools is investigated over different circumstances: overhangs, clearance gaps, excitation forces, excitation frequencies.

In the next subsection, the numerical results of the tools with *L/D = 7* will be presented as an example of a specific excitation force amplitude and a clearance gap between the balls and the cavity of the ID boring bar. Then there will be a summary of the rest of the overhangs keeping the specific force and clearance gap. Because there is a number of measurements for this specific gap and overhangs which could validate the dynamics of the tool. Finally, parametric computations will be performed on different excitation forces, clearance gaps and balls in order to find highest damping or smallest average displacements.

4.2.3 Numerical computation of two-span Winkler-supported boring bars with overhang of 112 mm (*L/D = 7*) *with and without impact damper*

The main purpose of this subsection is to demonstrate the method what will be used in the following subsections for different parameters of the tools. The excitation force necessary to plot Figure 18 and Figure 19 (time-displacement at the tip of the standard boring bar in *X* direction when *L/D = 7*), also summarized in Table 7 was calculated considering the RMS acceleration amplitude of the standard boring bar in Table 12 and Figure 36(a). The measured RMS acceleration amplitude of *16.189* m/s^2, was approximately processed to RMS displacement amplitude $A = 1.30 \times 10^6$ m in the time domain for stable cutting conditions. The shape of the signals is complex and do not follow a pattern, but the main analysis was based on the amplitude of the displacement signal for the standard boring bar, with an overhang of $L_1 = 112$ mm and a natural frequency of $\omega_1 = 725.15$ Hz. The excitation force was re-calculated by the product of the amplitude displacement and the stiffness of a cantilever Euler–Bernoulli beam, estimated using the following equation $k_b = 3(EI/L^3)$ [182], $k_b = 1.37 \times 10^{-6}$ N/m, resulting in $F_{exc} = 1.78$ N.

Typically, in an internal turning operation, the tangential cutting force F_{y0} is the largest. It acts perpendicular to the cutting insert rake surface and pushes the boring bar "downward"—that is, below the centerline. The radial force is about *20%* of the tangential force and perpendicular to the tangential and feed forces and pushes the bar away from the side of the bore [199]. At this point, the excitation forces in radial and tangential directions will be considered $F_{x0} = 1.78$ N and $F_{y0} = 1.2 \times F_{x0}$.

DOI: 10.14750/ME.2023.032

Considering the schematic dimensions and parameters in Figure 17 the position of the ball, z_n can be calculated in meters as follows:

$$z_n = 0.025 + r_b[1 + 2(n-1)] + A + nB \tag{50}$$

where the parameter A is the clearance between the ball and the top face of the adjusting screw, B is the clearance between the balls, C is the clearance between the ball and the bottom of the cavity, r_b is the ball radius and n is the position number of the ball.

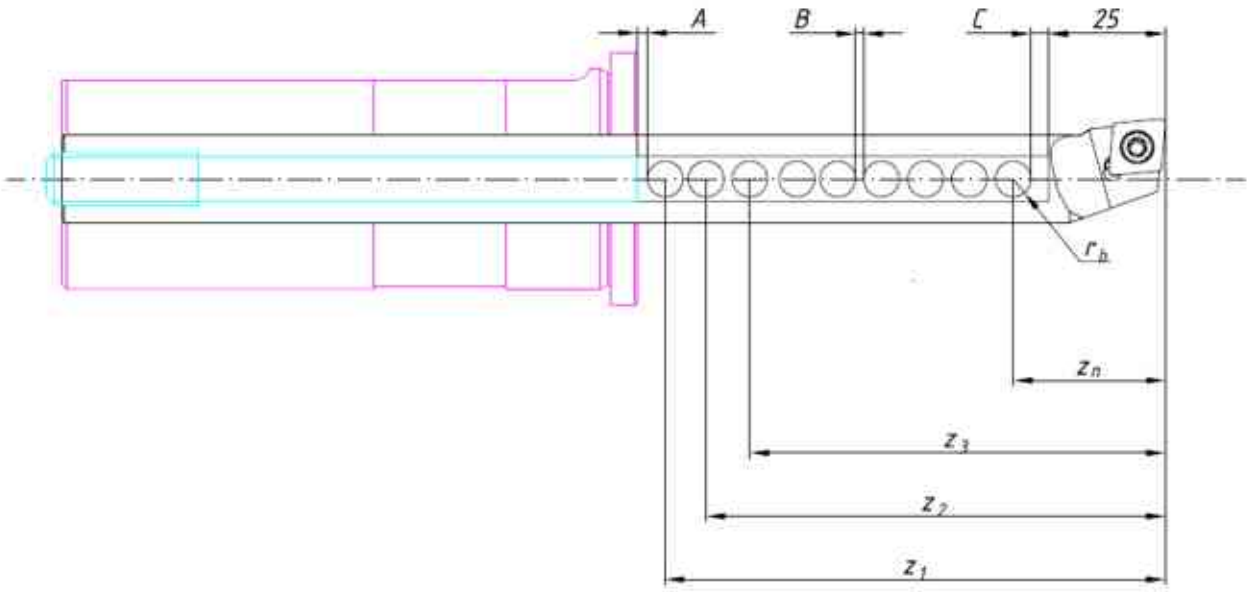

Figure 17. Position of the ball to calculate the displacement of the tool when L/D = 7

Considering the parameters A, B and C with the same value and constant of 0.083 mm, and $r_b = 4$ mm, there are the ball positions calculated in Table 6 for $L/D = 7$. It is also necessary to mention the values of the eigenfunctions $\Phi_i(z)$ at the locations of balls in Z direction, by applying (28).

DOI: 10.14750/ME.2023.032

Table 6. Ball position (mass center) in milimiters for L/D = 7

Modes *i* (Eigenfrequency)	Ball number *(n)*	Ball position *(z_n)*	Function value of $\Phi_i(z)$
No. *1* *(725.150 Hz)*	*1*	*0*	*0.1479932*
	2	*29.125*	*0.3076105*
	3	*37.250*	*0.5184362*
	4	*45.375*	*0.7744116*
	5	*53.500*	*1.0695857*
	6	*61.625*	*1.3981682*
	7	*69.750*	*1.7545894*
	8	*77.875*	*2.1335676*
	9	*86.000*	*2.53018212*
	10	*94.250*	*2.9399515*
	11	*102.375*	*3.35891228*
	Tip of the tool	*217.000*	*4.891985*
No. *2* *(4489.691 Hz)*	*1*	*0*	*0.8704131*
	2	*29.125*	*1.5322813*
	3	*37.250*	*2.2278827*
	4	*45.375*	*2.8463323*
	5	*53.500*	*3.294178*
	6	*61.625*	*3.5001459*
	7	*69.750*	*3.4185716*
	8	*77.875*	*3.0309611*
	9	*86.000*	*2.3453246*
	10	*94.250*	*1.3931365*
	11	*102.375*	*0.2239803*
	Tip of the tool	*217.000*	*-4.8453013*

Having said that, the contact forces acting between the ball and the cavity are considered to be collinear and occur in the *X* and *Y* directions. It is assumed same eigenvibrations take place in *x-z* and *y-z* planes. Eigenfrequency for the first mode $\omega_{n1} = 725.150$ Hz obtained from (3.14) was used in analysis of standard and ID boring bars, considering the boundary conditions (3.4) to (3.6) of two-span Winkler-supported tools. The present investigated examples have an overhang of *112* mm or *L/D = 7*. It was used the parameter values of Section 3.2 and the proposed mathematical model for ID in (3.15) by programming them in *SciLab* software. Though the excitation force has *X* and *Y* components the displacement amplitude RMS of the boring bar has been analyzed in *X* direction because it is related to the roughness of the turned workpiece.

Firstly, the results are shown in Figure 18 as a typical displacement curve of a standard boring bar. Secondly, Figure 19 presents for each excitation frequency, ω_i, the displacement on the tip of the ID boring bar in *X* direction versus time, as a non-harmonic curve, because of the chaotic motion behaviour of the balls inside the cavity. In order to make the results of the standard bar and the ID bar comparable, the Root Mean Square (RMS) of the displacements is determined for both of them. For example, the points of the curve FRF are given also by RMS of the displacements in

DOI: 10.14750/ME.2023.032

direction *X*. It means that the average displacement at the tip of the tool is determined instead of its amplitude.

The root mean square (RMS) average amplitude with standard and ID signals shown in Figure 18 and Figure 19 are given as:

$$X_{rms} = \sqrt{\frac{1}{N}\sum_{i}^{N}(X_i)^2} \tag{51}$$

where X_{rms} is RMS value of the displacements, N is the number of sampling points X_i is the equidistant sampling displacements [110].

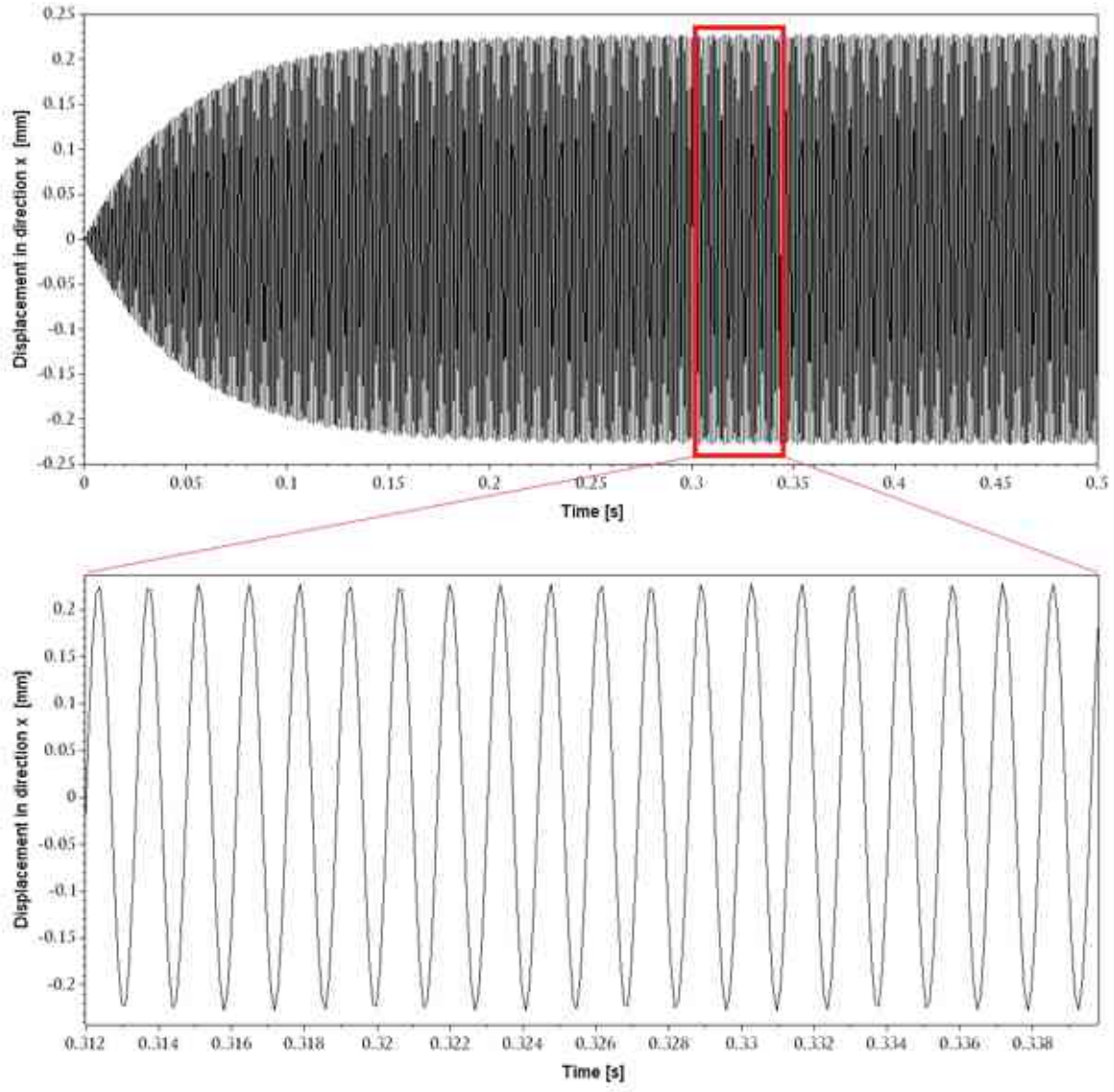

Figure 18. Time-displacement at the tip of the standard boring bar in X direction when L/D = 7

DOI: 10.14750/ME.2023.032

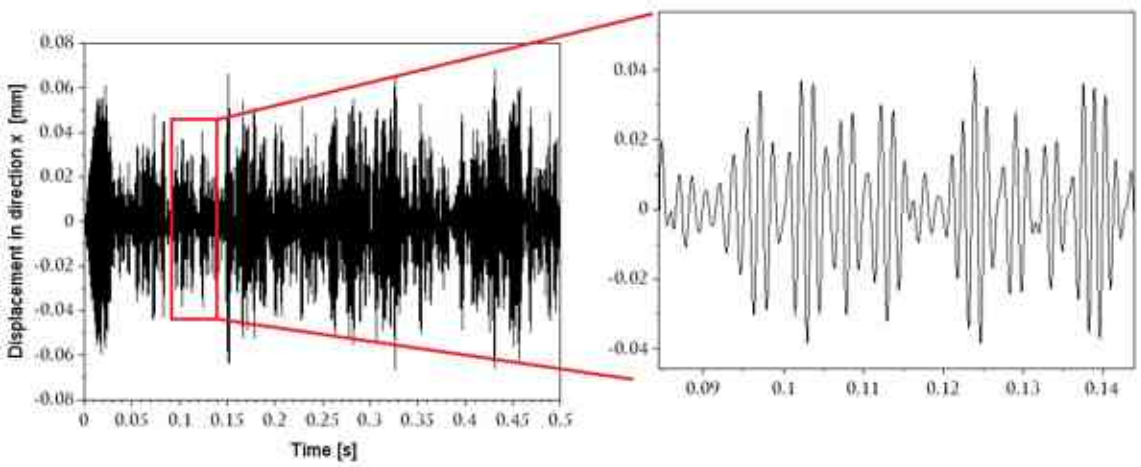

Figure 19. Time-displacement at the tip of the ID boring bar in X direction when L/D = 7

Applying (3.40) for the displacements shown in Figure 18 and Figure 19 the X_{rms} values are *0.148975336* mm and *0.0217333724* mm.

The computation of the ID tool also provides the displacements of the centres of balls. For the case of the ball trajectory, it is more convenient to express the clearance gap between the ball and the tool cavity than simply using their respective radius or diameter values. The centre of the balls is practically always within the circle of radius equal to the clearance gap (s). Thus, the clearance gap (s) is expressed as the difference between the cavity (r_s) and ball radius (r_b).

In this way, when the ball collides eccentrically against the circular tool cavity, can admit different trajectories, which will depend on the clearance gap, the excitation force, the coefficient of restitution and the contact force which is influenced by the friction coefficient. As an example, consider the response is shown in Figure 20 when using an excitation force of *1.78* N. These trajectories are related to the inertial frame.

Figure 20 illustrates the relative displacement of the balls for the same excitation force and clearance gap, with the force being applied only at the tip of the tool. The displacements of the cross-sections along the bar will differ due to the linear combination of the eigenshapes found in Table 6 and obtained by Eq. (48). As a result, the displacements are expected to be higher close to the tip of the tool compared to the vicinity of the Winkler foundation. Hence, the ball motions exhibit different patterns at the tip of the tool, middle of the tool, and close to the clamping system. This implies that the balls and the tooltip are not always in phase with each other, which is a typical characteristic of chaotic motion during multiple collisions in the tool cavity.

Figure 20 presents different types of trajectories of the ball on the cavity surface. From this point on, we will say that trajectory *1* (Figure 20(a)) is represented when the ball collides continuously on the cavity, while trajectory *2* (Figure 20(e)) is when the ball has fewer collisions than trajectory *1*, and trajectory *3* (Figure 21(h)) has even fewer collisions than trajectory *2*. Therefore, trajectories *2* and *3* represent the transition between trajectory *1*, and trajectory *4* (Figure 20(k)), in which few collisions occur on the cavity wall and the damping efficiency is the lowest among all trajectories found for the balls inside the cavity. We can say that the displacement values in Table 6 are higher for trajectory *1* and gradually decrease until reaching the lowest values that correspond to

DOI: 10.14750/ME.2023.032

trajectory *4*. This facilitates the numerical understanding of the relative displacements of the balls inside the tool cavity.

When comparing the trajectories *1* and *4*, respectively in Figure 20(a) and Figure 20(k), trajectory *1* has higher damping performance than trajectory *4*. The numerical calculation indicates that the balls prescribe an angular movement in relation to the centre of the cavity, which contributes to an increase in the number of impacts. This result is only possible if the excitation force is high enough to keep the impacts. On the contrary, a lower number of impacts were identified in trajectory *4* (Figure 20(k)), with aleatory motion of the balls to many directions minimizing the efficiency of the absorber. The simulation indicates that the low magnitude of the excitation force where these balls are located along the tool makes the impact damper have low efficiency. It might be because there are few numbers of impacts inside the cavity and no presence of sliding motion.

Furthermore, trajectory *1* provides a practically unidirectional movement to the ball, which approaches an ideal condition of collinear impacts. In the results of trajectories *2* and *3*, it is possible to notice that the trajectories indicate the presence of many impacts. The fact that the impacts are distributed in various directions, instead of concentrating along the direction of the excitation force application, causes the damping efficiency to be minimized. The efficiency decreases even further in the case of trajectory *4*, where there are almost no impacts on the tool cavity. Thus, it is demonstrated that the presence of high-frequency harmonic forces contributes to the occurrence of impacts. Excitations of this nature can be easily found in real applications, such as internal turning of deep holes in hardened materials.

However, it is crucial to note that the angular motion of the cavity is a parameter that can modify the ball's trajectory, changing the numerical response obtained. This is because it is a parameter directly related to the tangential force developed at the contact point. Additionally, the results presented in this section are based on simulations that consider a bidirectional harmonic excitation with a natural frequency, and the actual excitation force in real systems may not be of the same nature as the force applied in the simulations. Real systems may be subject to excitations in various directions, combining different amplitudes and frequencies, whether they are harmonic or not, leading to modifications in the occurrences of impacts.

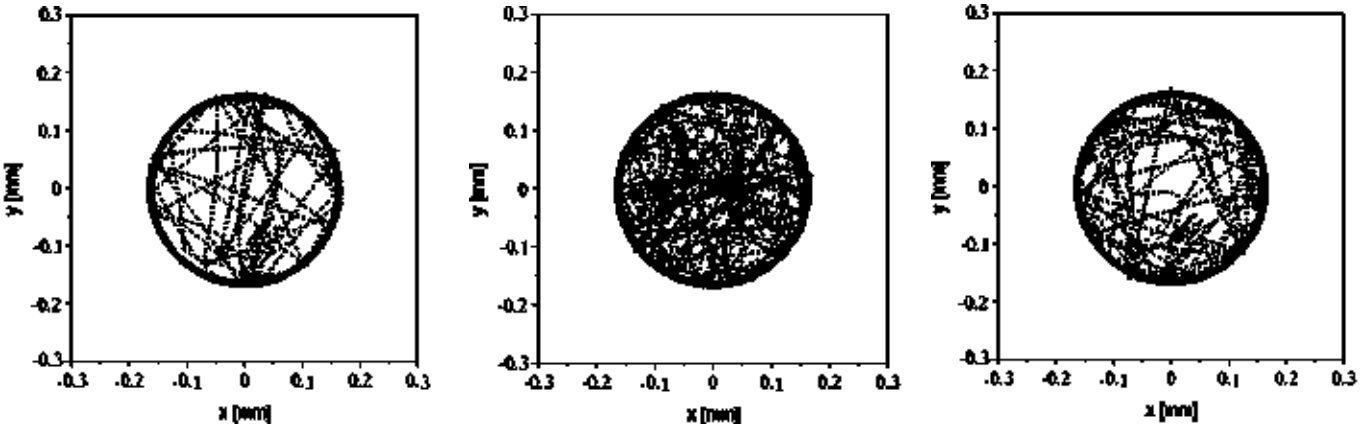

(a) (b) (c)

DOI: 10.14750/ME.2023.032

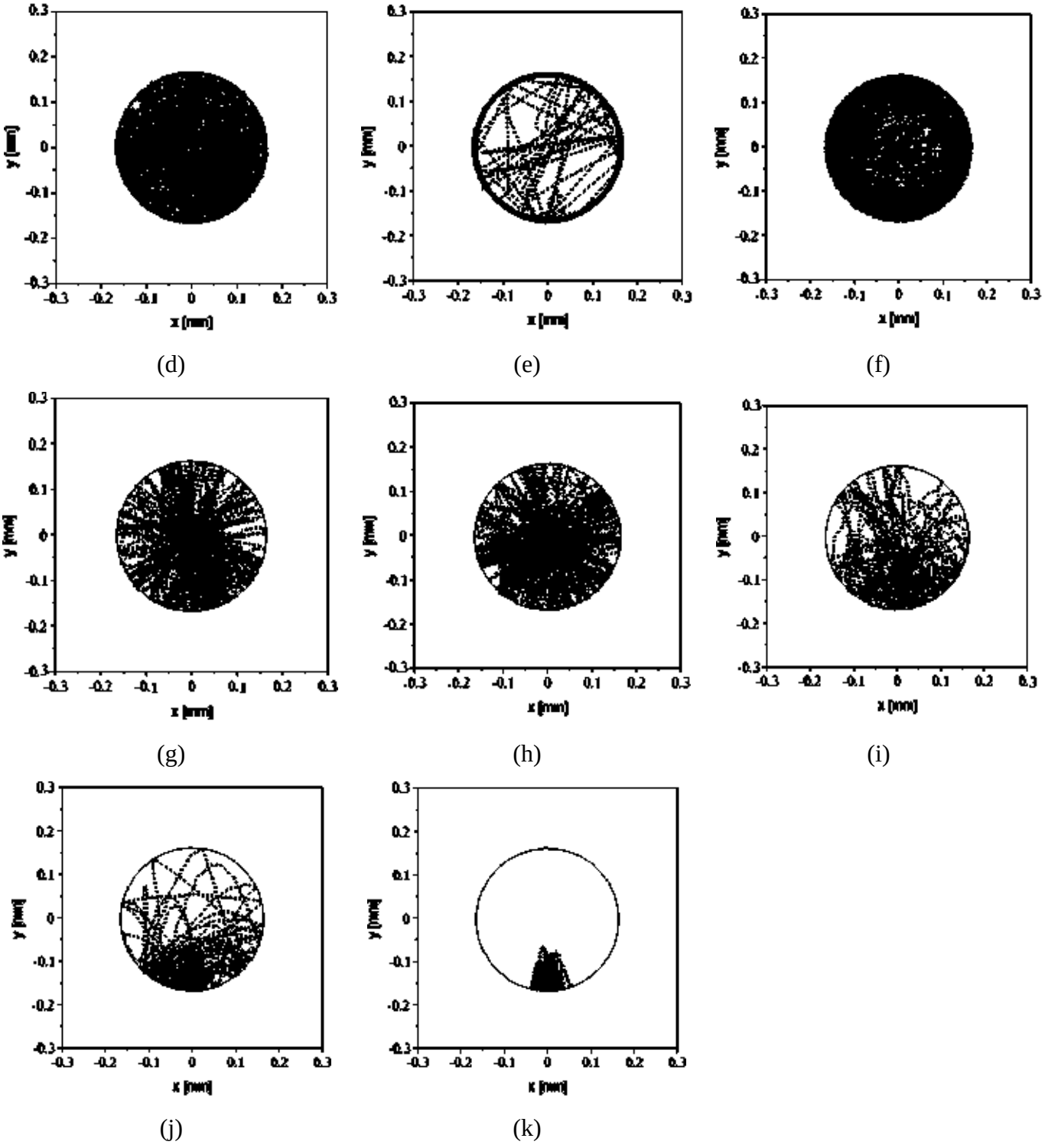

Figure 20. Trajectories of the balls (a) – (k) in the boring bar while cutting when L/D = 7 with 11 balls

In this section, the clearance gap and the excitation force are constant and established. It is notable that in Figure 21, it was necessary to determine the frequency response of the system at least for the neighborhood of the first eigenfrequency of the tools which is $\omega_1 = 725.150$ Hz. It is observed that the passive damper systems reduce the peak value of the frequency response in $\left|G(i\omega)\right|_{standard}$

DOI: 10.14750/ME.2023.032

= *109.02* to $|G(i\omega)|_{ID}$ | = *16.875*. It represents a damping ratio between the standard and the ID bar of 6.455, which proves the efficiency of the ID damper mechanisms to minimize the vibration amplitude of the tool during the internal turning operation of hardened materials.

Figure 21 proves that in free vibration the balls do not decrease the resonant peak, but when it is forced vibration the damping capacity of the balls is activated altering slightly the frequency and decreasing strongly the amplitude of the tool, as shown in Figure 19.

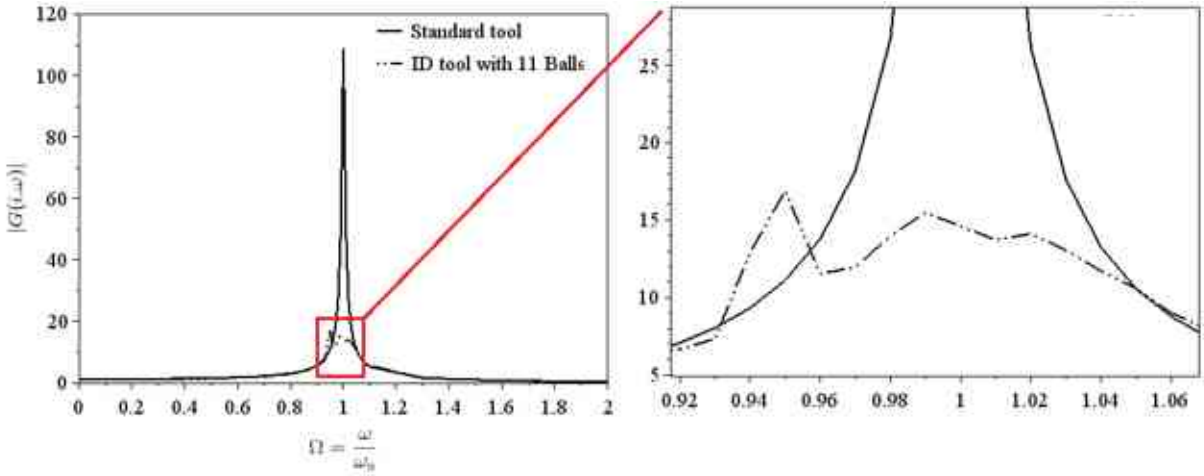

Figure 21. FRF curve obtained by the proposed mathematical model for standard and ID boring bars when L/D = 7

Consequently, in Figure 21, each peak value determines the Lehr damping of the specific tool with the following equation [204]:

$$|G(i\omega)|_{\max} = \frac{1}{2\zeta_i\sqrt{1-\zeta_i^2}} \tag{52}$$

The peak values of the FRFs and the corresponding Lehr damping are listed in Table 7. As regards the Lehr damping, ID provides much higher damping ratios than the standard boring bar.

Table 7. Damping ratios calculated from Equation (52) from the Figure 21 of the standard and ID boring bar when L/D = 7

Tool type	X_{RMS}	**Ω**	$\|G(i\omega)\|_{max}$	ζ_i
standard	*0.14897*	*1.0*	*109.02*	*0.00459*
ID	*0.0251*	*0.95*	*16.875*	*0.02963*

The boundaries of the stability lobe plot in Figure 22 define the split line between the stable and unstable cutting zones. Considering the parts of the tool's receptance FRF spectrum and assuming that the tool transfer function $H(j\omega)$, the specific cutting coefficient K_f, dynamic stiffness k_{do}, the natural frequency ω_i and the chatter frequency ω_c of the tool are known or measured, the procedure for plotting the stability lobes of the standard and ID boring bar can be summarized as follows [14], [25], [26], [199], [194]:

DOI: 10.14750/ME.2023.032

$$H(j\omega)=\frac{-2\zeta_i r_c}{k_{do}\left[\left(1-r_c^2\right)^2+\left(2\zeta_i r_c\right)^2\right]},\quad r_c=\frac{\omega_c}{\omega_i}\sqrt{1+2\zeta_i} \tag{53}$$

After that, the critical depth of cut, a_{lim} is calculated as [14], [25], [26], [199], [194]:

$$a_{\text{lim}}=\frac{k_{do}}{K_f}2\zeta_i(1+\zeta_i) \tag{54}$$

Finally, the lobes, i.e., k_a = 0, 1, 2, can be plotted from the relation between (53) and the spindle speed, S, of the workpiece written as [14], [25], [26], [199], [194]:

$$S=\frac{60\omega_c}{(2k_a+3)\pi+\tan^{-1}\left(H(j\omega)\right)} \tag{55}$$

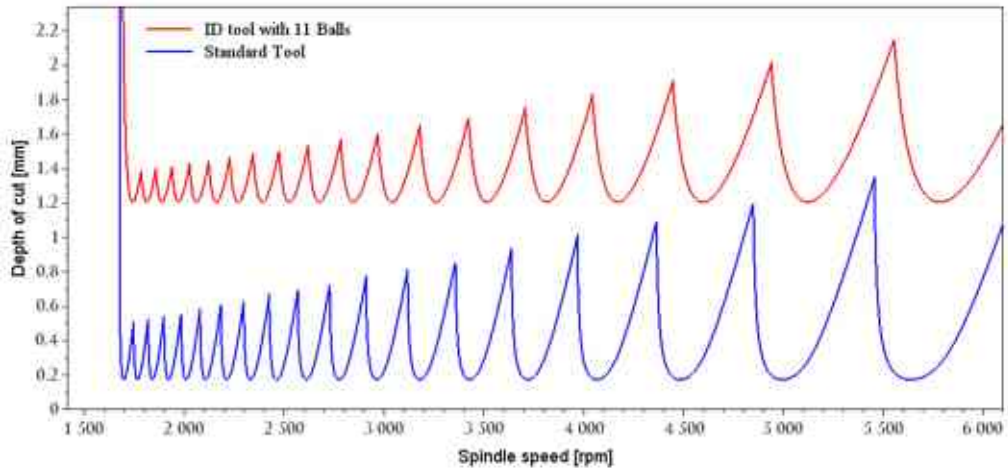

Figure 22. Stability lobe diagram for standard and ID boring bars when L/D = 7

4.2.4 Numerical computation of two-span Winkler-supported boring bars with overhang between 3 and 9 with and without impact damper

In an internal turning tool operation, it is critical to determine the maximum overhang that the tool can handle without experiencing chatter. This is particularly important for long overhangs, defined as $L/D \geq 5$ [149], [205], which can limit the cutting operation. This section analyzes the behaviour and dynamic properties of the tool under different overhangs.

All the time-displacement curves analyzed for overhangs between *3* and *9* are similar to those shown in Figure 18 and Figure 19 in Subsection 4.2.3. The curves for the standard tool are more regular, showing a harmonic pattern, while those for the ID boring bar are non-harmonic. Both tools show that as the overhangs increase, the displacement parameter also increases, but the ID boring bar has a lower amplitude than the standard boring bar in all situations studied. This indicates that the balls are effective in suppressing the tip of the tool displacement for all overhangs studied.

However, not all balls inside the tool can work with full damping efficiency. Table 8 separates the trajectory of each ball during cutting, as discussed in Subsection 4.2.3 and illustrated in Figure 20. The table shows the number of balls and their respective trajectories inside the tool cavity. It is

DOI: 10.14750/ME.2023.032

observed that trajectory *1* is present only in long overhangs (*L/D* ≥ *5*). This suggests that the ID damping system is an alternative to suppress the tool vibration in different overhangs, especially in higher ones.

Table 8 uses the symbols ◯, ⊗, *, and | to represent trajectories *1, 2, 3*, and *4*, respectively, as shown in Figure 20.

Table 8. Balls trajectory that might appear in the ID boring bar for different overhangs when the when excitation force is F_0 = 1.78 N and Gap_0 = 0.33 mm

L/D	*N° balls*	*1°*	*2°*	*3°*	*4°*	*5°*	*6°*	*7°*	*8°*	*9°*	*10°*	*11°*	*12°*	*13°*	*14°*	*15°*
3	*3*	*	*	*												
4	*5*	*	*	*	⊗	⊗										
5	*7*	*	*	⊗	⊗	◯	◯									
6	*9*	|	*	*	⊗	⊗	◯	◯	◯	◯						
7	*11*	|	|	*	*	*	⊗	◯	◯	◯	◯	◯				
8	*13*	|	|	*	*	*	*	◯	◯	◯	◯	◯	◯	◯		
9	*15*	|	|	|	*	*	*	⊗	*	◯	◯	◯	◯	◯	◯	◯

The FRF curves of standard tool are quite smooth and uniform, but the same is not true with the FRF curves of the tool when the ID is implemented. It is because the shock between the balls and the tool cavity has a chaotic motion. However, this condition is necessary to change the eigenfrequency of the tools and minimize the amplitude peak of the tool in the cutting operation, especially in long overhangs.

Table 9 contains the dynamic parameters calculated for the tool in order to obtain the damping ratio for different overhangs. It is important to highlight that for long overhangs (*L/D* ≥ *5*), the ID boring bar presented at least *1.5* times better damping ratio than the standard tool. The best damping ratio was obtained for *L/D = 8*. In short overhangs the damping ratio is not relevant compared to long ones. It lets us conclude that the ID system is advantageous to use mainly for long overhangs but it is also not worse for short ones. In that way, higher depth of cut is possible during the internal turning operation, because the ID tool can absorb more vibration energy during cutting compared to the standard tool. Consequently, the productivity of the manufactured workpieces increases and the chatter can be avoided.

Table 9. Lehr Damping of the standard (ζ_{iS}) and ID (ζ_{iID}) boring bar for different overhangs when excitation force is F_0 = 1.78 N and Gap_0 = 0.33 mm

L/D	**standard**				**ID**				**Ratio**
	X_{RMS}	**Ω**	$\|G(i\omega)\|_{standard}$	ζ_{iS}	X_{RMS}	**Ω**	$\|G(i\omega)\|_{ID}$	ζ_{iID}	ζ_{iID}/ζ_{iS}
3	*0.00356*		*21.111*	*0.02368*	*0.00349*	*1.0*	*20,678*	*0.0241*	*1.021*
4	*0.00872*		*26.319*	*0.01899*	*0.00788*	*1.0*	*23.768*	*0.0210*	*1.107*
5	*0.02989*		*51.987*	*0.00961*	*0.02225*	*1.01*	*38.703*	*0.0129*	*1.343*
6	*0.08405*	***1.0***	*91.799*	*0.00544*	*0.02368*	*1.02*	*25.870*	*0.0193*	*3.548*
7	***0.14897***		***109.02***	***0.00459***	***0.0251***	***0.95***	***16.875***	***0.02963***	***6.455***
8	*0.27123*		*138.799*	*0.00360*	*0.0327*	*0.95*	*16.775*	*0.02980*	*8.274*
9	*0.34172*		*127.291*	*0.00392*	*0.18791*	*0.92*	*69.998*	*0.00714*	*1.818*

DOI: 10.14750/ME.2023.032

Maximum Average Displacements of the tool as a function of the overhang for a standard (blue chart) and ID boring bar (orange chart) is shown in Figure 23. It aims to demonstrate the damping efficiency of the ID boring bar in the range of $5 \leq L/D \leq 9$.

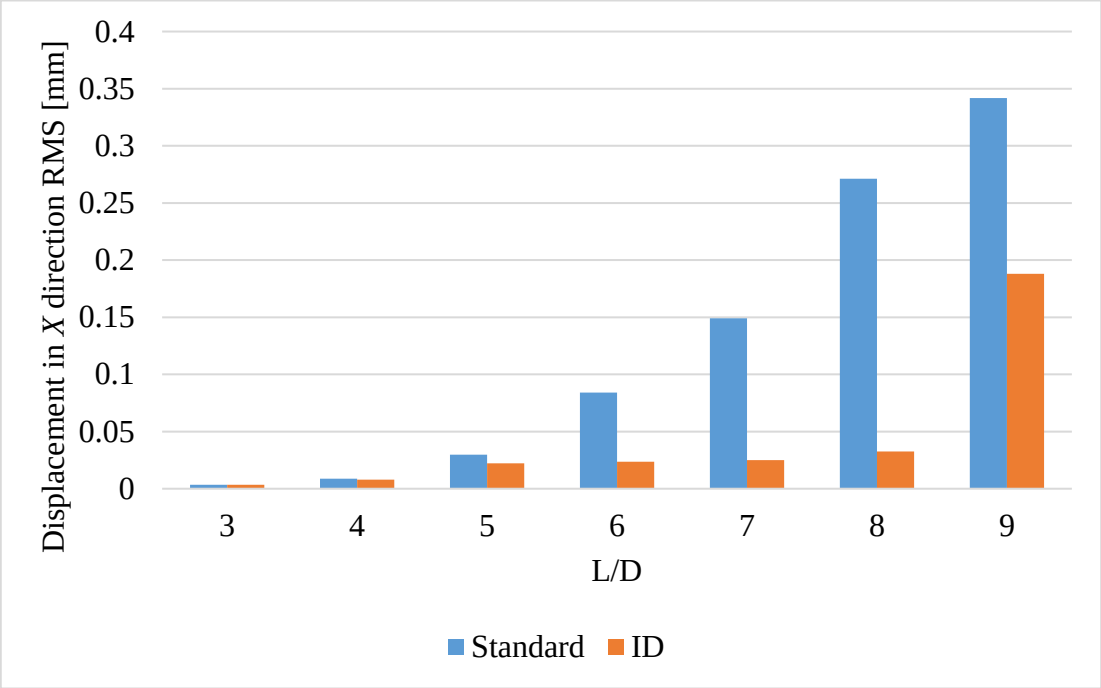

Figure 23. X_{rms} vs L/D for standard and ID boring bars when excitation force is F_0 = 1.78 N and Gap_0 = 0.33 mm

4.2.5 Parametric studies

In this section, we will examine the best design of an impact damper boring bar with *L/D = 7*, as analyzed in Section 4.2.4. We will use the same clamping system parameters as before in Section 3.2, where the Winkler foundation modulus, mode shape, damping ratio, and eigenfrequencies are constants. To ensure that the dimensions of the cavity are within the stiffness and mass limits [11], [109], [76], we will use $Gap_0 = 0.33$ mm multipliers of *0.25, 0.5, 0.75, 1.0, 1.25, 1.50, 1.75,* and *2*. Similarly, we will multiply the amplitude of the excitation force $F_0 = 1.78$ N with coefficients of *0.25, 0.5, 0.75, 1, 1.25, 1.5, 1.75, 2, 3,* and *4*.

We will determine the peak values of X_{RMS} for the range of clearance gaps and excitation forces mentioned above. Figure 24 and Figure 25 provide a couple of examples of how the peak values were obtained for different forces and gaps, respectively. By taking all the results for the peak of the above ranges of clearance gaps and excitation forces, we obtained a map graph shown in Figure 26. The smallest average peak amplitudes were found within the gap interval of *0.30* mm to *0.60* mm, which means that the tool used in the experiments is within this range. Meanwhile, the excitation force amplitude can be up to *2.5* N.

To explore this further, we took vertical sections of the map graph shown in Figure 26 at $1F_0$, $1.5F_0$, and $2F_0$, which provide the functions of X_{RMS} versus gap shown in Figure 27. Similarly, we took horizontal sections at $0.25Gap_0$, $1Gap_0$, and $2Gap_0$, which provide the functions of the X_{RMS} versus force shown in Figure 27. Figure 27(a) shows that very small vibration amplitudes were

DOI: 10.14750/ME.2023.032

obtained for a clearance gap of *0.33* mm up to the excitation force of *2* N. Figure 27(b) displays that when the excitation force is $F_0 = 1.78$ N, the displacement amplitude is very small when the clearance gap is within the interval of *0.33* mm and *0.66* mm.

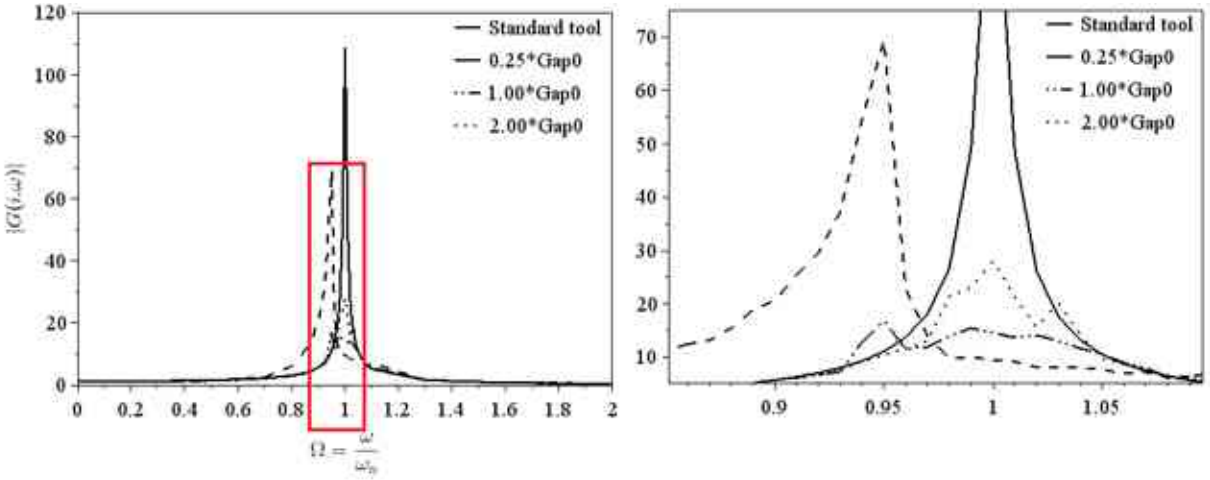

Figure 24. FRF curve to different forces when L/D = 7

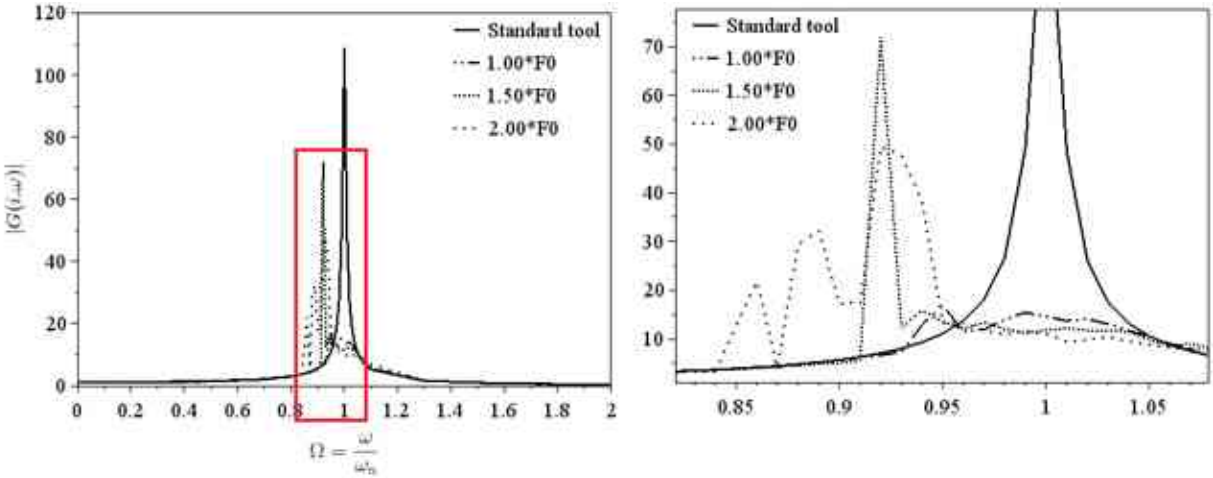

Figure 25. FRF curve to different clearance gaps when L/D = 7

DOI: 10.14750/ME.2023.032

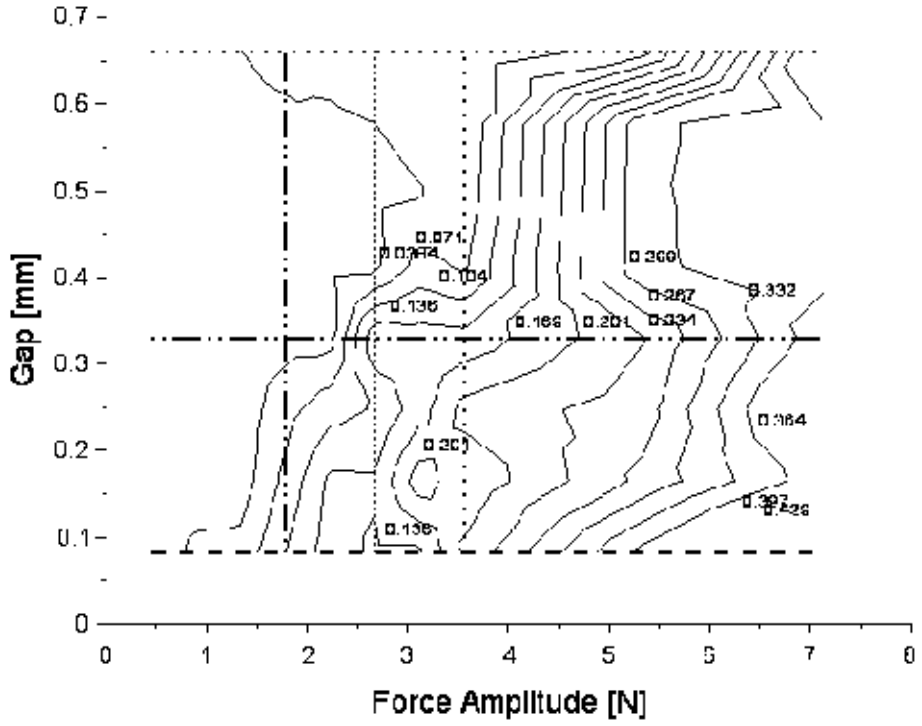

Figure 26. X_{rms} of the tool over different excitation forces and total clearance gaps when L/D = 7

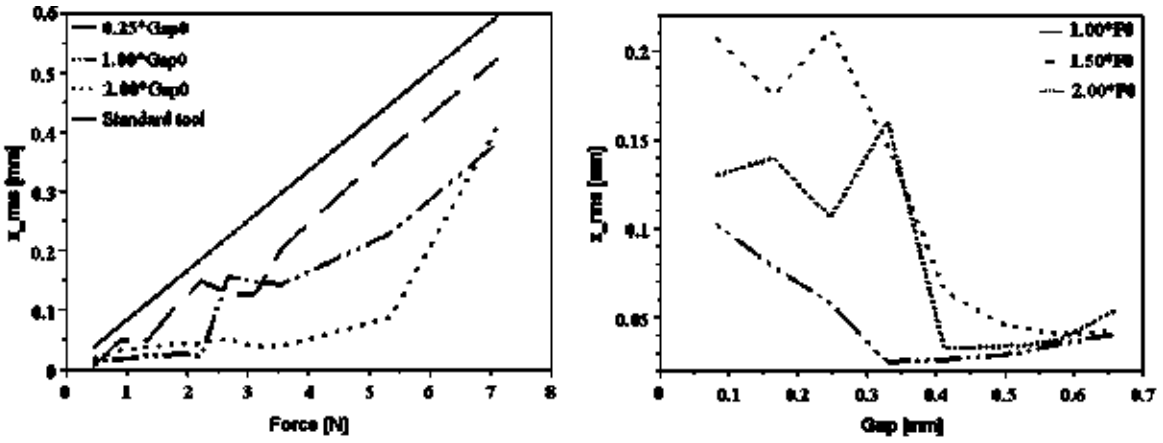

(a) (b)

Figure 27. Displacement (RMS) of the tool over different clearance gaps (a) and excitation forces (b) for L/D = 7

The damping ratio can also increase depending on the number of balls inside the tool cavity. Figure 28 shows that for more than *2* balls the damping ratio is always higher than for *1* ball. For each *L/D* a precise analysis should be made to check the necessary number of balls to reach the highest damping ratio. As an example, in Figure 28, the best scenario is nine balls inside the cavity to reach a maximum damping ratio equal to *0.032*. For that, the *9* balls should be allocated along the cavity starting from the tip of the tool and blocked by the adjusting screw as represented in Figure 5(b) in Section 3.2.

DOI: 10.14750/ME.2023.032

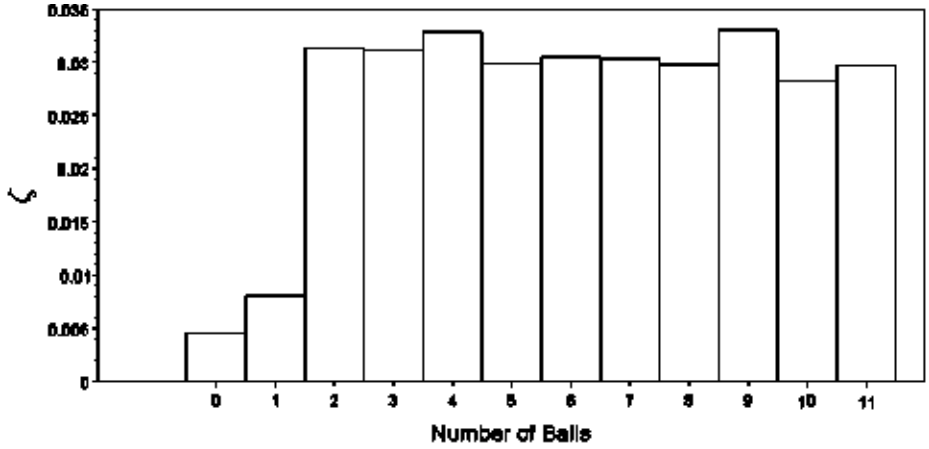

Figure 28. The damping ratio of the tool over different numbers of balls along the tool with constants values of force F_0 = 1.78 N, total Gap_0 = 0.33 mm and L/D = 7

After selecting the appropriate number of balls in Figure 28, Table 10 displays the best configuration for the ID tool with a clearance gap of *0.33* mm and excitation force of *1.78* N, which achieves the highest possible damping ratio. The analysis shows that an impact damper can be improved, where for *L/D = 7, 9* balls can achieve a Lehr damping of 0.*03303* after the parametric study (ζ_{ipID}), and *11* balls can achieve a Lehr damping of *0.02963* before the parametric study (ζ_{iID}).

Table 10. Comparison of the highest Lehr damping in an ID boring bar before (ζ_{iID}) and after (ζ_{ipID}) the parametric study for different overhangs when excitation force is F_0 = 1.78 N and Gap_0 = 0.33 mm

L/D	**N° of the ball**	ζ_{ipID}	**N° of the ball**	ζ_{iID}	ζ_{ipID}/ζ_{iID}
3	*1*	*0.24364*	*3*	*0.0241*	*1.01*
4	*4*	*0.024047*	*5*	*0.0210*	*1.15*
5	*3*	*0.015403*	*7*	*0.0129*	*1.20*
6	*3*	*0.023238*	*9*	*0.0193*	*1.20*
7	***9***	***0.03303***	***11***	***0.02963***	***1.12***
8	*11*	*0.03102*	*13*	*0.02980*	*1.04*
9	*11*	*0.008804*	*15*	*0.00714*	*1.23*

Similarly, the results of Table 11 demonstrate the highest damping ratio for different overhangs by considering various clearance gap and force multipliers. The advantage of using Table 11 is that it can help in the production of an appropriate ID tool for achieving the highest damping ratio.

DOI: 10.14750/ME.2023.032

Table 11. Comparison of the highest Lehr damping in an ID boring bar before (ζ_{iID}) and after (ζ_{ipID}) the parametric study for different overhangs, gaps multipliers and forces multipliers

L/D	Gap Multiplier	Force Multiplier	N° of the ball	ζ_{ipID}	N° of the ball	ζ_{iID}	ζ_{ipID} / ζ_{iID}
3	0.25	2.00	3	0.026696	3	0.0241	1.11
4	0.25	1.00	5	0.025049	5	0.0210	1.19
5	1.00	1.00	3	0.015403	7	0.0129	1.20
6	0.75	2.00	3	0.029043	9	0.0193	1.50
7	**1.00**	**1.00**	**9**	**0.03303**	**11**	**0.02963**	**1.12**
8	1.00	1.00	11	0.03102	13	0.02980	1.04
9	1.50	0.25	14	0.017214	15	0.00714	2.41

Once the appropriate number of balls, clearance gap multiplier, and force multiplier are selected to achieve the highest damping ratio, it is possible to plot Figure 29, which illustrates the (SLD) for *L/D = 7*. Based on this information, the cutting parameters can be reprogrammed to improve the performance of the tool and enhance the production process.

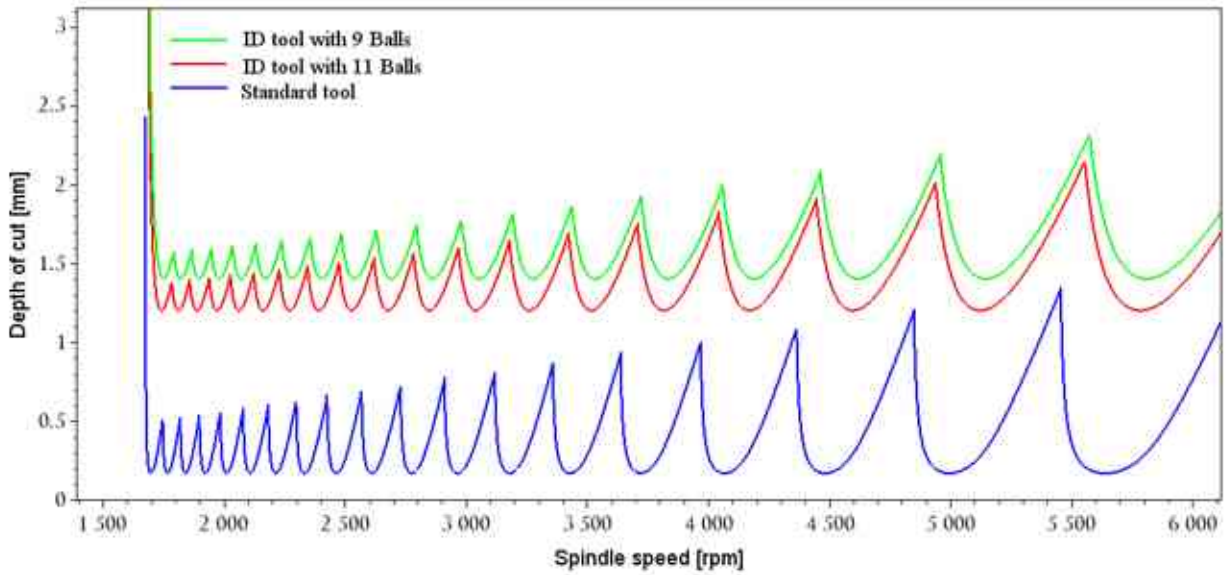

Figure 29. Stability lobe diagram for a standard boring bar, an ID boring bar with 9 balls, and an ID boring bar with 11 balls, with Gap_0 = 0.33mm, excitation force F_0 = 1.78 N, and L/D = 7

4.2.6 Experimental studies

In this section, the measurements of the standard and ID bar are performed. The impact of roughness profile and cylindricity profile on stable and unstable vibration conditions during internal turning operations in hardened materials is investigated. The aim is to determine the highest overhang possible in a stable condition and to validate the theoretical data for the previous sections. For that reason, an accelerometer was positioned to measure vibration in the radial direction in order to collect the vibration amplitudes. Thus, the stable and unstable limits were settled to different overhangs and tested at the same cutting conditions of $v_c = 360$ m/min, $f = 0.14$ mm and $a_p = 0.1$ mm.

DOI: 10.14750/ME.2023.032

Figure 30 shows the excitation frequencies generated by cutting the standard and ID boring bar at different tool overhangs. It was observed that the excited vibration signals are widely distributed and have low acceleration amplitude, which is why the highest harmonic value was sought in each overhang during the cutting process.

Analyzing Figure 30(a), it is possible to notice that the frequency spectrum of the vibration generated by the standard bar presented a dominant frequency range, with distinct values of excitation amplitude between stable and unstable cutting, and the stable cutting being much larger than the unstable cutting. On the other hand, in Figure 30(b), when using the ID bar, although there is a frequency range with higher amplitude than other frequency ranges, it is not as higher as in the standard bar. This is probably due to the detection of impacts of the balls with the cavity wall of the tool at various frequencies, generating a more distributed vibration signal.

Furthermore, when comparing the amplitude values of the tool in stable cutting between the standanrd bar and the ID bar, it is possible to observe that the ID bar has a much lower excitation amplitude than the standard bar, by approximately *6* times peak to peak, as shown in Figure 30. It is important to note that, despite the tool (both standard and ID bars) mainly vibrating at its natural frequency, this does not generate instability in the process.

Finally, it is possible to explain that the ID boring bar generates a more distributed vibration signal due to the damping system of the tool. This damping occurs due to the interaction of the balls with the cavity wall, dissipating part of the mechanical energy of the tool. As a result, the vibration amplitude is reduced, and the spectral distribution is more uniform in relation to the standard bar, which does not have damping. This leads to an excitation amplitude of the FFT signals with higher values in the standard bar compared to the ID boring bar.

DOI: 10.14750/ME.2023.032

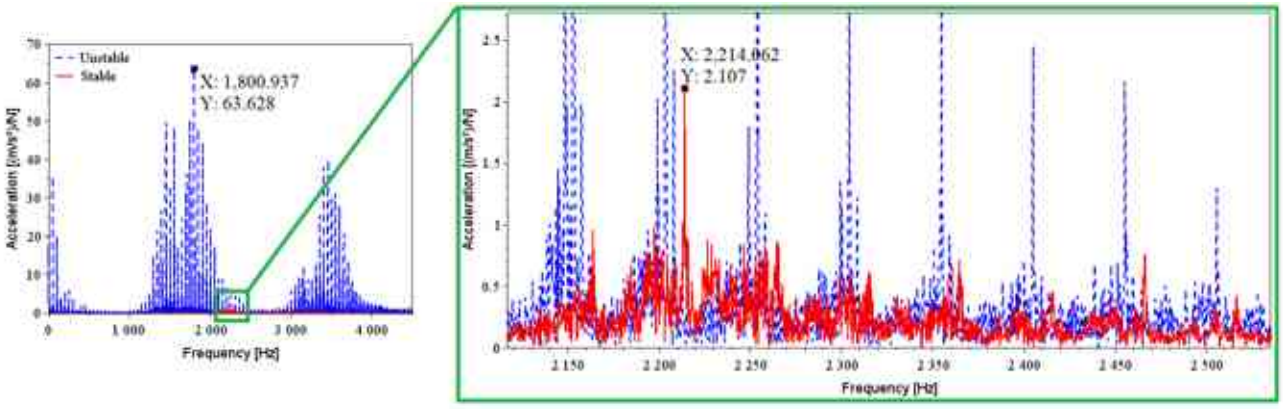

(a)

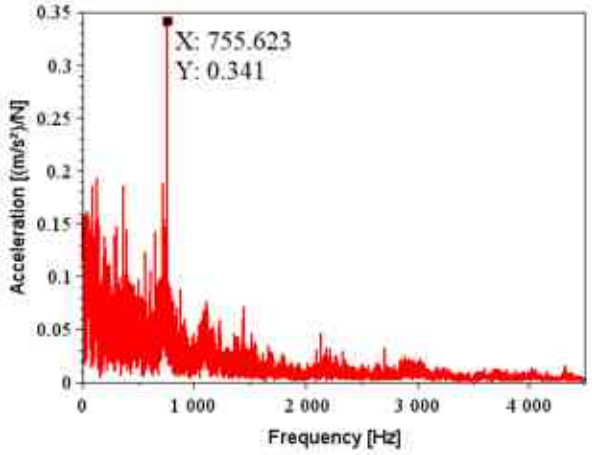

(b)

Figure 30. Excitation signal FFT obtained experimentally for (a) stable L/D = 4 and unstable L/D = 5 with standard boring bar (b) stable L/D = 7 with ID boring bar

The feed rate, depth of cut, and tip radius of the tool, which determine the theoretical roughness of the part, were kept constant during the tests, and vibration was observed. The static stiffness of the toolbar was found to be the main factor affecting the stability of the machining process, and its influence was tested at different overhangs.

The stability of the machine-tool-workpiece system was found to have a significant impact on the surface finish, regardless of the cutting conditions. The limits of *L/D* ratio that caused an abrupt increase in roughness for both the standard and ID boring bar were attributed to the low stability of the system, which made longer overhangs unfeasible. The irregular roughness profile observed in Figure 31(b) and Figure 33(b) was attributed to the instability of the tool due to low static stiffness in long overhangs, as shown in Figure 31 and Figure 33. This instability caused deflection that interfered with the circularity profile of the turned workpiece, as observed in Figure 32 and Figure 34.

Radial movement of the tool was found to influence both the roughness and geometric tolerance of the workpiece, irrespective of the tool type. As the overhang increased, form errors fluctuated, and exceeding the tool stability limit caused premature breakage of the insert, generating an

DOI: 10.14750/ME.2023.032

irregular geometric error as illustrated in Figure 32(c)(d) and Figure 34(c)(d). This impairment of interchangeability of parts can be avoided by adjusting the tool clamp to the smallest possible overhang (*L/D = 3*) or by implementing damping systems in the boring bar, as recommended by Thomas et al. [20] and other researchers.

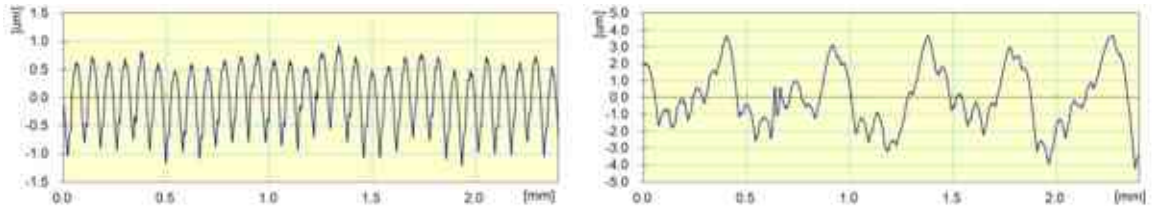

(a) (b)

Figure 31. Roughness profile of the workpiece when cutting with a standard boring bar: (a) in stable conditions at L/D = 4; (b) in unstable conditions at L/D = 5

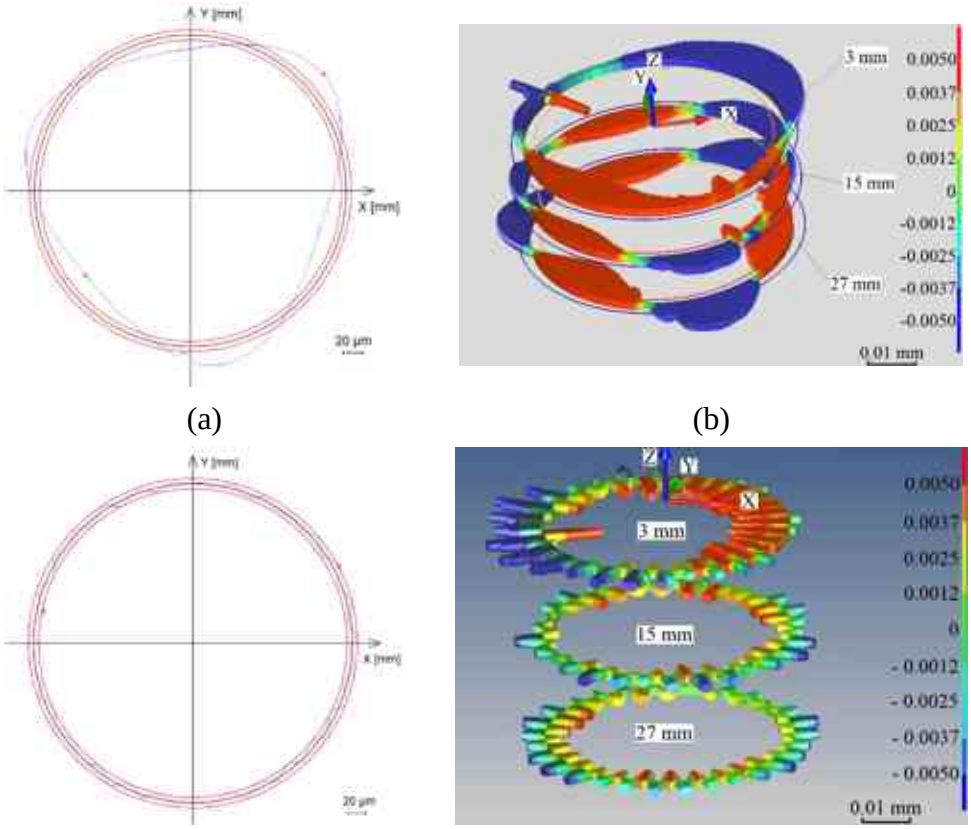

(a) (b)

(c) (d)

Figure 32. Circularity profile of the workpiece when cutting with a standard boring bar: (a) in stable condition in 2D and section 15 mm; (b) in stable condition in 3D at L/D = 4; (c) unstable condition in 2D and section 15 mm; (d) unstable condition in 3D at L/D = 5

DOI: 10.14750/ME.2023.032

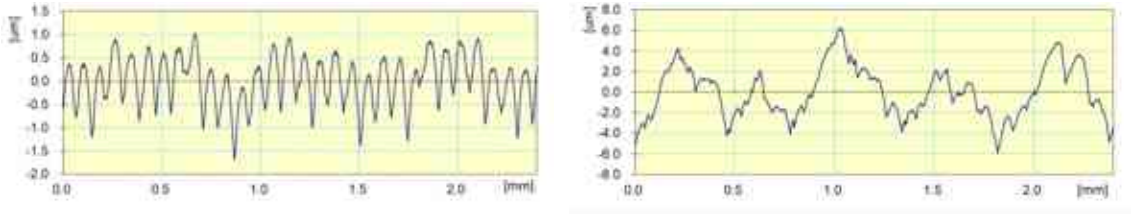

(a) (b)

Figure 33. Roughness profile of the workpiece when cutting with a ID boring bar: (a) in stable conditions at L/D = 7; (b) in unstable conditions at L/D = 9

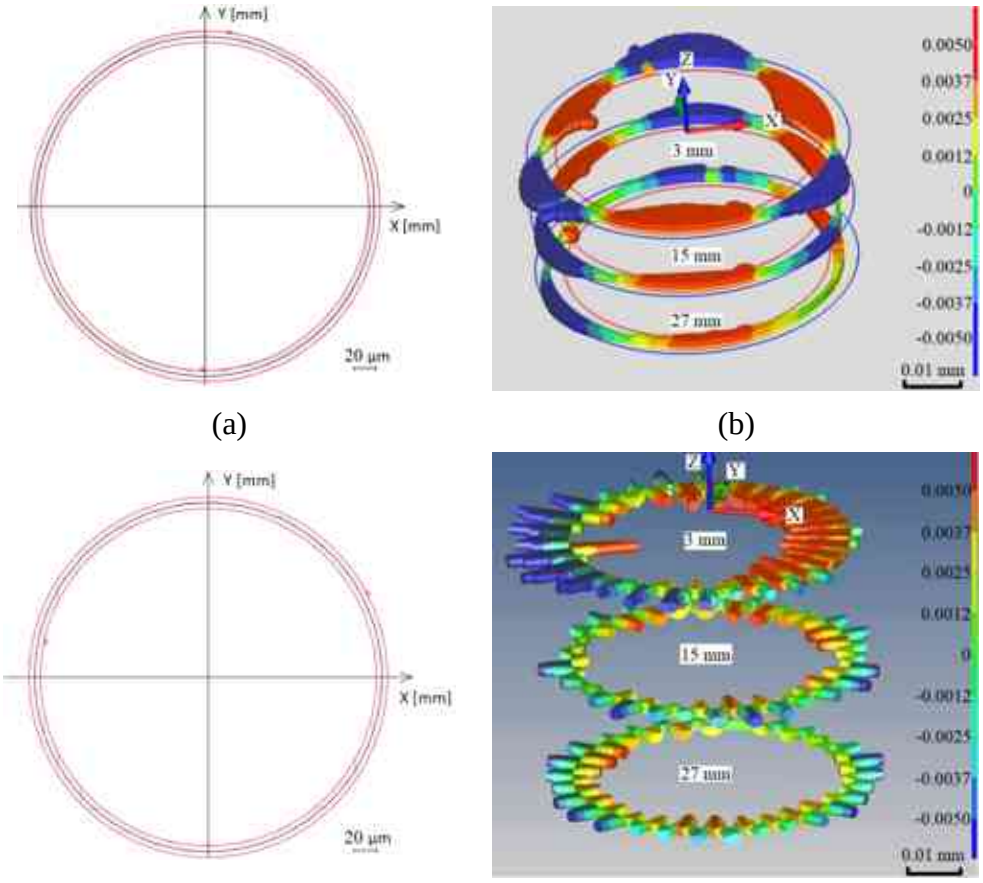

(a) (b)

(c) (d)

Figure 34. Circularity profile of the workpiece when cutting with a ID bar: (a) in stable condition in 2D and section 15 mm; (b) in stable condition in 3D at L/D = 7; (c) unstable condition in 2D and section 15 mm; (d) unstable condition in 3D at L/D = 9

To evaluate each experiment, the following postulates were constructed:

(1) The turning process was stable: No vibration marks were visible on the workpiece's surface, and at the same time, the value of the arithmetic average roughness (R_a) was less than *0.8* µm (see Figure 35(a)).

(2) The turning process was unstable: There were visible signs of chatter on the surface of the workpiece, and at the same time, the value of the arithmetic average roughness (R_a) was greater

DOI: 10.14750/ME.2023.032

than *0.8* μm. Tool marks on the surface of the workpiece (internal hole) during an unstable turning process can be observed in Figure 35(b).

We observed that when the value of the arithmetic average roughness (R_a) was greater than *0.8* μm, the chatter marks of Figure 35(b) started to appear in the workpiece. The chatter marks are a collection of analyzed factors, where the highlighted main points are the long overhangs that cause a decrease in dynamic stiffness. Therefore, there is an increase in the tool's deflection as a result of higher displacement amplitudes at the tip of the tool, and similarly, there are higher amplitudes in the roughness and circularity profile.

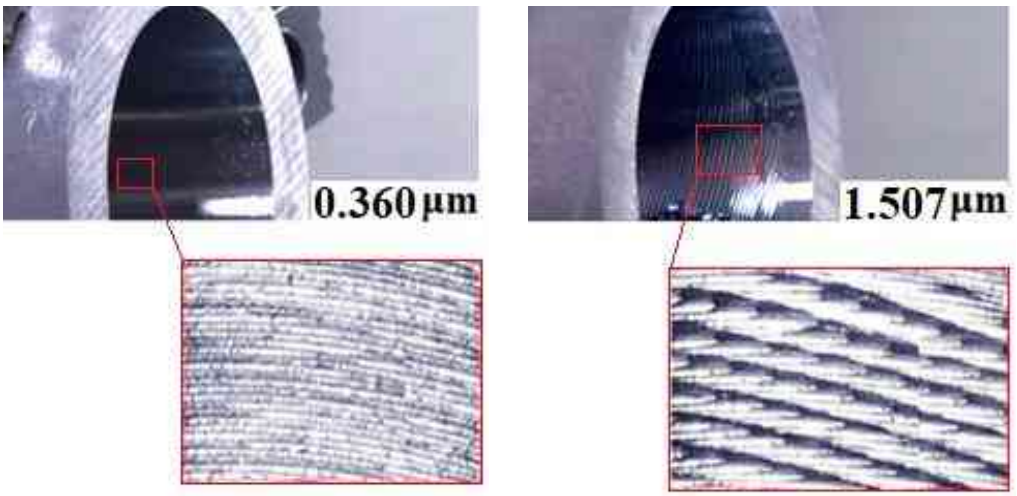

(a) (b)

Figure 35. Arithmetic average roughness (Ra) for the workpiece when cutting with a standard boring bar in (a) stable condition L/D = 4 and (b) unstable condition L/D = 5

Table 12 summarizes the results of surface roughness measurements when machining different types of holders at different *L/D* ratio. It can be observed in Table 12 that there are limits to the tool's working range in stable and unstable modes. It is clear that all tools can retain similar roughness and acceleration amplitudes until their overhang is limited in the stable regime; on the other hand, in the unstable regime, roughness and the acceleration amplitude are high and produce substantial fluctuations among the values; this is typical chatter behavior.

Table 12 is an important reference for guiding the selection of tools for an internal turning operation. It describes the exact overhang limits for tools with different structural configurations and dynamic properties. If we assume that short overhangs are up to *5* and over, this limit is a long overhang, and we can conclude that the best choice for operations with long holes comprises ID boring bars with a maximum *L/D* equal to *8*. This proves the efficiency of the damper mechanisms of the multiple numbers of balls inside the cavity of the ID tool that can minimize the vibration amplitude of the tool during internal turning operations with respect to hardened materials. Another point to be mentioned is that when Table 3 and Table 12 are compared, the damping efficiency of the ID with respect to forced vibrations (during cutting) is superior compared to the standard boring bar in free vibration conditions. This can be explained by the dynamics of the bouncing balls as the excitation amplitude increases and more balls are activated within the cavity to decrease the tool's vibration amplitude. When a ball is actively participating in the suppression of a tool's vibration, it performs an approximately circular motion in the cavity. In other words,

DOI: 10.14750/ME.2023.032

the ball is not spinning purely on the wall of the cavity but bounces over it as it moves along a non-smooth circular path.

Table 12. Average values of roughness (deviation ± 0.02 mm) in longitudinal direction and acceleration amplitude (deviation ± 0.1 m/s²) of the tip of the tool

Tool Type	***L/D***	**Stability**	**R_a [µm]**	**R_z [µm]**	**RMS [m/s^2]**
standard	*< 4.5*	Stable	*0.360*	*1.860*	*16.189*
	≥ 4.5	Unstable	*1.507*	*7.002*	*347.795*
ID	*≤ 8*	Stable	*0.460*	*2.249*	*2.318*
	> 8	Unstable	*1.820*	*8.000*	*2.318*

Figure 36 and Figure 37 show the experimental results of the acceleration signal that were processed relative to velocity and displacement in the time domain for the unstable and stable cutting conditions of all tools. Table 12 and the excitation signals shown in Figure 36 and Figure 37 are a set of data that illustrate the vibration amplitude achieved by different boring bars in stable overhangs. It is possible, therefore, to observe that the signals are periodic, and even in the time range of *0.20* s, the behaviour of the signal is repeated throughout all tests.

The shape of the signal is complex and does not follow a pattern, but the main analysis was based on the amplitude of the displacement signal for each tool. The unstable amplitudes of standard boring bar (RMS acceleration amplitude higher than *300* m/s^2) are substantially higher compared to the stable ones (RMS acceleration amplitude lower than *50* m/s^2), except for the ID bar that did not show significant amplitudes relative to the long overhangs (RMS acceleration amplitude lower than *3* m/s^2); because of this, there are no unstable signals in Figure 37.

For the cutting operation, the analysis demonstrated that the frequency of the tool at $\omega_i = 725.15$ Hz caused higher amplitudes for the standard than ID boring bar for both maximum overhangs. In contrast, in stable conditions, the resultant roughness values follow the same behaviour of the displacement of the tip; when the roughness values are under *0.8* µm, the tools were stable contrary to the roughness values, and this limited their instability during the cutting process.

The operational range of the ID is higher than the standard boring bar, which makes the tool more flexible for cutting long and short overhangs; this avoids the need to change the tool during the process and saves time by limiting the changes made to the tool's setup.

DOI: 10.14750/ME.2023.032

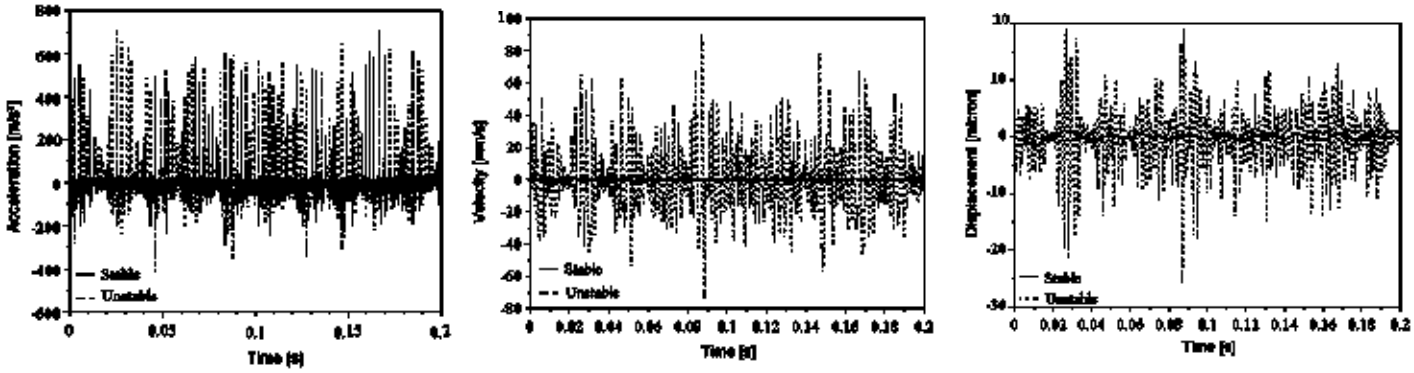

(**a**) (**b**) (**c**)

Figure 36. Excitation signal obtained experimentally (a) acceleration, (b) velocity and (c) acceleration for stable L/D = 4 and unstable L/D = 5 with standard boring bar

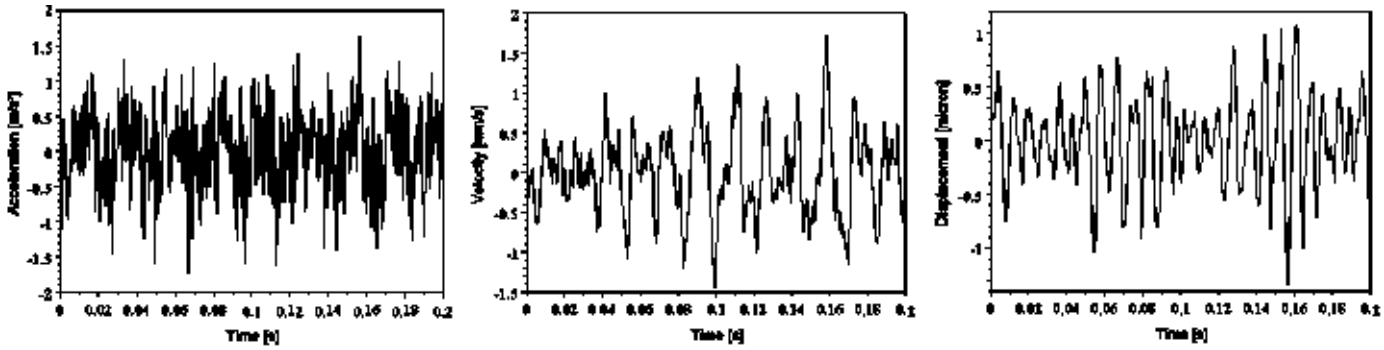

(**a**) (**b**) (**c**)

Figure 37. Excitation signal obtained experimentally (a) acceleration, (b) velocity and (c) acceleration for stable L/D = 7 with ID boring bar

It is possible to verify that among all the bars tested, the acceleration amplitudes in the stable cutting regime are similar. It is important to remember that the variables that cause excitation at the tool's tip are, in general, the dynamic parameters of the tool, which are completely dependent on time. Therefore, to reduce the vibration amplitude of the system, it was necessary to modify the inertial and elastic conditions of the tool. These modifications may cause an increase in the damping capacity due to the balls (ID bar). In this manner, the vibrational energy produced by the harmonic movement of the tool is significantly reduced, and the vibration spectrum becomes smoother [1].

Using the ID boring bar—where the total length of the tool was out of the clamp system—with an overhang limit *L/D = 9*, no abrupt increase in the acceleration signal was detected. However, for this condition, roughness increased abruptly when the bar exceeded *L/D = 8*, where the unstable regime was present. The most accepted hypothesis for explaining how roughness grew significantly without growth in acceleration comes from the vibration theory: for simple harmonic motions, acceleration is proportional to the displacement amplitude, and it is proportional to the square of the frequency. In that case, the acceleration amplitudes can be equal for short and long overhangs, as it was experimentally experienced, but the displacement amplitudes exhibit a different behaviour because of their different natural frequencies. Hereafter, one can conclude that the ratio of the roughness is reciprocally proportional to the ratio of the square of the natural frequency of the tool.

DOI: 10.14750/ME.2023.032

After analyzing both the numerical results and experimental tests, it was found that the damping ratio played a crucial role in determining the stability of the tool during cutting. Remarkably, there was a close correspondence between the numerical and experimental results in terms of the damping ratios obtained. The numerical calculations showed that the damping ratio increased up to a maximum value at $L/D = 8$, beyond which it started decreasing. Similarly, in the experiments, the stability limit of the ID bar was observed to be at $L/D = 8$, beyond which the cutting was unstable. This can be attributed to the clearance gap, which has a range of frequency that allows for the highest possible damping ratio of the tool. It is also dependent on the excitation force and cutting conditions employed during the internal turning operation. In the numerical study, a damping ratio of *0.0298* (see Table 9) was achieved for $L/D = 8$ with $Gap_0 = 1$ and $F_0 = 1$. It is worth noting that the highest damping ratio found in the numerical results was also found in the experimental tests during cutting process, highlighting the importance of numerical simulations in predicting the stability of machining processes.

It is also important to observe that comparing the damping ratio obtained in the of the numerical simulation already mentioned and the impact test with a damping ratio of *0.0033* (see Table 3), it is possible to affirm that the damping ratio in forced vibration increased more than 9 times when compared to forced vibration. It is essential to remember that the variables that cause excitation at the tooltip are generally the tool's dynamic parameters totally dependent on time. Therefore, to reduce the vibration amplitude of the system, it was necessary to interfere with the inertial and elastic conditions of the tool. These modifications caused an increase in the damping capacity due to the cavity dimensions ($Ø\ 8.33 \times 180$ mm) and also the $Ø\ 8$ mm balls inside. In this way, the flow of vibrational energy generated by the tool's harmonic movement is significantly reduced. The energy flow contours of the vibration spectrum become smoother since the kinetic energy dissipation of the bar is reduced by rapidly transferring linear momentum from the balls in a combination of multiple inelastic collisions, friction between balls, and between balls and cavity walls to achieve damping. It is enough to observe the equation of the total mechanical energy of simple harmonic motion, which establishes that the energy of vibration is proportional to the square of the amplitude of oscillation, given a conservative system (constant mechanical energy). By demonstrating the practical advantages of the impact damper tool in the metal cutting industry and providing guidance for its optimal use in real cutting operations, this study aims to enhance the use of the tool in practical applications.

DOI: 10.14750/ME.2023.032

5. THESES – NEW SCIENTIFIC RESULTS

T1. A) A novel multi-span boring bar model was proposed based on the Euler-Bernoulli beam theory. The bar is partially supported by a Winkler foundation of constant stiffness that represents the clamping of the tool. Numerical evaluation of the model was carried out, paying attention to the modal parameters for various overhangs, or length-to-diameter (*L/D*) ratios. The selected typical *L/D = 3...9* geometries are commercially used by the industry. Analysis results revealed how the mechanical properties, like mode shapes, Lehr damping, natural frequencies, dynamic and static stiffness depend on the overhang.

T1. B) The stiffness of the clamping mechanism has a significant impact on the natural frequencies of the boring bar and influences its mode shapes also. Using a trial-and-error method, the preferable Winkler foundation stiffness was determined to be $k = 1.0 \times 10^{11}$ N/m, which was found to operate the ID and standard boring bar for all studied overhangs. The analytical model shows excellent accuracy with experiments in long overhangs, with a maximum absolute error of less than 3%.

T2. A) A novel non-linear viscoelastic model was proposed to calculate the contact force of the impact damper (ID) bar by incorporating a damping coefficient and contact stiffness based on the Hertz theory. This model is also effective in calculating the contact force and is highly sensitive to variations in the clearance gap between the cavity wall of the tool and the balls within. The investigation presented uses a novel approach to model the damping mechanism of the ID bar. It is noted that not all balls within the cavity have the same efficiency as regard the damping. The trajectory of a ball depends on multiple factors such as clearance gap, excitation force and the location of the ball, i.e., distance from the tip. The balls near the tip of the tool have greater displacements compared to those close to the Winkler-type foundation.

T2. B) In forced vibration, the damping capacity of the balls is activated, leading to a significant decrease in the tool's vibration amplitude. For given clearance gap, excitation force, and first eigenfrequency of the tool, it can be observed that the ID boring bar reduces the frequency response peak by up to *85*% meaning a *6.4* times higher damping ratio than a standard tool.

T2. C) The damping ratio is improved depending on the number of balls within the tool cavity. For more than two balls, the damping ratio is consistently higher than for a single ball. Parametric studies proved that more balls do not necessarily mean better Lehr damping. With the technique developed, a map graph was drawn to select the highest damping ratio in terms of clearance gap multiplier and force multiplier. This makes it possible to plot of the stability lobe diagram (SLD) for different overhangs.

T3. A) There is a close correspondence between the numerical and experimental results regarding the obtained damping ratios. Both methods confirmed that the stability limit of the ID bar is *L/D = 8*. The ID boring bar can operate in a frequency range up to two times broader than a

DOI: 10.14750/ME.2023.032

standard tool. Additionally, it can operate in a higher range of overhang in stable cutting ($L/D \leq 8$) than a standard tool ($L/D < 4.5$). When using both ID and standard bars at the limit of their stability, the ID bar exhibits a lower excitation amplitude than the standard bar, by approximately six times peak to peak.

T3 B) The irregular roughness and circularity profile in the experiments is attributed to the instability of the tool due to low static stiffness in long overhangs. It was observed that when the value of the arithmetic average roughness was greater than 0.8 μm, chatter marks started to appear in the workpiece. The unstable amplitudes of the standard boring bar (RMS acceleration amplitude > 300 m/s^2) were substantially higher compared to the stable ones (RMS acceleration amplitude < 50 m/s^2), except for the ID bar that did not show significant amplitudes relative to the long overhangs (RMS acceleration amplitude < 3 m/s^2).

DOI: 10.14750/ME.2023.032

6. SUMMARY

This work focuses on investigating the stability of internal turning operation using the ID boring bar, the dynamic properties of the tool and clamping system. The study starts with a review of relevant literature on the ID boring bar and its effect on metal cutting stability. This includes a discussion on the current techniques used to avoid chatter, such as active, passive, and hybrid dampers.

To address the dynamic problem of the ID boring bar, the methodology used in this work is formulated mathematically and investigated experimentally. The results of the dynamical behaviour of the ID boring bar are compared to a standard tool in both free and forced vibrations. In free vibration, an analytical mathematical model is proposed and calculated to define the natural frequencies of the tool and corresponding mode shapes. Additionally, the dynamic properties of the tools are experimentally tested, including the natural frequency, damping ratio, and static stiffness.

In forced vibration, the equation of motion is set up and analyzed using a series of numerical computations to understand the behaviour of the balls inside the cavity and the damping capacity of the tool for different forces, clearance gaps, and overhangs. After parametric studies, many experiments are performed to validate the results in terms of stability, roughness, cylindricity, and vibration measurements.

Finally, the new scientific results obtained from this study are highlighted to emphasize the novelty of the thesis, including the relevant references used throughout the work. Overall, this work presents a detailed investigation into the ID boring bar and its impact on metal cutting stability, and provides valuable insights into the dynamic properties of the tool and its effectiveness in minimizing chatter.

DOI: 10.14750/ME.2023.032

ACKNOWLEDGEMENTS

This work would not have been possible without the invaluable support and contributions of several individuals, to whom I extend my deepest gratitude:
First and foremost, I express my gratitude to God for granting me the gift of life, good health, and wisdom to carry out this work.
I would like to extend my special thanks to my family for their constant love, support, and patience throughout my journey.
I am deeply grateful to my advisor, Dr. László Péter Kiss, for sharing his knowledge, guidance, and expertise, which have helped me to become a more competent and responsible researcher. I also appreciate his understanding and cooperation during the PhD program.
I would like to thank Dr. Tamás Szabó for his collaboration on this work and for his valuable guidance along with my advisor.
I am indebted to Professor and friend Dr. Jozef Peterka, Dr. Rouben Rostamian, Dr. Anselmo Eduardo Diniz, and my friend Marcos Vieira de Albuquerque for their collaboration and valuable discussions during my PhD program.
I express my gratitude to the SENAI SP Faculty and University of Campinas in Brazil, as well as MTF STU in Slovakia for their partnership with the University of Miskolc.
I am deeply grateful to Dr. Rónai László for his indispensable assistance.
I would like to thank my friends from University of Miskolc, SENAI SP Faculty, University of Campinas, and MTF STU, including Zsombor Fülöp, Fábio Kuranaka, Marcus Begossi, Alex Payao, Daniel Suyama, Antonio Cazzani, Sebastian Cabezas, Messaoudi Abderrazek, Al-zgoul Mohammad, Okhunjon Sayfidinov, Baibhaw Kumar Singh, Jamal Karmoua, Raid Meknassi, Yasser Dakhel, Mahmoud Saleh, Flora, Abel, Lucas Alexandre, Matheus Nobre, Guilherme Hollo, Verônica Mandelli Grasselli, Amal Zarrami, Chaima Sayari, Houssèm Bahbah, Jakub Hrbál, Tomas Vopat, Róbert Straka, and Marian Nemeth, for their support and encouragement.
Lastly, I would like to express my appreciation to all those who contributed to this work in some way and whom I may have inadvertently forgotten to mention due to carelessness.
I would also like to dedicate this work to the memory of my supervisor, Dr. Attila Szilágyi, and my grandmother Cleuza Alves Pereira da Silva, who supported me throughout my PhD journey.
To all of you, I extend my sincere thanks and gratitude.

DOI: 10.14750/ME.2023.032

REFERENCES

[1] Pereira, A. G. Piezoelectric shunt application for passive chatter control in the alloy Ti-6Al-4V turning process. (In Portuguese). Master dissertation. UFSCAR, Sao Carlos, Brazil. 2022.

[2] Ma, H. Wu, J. and Yang, L. and Xiong, Z. Active chatter suppression with displacement-only measurement in turning process. Journal of Sound and Vibration. Elsevier Ltd. v. 401, p. 255–267. ISSN 10958568. 2017. DOI: 10.1016/j.jsv.2017.05.009.

[3] Altintas, Y. Manufacturing automation: metal cutting mechanics, machine tool vibrations, and CNC design. 2nd edition. ed. [S.I.]: Cambridge University Press. 365 p. ISSN 17410509. ISBN 9780521172479. 2012.

[4] Saciotto, V.R. and Diniz, A.E. An experimental evaluation of particle impact dampers applied on the tool for milling of hardened steel complex surface. The International Journal of Advanced Manufacturing Technology. 119. 7579–7597. 2022. DOI: 10.1007/s00170-022-08782-4

[5] Quintana, G. and Ciurana, J. Chatter in machining processes: A review. International Journal of Machine Tools and Manufacture, v. 51, n. 5, p. 363–376. 2011. DOI: 10.1016/j.ijmachtools.2011.01.001.

[6] Urbanski, J.P., Koshy, P., Dewes, R.C. and Aspinwall, D.K. High speed machining of moulds and dies for net shape manufacture. Materials & Design, v. 21, n. 4, p. 395–402. 2000. DOI: 10.1016/S0261-3069(99)00092-8.

[7] Munoa, J., Beudaert, X., Dombovari, Z., Altintas, Y., E. Budak, Brecher, C., Stepan, G. Chatter suppression techniques in metal cutting. CIRP Annals - Manufacturing Technology, CIRP, v. 65, n. 2, p. 785–808, ISSN 17260604. 2016. DOI: 10.1016/j.cirp.2016.06.004.

[8] Prasad, B. B., Duvigneau, F., Woschke, E. and Juhre, D. Wind turbine blade and generator test specimen for evaluating a passive vibration reduction concept based on granular materials. In Proceedings of the ISMA. 2020.

[9] Wang, L., Cheng, T. H., Tang, X. D. and Qian. J. G. Vibration and Damping Analysis of Carbon Fiber Wind Turbine Blade with Viscoelastic Damping Treatment. In Advanced Materials Research, vol. 1008, pp. 192-196. Trans Tech Publications Ltd. 2014.

[10] Prasad, B. B., Duvigneau, F., Juhre, D., and Woschke, E. Damping performance of particle dampers with different granular materials and their mixtures. Applied Acoustics 200. 2022. DOI: 10.1016/j.apacoust.2022.109059.

[11] Thomas, W., Diniz, A. E., Pederiva, R., Suyama, D. I. and Marcos. V. A new type of impact damper with long overhangs in the internal turning of hardened materials. Procedia CIRP 82. 2019. DOI: 10.1016/j.procir.2019.04.147.

[12] Lawrance, G., P. Sam, P., Joshwa, D., Sharvilin, S., Sudarsan, K., and Arun, R. Effect of particle damper technique on tribological properties during hard turning process. Materials Today: Proceedings 49. 2022. DOI: 10.1016/j.matpr.2021.06.372.

[13] Diniz, A.E., da Silva, W.T.A., Suyama, D.I. Evaluating the use of a new type of impact damper for internal turning tool bar in deep holes. The International Journal of Advanced Manufacturing Technology. 101, 1375–1390. 2019. DOI: 10.1007/s00170-018-3039-x

[14] Wu, D., Wang, X., and Yang, Y. Design and optimisation of a turning cutter embedded with impact damper. International Journal of Mechatronics and Manufacturing Systems 13, no. 3: 185-198. 2020. DOI: 10.1504/IJMMS.2020.111280.

[15] Peterka, J., De Silva, W. T., Straka, R., Vopát, T., Hrbál, J. and Kritikos, M. Analysis of form Error and Roughness of Hardened Steel Workpieces Internally Turned with Different Tools in Long Overhangs. Research Papers Faculty of Materials Science and Technology Slovak University of Technology 30, no. 50. 2022. DOI: 10.2478/rput-2022-0003

[16] Peterka, J., Martinovic, J., De Silva, W. T., and Kolesnyk, V. Analysis of Physical Causes of Machined Surfaces in Selected Machining Methods. MM Science Journal. 2022. DOI: 10.2507/33rd.daaam.proceedings.xxx.

[17] Zyl, D.V., Altintas, Y. and Ostling, D. Parametric design of boring bars with adaptive tuned mass dampers. CIRP Journal of Manufacturing Science and Technology 38. 2022. DOI: 10.1016/j.cirpj.2022.06.003

[18] Dogan, H. Investigation of Inerter-based Vibration Absorbers for Machining Chatter Stability. PhD dissertation. University of Sheffield. 2021.

[19] Hou, J., Niu, J., Y. Shen, Yang, S. and Zhang, W. Dynamic analysis and vibration control of two-degree-of-freedom boring bar with fractional-order model of magnetorheological fluid. Journal of Vibration and Control. 2021. DOI: 10.1177/10775463211023368.

[20] Thomas, W., Fulop, Z. and Szilágyi, A. Passive damping techniques for vibration suppression in boring operation with long overhangs. In Vehicle and Automotive Engineering, pp. 256-264. Springer, Singapore. 2020. DOI: 10.1007/978-981-15-9529-5_22.

[21] Sentyakov, K., Peterka, J., Smirnov, V., Bozek, P. and Sviatskii, V. Modeling of boring mandrel working process with vibration damper. Materials 13, no. 8. 2020. DOI: 10.3390/ma13081931.

[22] Yadav, A., Talaviya, D., Bansal, A., and Law, M.. Design of chatter-resistant damped boring bars using a receptance coupling approach. Journal of Manufacturing and Materials Processing 4, no. 2. 2020. DOI: 10.3390/jmmp4020053.

[23] Li, L., Sun, B., and Hua, H. Analysis of the vibration characteristics of a boring bar with a variable stiffness dynamic vibration absorber. Shock and Vibration. 2019. DOI: 10.1155/2019/5284194.

[24] Li, Lie, Beibei Sun, and Haitao Hua. Nonlinear system modeling and damping implementation of a boring bar. The International Journal of Advanced Manufacturing Technology 104, no. 1. 2019. DOI: 10.1007/s00170-019-03907-8

[25] Fallah, M., and Moetakef-Imani, B. Analytical prediction of stability lobes for passively damped boring bars. Journal of Mechanics 33, no. 5. 2017. DOI: 10.1017/jmech.2017.22.

[26] Sørby, K. Development and optimization of vibration-damped tool holders for high length-to-diameter boring operations. High Speed Mach 2. 2016. DOI: 10.1515/hsm-2016-0005.

[27] Moradi, H., Bakhtiari-Nejad, F., and Movahhedy, M. R. Tuneable vibration absorber design to suppress vibrations: an application in boring manufacturing process. Journal of Sound and Vibration 318, no. 1-2. 2008. DOI: 10.1016/j.jsv.2008.04.001.

[28] Silva, W. T. A. Uma contribuição ao uso de barras de tornear com amortecimento de impacto por esferas (In Portuguese). Master's Thesis, State University of Campinas, Campinas Brazil. 2017.

[29] Bartarya, G., and Choudhury, S. K. State of the art in hard turning. International Journal of Machine Tools and Manufacture 53, no. 1. 2012. DOI: 10.1016/j.ijmachtools.2011.08.019.

[30] Smith, G. T. Cutting Tool Technology: Industrial handbook. Southampton (UK): Springer-Verlag. 2008.

[31] Klocke, F., Krämer, A., Sangermann, H., and Lung, D. Thermo-mechanical tool load during high performance cutting of hard-to-cut materials. Procedia CIRP 1. 2012. DOI: 10.1016/j.procir.2012.04.053.

[32] Barry, J., Byrne, G. Cutting tool wear in the machining of hardened steels: Part I: Alumina/TiC cutting tool wear. Wear, v. 247, n. 2, p. 139-151. 2001. DOI: 10.1016/S0043-1648(00)00531-7.

[33] Tönshoff, H. K., Arendt, C., and Amor, R. B. Cutting of hardened steel. CIRP Annals-Manufacturing Technology, v. 49, n. 2, p. 547-566, 2000. DOI: 10.1016/S0007-8506(07)63455-6.

[34] Matsumoto, Y., Hashimoto, F., and Lahoti, G. Surface integrity generated by precision hard turning. CIRP Annals-Manufacturing Technology, v. 48, n. 1, p. 59-62, 1999. DOI: 10.1016/S0007-8506(07)63131-X

[35] Thiele, J. D., and Melkote, S. N. Effect of cutting edge geometry and workpiece hardness on surface generation in the finish hard turning of AISI 52100 steel. Journal of Materials Processing Technology, v. 94, n. 2-3, p. 216-226, 1999. DOI: 10.1016/S0924-0136(99)00111-9.

[36] Strafford, K. N. and Audy, J. Indirect monitoring of machinability in carbon steels by measurement of cutting forces. Journal of Materials Processing Technology, v. 67, n. 1-3, p. 150-156, 1997. DOI: 10.1016/S0924-0136(96)02835-X.

[37] Rogov, V. A. and Siamak, G. Optimization of Surface Roughness and Vibration in Turning of Aluminum Alloy AA2024. Engineering and Technology International Journal of Mechanical, vol. 1, p. 1 - 10, 2013.

[38] Lazoglu, I., Atabey, F., and Altintas, Y. Dynamics of boring processes: Part III-time domain modeling. International Journal of Machine Tools and Manufacture 42, no. 14. 2002. DOI: 10.1016/S0890-6955(02)00067-6.

[39] Yuvaraju, B. A. G., Nanda, B. K., and Srinivas, J. Investigation of stability in internal turning using a boring bar with a passive constrained layer damping. FME Transactions 49, no. 2. 2021. DOI: 10.5937/fme2102384Y.

[40] Dorian Tool, Catalog Solution Tool. The anti-vibration tunable boring bars & high performance carbide boring bar. http://www.doriantool.com/wp-content/uploads/Sec-D-DEEP-HOLE-BORING2015.c2.pdf. 2015.

[41] Jang, D. Y., Choi, Y., Kim, H., and Alex, H. Study of the correlation between surface roughness and cutting vibrations to develop an on-line roughness measuring technique in hard turning. International Journal of Machine Tools and Manufacture, UK, vol. 36 p. 453 - 464, June. 1996. DOI: 10.1016/0890-6955(95)00074-7.

[42] Costa, D. D. Análise dos parâmetros de torneamento de aços endurecidos. (in Portuguese). Master dissertation, UNICAMP. Campinas, Brazil. 1993.

[43] Sandvik. Modern Metal Cutting: A Pratical Handbook. Sandvik Coromant Technical Editorial: Sandviken, Sweden. 2010.

[44] Schneider, G. Cutting tool applications chapter 10: boring operations and machines. American Machinist. Modern Machine Shop. http://www.americanmachinist.com/. 2010.

[45] Sims, N. D. Vibration absorbers for chatter suppression: A new analytical tuning methodology. Journal of Sound and Vibration. Sheffield (UK). 2006. DOI: https://doi.org/10.1016/j.jsv.2006.10.020.

[46] Alves da Silva, W. T., Fülöp, Z., and Szilágyi, A. Evaluating Cbn Tool Life in Hardened Boring Operations in Long Overhangs. Design Of Machines And Structures: A Publication Of The University Of Miskolc 10, no. 2. 2020. DOI: 10.32972/dms.2020.026.

[47] Thomas, W., Diniz, A. E., and Szilágyi, A. Performance Of CBN Insert Over Internal Turning Operation. Proceedings of the World Congress on Engineering 2021. WCE 2021, London, U.K. 2021.

[48] Lee, D. G. Manufaturing and testing of chatter free boring bars. Korea Institute of Technology, Korea, p. 1 - 4, Janeiro, 1988.

[49] Paris, H., Peigne, G., and Mayer, R. Surface shape prediction in high-speed milling. International Journal of Machine Tools and Manufacture 44, no. 15. 2004. DOI: 10.1016/j.ijmachtools.2004.06.005

[50] Cheng, K. Machining Dynamics: Fundamentals, Applications and Practices. Middlesex (UK): Springer-Verlag. 2008.

[51] Suyama, D. I. Uma contribuição ao estudo do torneamento interno em aços endurecidos. (in Portuguese), PhD thesis, Unicamp, Campinas, São Paulo, Brazil. 2014.

[52] Suyama, D. I., Diniz, A. E., and Pederiva, R. The use of carbide and particle-damped bars to increase tool overhang in the internal turning of hardened steel. The International Journal of Advanced Manufacturing Technology, v. 86, n. 5-8, p. 2083-2092, 2016. DOI: 10.1007/s00170-015-8328-z.

[53] Siddhpura, M. and Paurobally, R. A review of chatter vibration research in turning. International Journal of Machine tools and manufacture, Elsevier, v. 61, p. 27–47, 2012. DOI: 10.1016/j.ijmachtools.2012.05.007

[54] Aguirre, G., Gorostiaga, M., Porchez, T., and Muñoa, J. Self-tuning semi-active tuned-mass damper for machine tool chatter suppression. ISMA2012-USD2012 1. 2012.

[55] Yao, Z., Mei, D., and Chen, Z. On-line chatter detection and identification based on wavelet and support vector machine. Journal of Materials Processing Technology, Hangzhou. China, p. 713 - 719, November, 2009. DOI: 10.1016/j.jmatprotec.2009.11.007.

[56] Bhaskaran, J. Process monitoring of hard turning using acoustic emission technique. 2011. Master Thesis. Available: http://shodhganga.inflibnet.ac.in/handle/10603/25391.

[57] Yang, W. p. and Tarng, Y. Design optimization of cutting parameters for turning operations based on the taguchi method. Journal of materials processing technology, Elsevier, v. 84, n. 1-3, p. 122–129, 1998. DOI: 10.1016/S0924-0136(98)00079-X.

[58] Saciotto, V. R. Desenvolvimento de ferramenta esbelta de fresamento com amortecedor de impacto. (In Portuguese). Master's Thesis, State University of Campinas, Campinas Brazil, 2020.

[59] Insperger, T., and Stépán, G. Updated semi-discretization method for periodic delay-differential equations with discrete delay. International journal for numerical methods in engineering 61, no. 1. 2004. DOI: 10.1002/nme.1061.

[60] Altintas, Y. and Weck, M. Chatter stability of metal cutting and grinding. CIRP annals 53, no. 2. 2004. DOI: 10.1016/S0007-8506(07)60032-8.

[61] Ertürk, A., Özgüven, H.N., & Budak, E. Analytical modeling of spindle–tool dynamics on machine tools using Timoshenko beam model and receptance coupling for the prediction of tool point FRF. International Journal of Machine Tools and Manufacture 46, no. 15. 2006. DOI: 10.1016/j.ijmachtools.2006.01.032.

[62] Rafal, R., Pawel,L., Krzysztof, K., Bogdan,K. and Jerzy,W. Chatter identification methods on the basis of time series measured during titanium superalloy milling. International Journal of Mechanical Sciences, v. 99, p. 196–207. 2015. DOI: 10.1016/j.ijmecsci.2015.05.013.

[63] Ding, L., Sun, Y., and Xiong, Z. Active chatter suppression in turning by simultaneous adjustment of amplitude and frequency of spindle speed variation. Journal of Manufacturing science and Engineering 142, no. 2. 2020. DOI: 10.1115/1.4045618.

[64] Rivin, E.I. and Kang, H. Enhancement of dynamic stability of cantilever tooling structures. International Journal of Machine Tools and Manufacture, S.I. v. 32, n. 4, p. 539-561. 1992. DOI: 10.1016/0890-6955(92)90044-H.

[65] Badadhe, A.M., Bhave, S.Y. and Navale, L.G. Optimization of cutting parameters in boring operation. Journal of Mechanical and Civil Engineering, pp. 10–15. 2005.

[66] Albuquerque, M.V. Modelagem e Análise Dinâmica de um Absorvedor de Vibrações por Efeito de Impacto (In Portuguese). Master's Thesis, State University of Campinas, Campinas Brazil. 2016.

[67] Kovacs, B. Vibration analysis of a damped arch using an iterative laminate model. Journal of sound and vibration. 2002. DOI: 10.1006/jsvi.2002.5004.

[68] Kovács, B. Vibration of multi-layered bands with interfacial imperfection. Journal of sound and vibration 300, no. 1-2. 2007. DOI: 10.1016/j.jsv.2006.01.018.

[69] Bankar, V.K. and Aradhye, A.S. A review on active, semi-active and passive vibration damping. International Journal of Current Engineering and Technology. 6, 2187–2191. 2016.

[70] Kovács, B. Vibration and Stability of layered circular ring segment. (In Hungarian) Canditate of Science Thesis. Miskolc, Hungary. 1992.

[71] Waydande, S., Mahajan, D.A., Gajjal, S.Y. A review on vibration attenuation of boring bar using passive dampers. International Journal of Research in Engineering and Technology 4(4), 117–122. 2014. DOI: 10.15623/ijret.2015.0407020.

[72] Rubio, L., Loya, J.A., Miguélez, M.H. and Fernández-Sáez, J. Optimization of passive vibration absorbers to reduce chatter in boring. Mechanical Systems and Signal Processing. 41, 691–704. 2013. DOI: 10.1016/j.ymssp.2013.07.019.

[73] Vinayaravi, R., Kumaresan, D., Jayaraj, K., Asraff, A.K. and Muthukumar, R. Experimental investigation and theoretical modelling of an impact damper. Journal Sound and Vibration. 332, 1324–1334 (2013). DOI: 10.1016/j.jsv.2012.10.032.

[74] Zhang, C., Chen, T., Wang, X. and Li, Y. Discrete element method model and damping performance of bean bag dampers. Journal Sound and Vibration. 333, 6024–6037. 2014. DOI: 10.1016/j.jsv.2014.07.011.

[75] Ema, S. and Marui, E. A fundamental study on impact dampers. International Journal of Machine Tools and Manufacture. 34(407), 407–421. 1994. DOI: 10.1016/0890-6955(94)90009-4.

[76] Ema, S. and Marui, E. Damping characteristics of an impact damper and its application. International Journal of Machine Tools and Manufacture. 36(3), 293–306. 1996. DOI: 10.1016/0890-6955(95)00073-9.

[77] Lu, Z., Lu, X. and Masri, S.F. Studies of the performance of particle dampers under dynamic loads. J. Sound Vib. 329, 5415–5433. 2010. DOI: 10.1016/j.jsv.2010.06.027.

[78] Dimarogonas, A. Vibration for Engineers, 2nd edn. Prentice Hall Upper Saddle River, New Jersey. 1996.

[79] Liu, X., Liu, Q., Wu, S., Liu, L. and Gao, H. Research on the performance of damping boring bar with a variable stiffness dynamic vibration absorber. The International Journal of Advanced Manufacturing Technology. 89, 2893–2906. 2017. DOI: 10.1007/s00170-016-9612-2.

[80] Bavastri, C.A.: Redução de Vibrações de Banda Larga em Estruturas Complexas por Neutralizadores Viscoelásticos (In Portuguese). PhD Thesis, UFSC, Florianópolis Santa Catarina, Brazil. 1997.

[81] Aralikatti, S. S., and Hemantha, K. Tool vibration isolation in hard turning process with magnetorheological fluid damper. Journal of Manufacturing Processes. 88. 2023. DOI: 10.1016/j.jmapro.2023.01.044.

[82] Hahn, R.S. Design of lanchester damper for elimination of metal-cutting chatter. Trans. ASME 73, 3. 1951.

[83] Kyocera Catalog boring - boring bars with interchangeable heads and anti-vibration dampener system. 2017. http://www.kyocera.com.sg/products/cuttingtools/wp-content/uploads/2015/02/F-Boring.pdf. Accessed 12 February 2023.

[84] Kanase, S.S., Patil, J.S. and Jadhav, S.M. Improvement of Ra value of boring operation using passive damper. International Journal Of Engineering And Science. 2, 103–108. 2013. DOI: 10.1016/S0924-0136(96)02835-X.

[85] Booty, C., Bowyer, E.P. and Krylov, V.V. Experimental investigation of damping flexural vibrations using granular materials. International Congress on Sound and Vibration Department of Aeronautical and Automotive Engineering. Loughborough University, Loughborough, Leicestershire, England. 2014.

[86] Vasanth, X.A., Paul, P.S., Lawrance, G. and Varadarajan, A.S. Vibration control techniques during turning process: a review. Australian Journal of Mechanical Engineering. 1–21. 2019. DOI: 10.1080/14484846. 2019.1585224.

[87] Alammari, Y., Sanati, M., and Freiheit, T., Investigation of Boring Bar Dynamics for Chatter Suppression. Procedia Manufacturing, v. 1, p. 768-778, 2015. DOI: 10.1016/j.promfg.2015.09.059.

[88] Yuvaraju, B.A., Ganesh, B.K., and Srinivas, J. Optimal cutting state predictions in internal turning operation with nano-SiC/GFRE composite layered boring tools. International Journal of Machining and Machinability of Materials 23, no. 1. 2021. DOI: 10.1504/IJMMM.2021.112714.

[89] Tarng Y.S., Kao J.Y. and Lee, E.C. Chatter suppression in turning operations with a tuned vibration absorber. Journal of Materials Processing Technology. 2000. DOI: 10.1016/S0924-0136(00)00585-9.

[90] Khatake, P. and Nitnaware, P.T. Vibration mitigation using passive damper in machining. International Journal of Modern Engineering Research. 3(6), 3649–3652. 2013.

[91] Ema, S. and Marui, E. Suppression of chatter vibration of boring tools using impact dampers. International Journal of Machine Tools and Manufacture, v. 40, n. 8, 1141–1156, 2000. DOI: 10.1016/S0890-6955(99)00119-4.

[92] Biju, C.V., Shunmugam, M.S. Investigation into effect of particle impact damping (PID) on surface topography in boring operation. International Journal of Advanced Manufacturing and Technology. 1219–1231. 2014. DOI: 10.1007/s00170-014-6201-0.

[93] Sathishkumar, B., Mohanasundaram, K., and Kumar, M. Impact of particle damping parameters on surface roughness of bored surface. Arabian Journal for Science and Engineering. v. 39, 7327–7334, 2014. DOI: 10.1007/s13369-014-1209-1.

[94] Thomas, W., Fülop, Z. and Szilágyi, A. Comparison between the performances of different boring bars in the internal turning of long overhangs. Nanomaterials Science & Engineering 2, no. 3. 2020. DOI: 10.34624/nmse.v2i3.19533.

[95] Ramesh, K., Alwarsamy, T., and Jayabal, S. 841. ANN prediction and RSM optimization of cutting process parameters in boring operations using impact dampers. Journal of Vibroengineering 14, no. 3. 2012.

[96] Paul, P.S., Raja, P., Aruldhas, P., Pringle, S. and Shaji, E. Effectiveness of particle and mass impact damping on tool vibration during hard turning process. Proceedings of the Institution of Mechanical Engineers, Part B: Journal of Engineering Manufacture. v. 232, n. 5, 776–786, 2018.

[97] Aguiar, H., Hassui, A., Suyama, D. and Magri, A. Reduction of internal turning surface roughness by using particle damping aided by airflow. The International Journal of Advanced Manufacturing Technology, v.106. 2020. DOI: 10.1007/s00170-019-04566-5.

[98] Ibrahim, R.A. Vibro-impact dynamics: modeling, mapping and applications. v. 43. Springer Science & Business Media, 2009. DOI: 10.1007/978-3-642-00275-5.

[99] Paget, A. Vibration in steam turbine buckets and damping by impacts. Engineering. 1937.

[100] De Albuquerque, M.V., Absorvedor de vibração por efeito de impacto aplicado em vigas com e sem rotação. (in Portuguese). PhD thesis, Unicamp, Brazil. 2022.

[101] Masri, S. General motion of impact dampers. The Journal of the Acoustical Society of America, v. 47, 229–237. 1969.

[102] Wong, C.; Daniel, M.C. and Rongong, J. Energy dissipation prediction of particle dampers. Journal of Sound and Vibration, v. 319, 91–118, 2009. DOI: 10.1016/j.jsv.2008.06.027.

[103] Du, Y. and Wang, S. Modeling the fine particle impact damper. International Journal of Mechanical Sciences, v. 52, 1015–1022. 2010. DOI: 10.1016/j.ijmecsci.2010.04.004.

[104] Duncan, M.; Wassgren, C. and Krousgrill, C. The damping performance of a single particle impact damper. Journal of Sound and Vibration, v. 286, 123–144, 2005. DOI: 10.1016/j.jsv.2004.09.028.

[105] Hang, Y., Wang, Y., Liu, B., and Jiang, X.Experimental study on the damping effect of multi-unit particle dampers applied to bracket structure. Applied Sciences 9, no. 14. 2019. DOI: 10.3390/app9142912.

[106] Bapat, C.N. and Sankar, S. Single unit impact damper in free and forced vibration. Journal of Sound and Vibration, v. 99(1), 85 – 94. 1985a.

[107] Friend, R. and Kinra, V. Particle impact damping. Journal of Sound and Vibration, v. 233 (1), 93–118, 2000. DOI: 10.1006/jsvi.1999.2795.

[108] Blazejczyk-Okolewska, B. Analysis of an impact damper of vibrations. Chaos, Solitons and Fractals, v. 12, n. 11, 1983 – 1988, 2001. DOI: 10.1016/S0960-0779(00)00146-6

[109] Cheng, C.C. and Wang, J.Y. Free vibration analysis of a resilient impact damper. International Journal of Mechanical Sciences, Volume 45, Issue 4, Pages 589-604, ISSN 0020-7403. 2003. DOI: 10.1016/S0020-7403(03)00116-4.

[110] Cheng, J. and Xu, H. Inner mass impact damper for attenuating structure vibration. International Journal of Solids and Structures, Volume 43, Issue 17, 2006, Pages 5355-5369, ISSN 0020-7683, DOI: 10.1016/j.ijsolstr.2005.07.026.

[111] Demiryurek, S G. Periodically Arranged Nonlinear Passive Particle Dampers Under Low-Amplitude Excitation. PhD dissertation., University of Sheffield, 2022.

[112] Yasuda, K. and Toyoda, M. The damping effect of an impact damper. Belletin of the JSME, v.21, (153), 424–431, 1978.

[113] Li, K. and Darby, A.P. Experiments on the effect of an impact damper on a multiple-degree-of-freedom system. Journal of Vibration and Control, v. 12, n. 5, 445–464, 2006b. URL: DOI: 10.1177/1077546306063504.

[114] Bapat, C.N. and Sankar, S. Multi-unit impact damper - reexamined. Journal of Sound and Vibration, v. 103 (4), 457 – 469, 1985b.

[115] Nigm, M. e Shabana, A. Effect of an impact damper on a multi-degree of freedom system. Journal of Sound and Vibration, v. 89, n. 4, 541–557, 1983. DOI: 10.1016/0022-460X(83)90356-5.

[116] Li, K. and Darby, A.P. A buffered impact damper for multi-degree-of-freedom structural control. Earthquake Engineering and Structural Dynamics, v. 37, n. 13, 1491–1510, 2008. DOI: 10.1002/eqe.823.

[117] Liu, W., Tomlinson, G. and Rongong, J. The dynamic characterisation of disk geometry particle dampers. Journal of Sound and Vibration, v. 280, n. 3, 849–861, 2005. DOI: 10.1016/j.jsv.2003.12.047.

[118] Lu, Z., Masri, S.F. and Lu, X. Studies of the performance of particle dampers attached to a two-degrees-of-freedom system under random excitation. Journal of Vibration and Control, v. 17(10), 1454–1471. 2010. DOI: 10.1177/1077546310370687.

[119] Flores, P., Machado, M., Silva, M.T. and Martins, J.M. On the continuous contact force models for soft materials in multibody dynamics. Multibody System and Dynamics., v. 25, 357–375. 2011. DOI: 10.1007/s11044-010-9237-4.

[120] Cundall, P.A. and Strack, O.D.L. A discrete numerical model for granular assemblies. Geotechnique, v. 29, n. 1, 47–65, 1979. DOI: 10.1680/geot.1979.29.1.47.

[121] O'Sullivan, Catherine. Particulate discrete element modelling: a geomechanics perspective. CRC Press, 2011. DOI: 10.1201/9781482266498.

[122] Hertz, H. Uber die Beruhrung Fester Elastischer Korper (On the Contact of Elastic Solids), J Reine Angew Math, Vol. 92, pp. 156-171. 1882.

[123] Di Renzo, A. and Di Maio, F. Comparison of contact-force models for the simulation of collisions in dem-based granular flow codes. Chemical Engineering Science, v. 59, 525–541, 02. 2004. DOI: 10.1016/j.ces.2003.09.037.

[124] Demiryurek, S. G., A. Krynkin, and J. Rongong. Modelling of nonlinear dampers under low-amplitude vibration. In Acoustics 2020 Proceedings. Institute of Acoustics, 2020.

[125] Mongillo, G. Discrete Element Method uses in Optimization of Modern Tunnel Boring Machine Designs. 2022. Acess 10/02/2023.

https://www.tunnelcanada.ca/members/documents/2022/papers/SESFCEXAW30O401HB_TAC2022_Paper_Mongillo_Nov_2022_V2_Submitted.pdf.

[126] Syed, Z., Tekeste, M. and White, D. A coupled sliding and rolling friction model for dem calibration. Journal of Terramechanics, v. 72, 9–20, 2017. DOI: 10.1016/j.jterra.2017.03.003.

[127] Walton, O.R. and Braun, R.L. Viscosity, granular-temperature, and stress calculations for shearing assemblies of inelastic, frictional disks. Journal of Rheology, v. 30, n. 5, 949–980, oct 1986.

[128] Cleary, P. W. DEM simulation of industrial particle flows: case studies of dragline excavators, mixing in tumblers and centrifugal mills. Powder technology 109, no. 1-3. 2000. DOI: 10.1016/S0032-5910(99)00229-6.

[129] Delaney, G.W. Inagaki, S. and Aste, T. Fine tuning DEM simulations to perform virtual experiments with three-dimensional granular packings. Granular and complex materials. pp. 169–185. 2007. DOI: 10.1142/9789812771995_0009.

[130] Malone, K.F. and Xu, B.H. Determination of contact parameters for discrete element method simulations of granular systems. Particuology, v. 6, n. 6, 521–528, 2008. Simulation and Modeling of Particulate Systems. DOI: 10.1016/j.partic.2008.07.012.

[131] Nagurka, M. and Huang, S. A mass-spring-damper model of a bouncing ball. American Control Conference. Proceedings of the 2004, v. 1, 2004.

[132] Seifried, R.; Schiehlen, W. e Eberhard, P. The role of the coefficient of restitution on impact problems in multi-body dynamics. Proceedings of Institution of Mechanical Engineers, Part K: Journal of Multi-body Dynamics, v. 224, 279–306, 2010.

[133] Lu, Z., Wang, Z., Masri, S.F. and Lu, X. Particle impact dampers: Past, present, and future. Structural Control and Health Monitoring, v. 25, n. 1, e2058, 2018. E2058 STC-17-0042.R1. DOI: 10.1002/stc.2058.

[134] Hunt, K.H. and Crossley, F.R.E. Coefficient of restitution interpreted as damping in vibroimpact. ASME Journal of Applied Mechanics, v. 42, 440–445, 1975. DOI: 10.1115/1.3423596.

[135] Lankarani, H. and Nikravesh, P. A contact force model with hysteresis damping for impact analysis of multibody systems. Journal of Mechanical Design, v. 112, 369–376, 1990. DOI: 10.1115/1.2912617.

[136] Hu, S. and Guo, X. A dissipative contact force model for impact analysis in multibody dynamics. Multibody System and Dynamics, v. 35, 131–151. 2015. DOI: 10.1007/s11044-015-9453-z.

[137] Filipe, D. G. and Nicoletti, R. Dampening of a cantilever beam with large particles in a small cavity: model and experiment. Archive of Applied Mechanics 91, no. 7: 2933–2942. 2021. DOI: 10.1007/s00419-021-01946-w.

[138] Rouben, R., Thomas, W. and Szilagyi, A. Dynamic Analysis of an Internal Turning Tool with Elastic Foundation (Winkler Model) ECCOMAS Thematic Conference on Multibody Dynamics. In ECCOMAS Thematic Conference on Multibody Dynamics, pp. 126-135. Budapest University of Technology and Economics, 2021.

[139] Akesson, H., Smirnova, L. and Claesson I.T. Analysis of dynamic properties of boring bars concerning different clamping conditions. Mechanical Systems and Signal Processing, 23:2629-2647, 2009. DOI: 10.1016/j.ymssp.2009.05.012.

[140] Daghini, L. Improving machining system performance through designed-in damping: modelling, analysis and design solutions. PhD dissertation, KTH Royal Institute of Technology, 2012. DOI: 10.13140/RG.2.1.2435.6007.

[141] Akesson, H., Smirnova, T., Hakansson, L. and Claesson I.T. Analog and digital approaches of attenuation boring bar vibrations during metal cutting operations. Published at the 12th ICSV conference, Lisabon, Portugal, July 11 – 14. 2005. DOI: 10.4271/2005-01-3402.

[142] Andren, L. Hakansson, L. Brandt, A. and Claesson I. Identification of dynamic properties of boring bar vibrations in a continuous boring operation. Journal of Mechanical Systems & Signal Processing, 18(4):869–901, 2004. DOI: 10.1016/S0888-3270(03)00093-1.

[143] Andren, L. Hakansson, L. Brandt, A. and Claesson. I. Identification of motion of cutting tool vibration in a continuous boring operation – correlation to structural properties. Journal of Mechanical Systems & Signal Processing, 18(4):903–927, 2004. DOI: 10.1016/j.ymssp.2003.09.009.

[144] Zhang, G.M. and Kapoor, S.G. Dynamic modeling and analysis of the boring machining system. Journal of Engineering for Industry, Transactions of the ASME, 109:219–226, August 1987. DOI: 10.1115/1.3187122.

[145] Kuster, F. Cutting dynamics and stability of boring bars. Annals of CIRP, 39(1):361–366, 1990. DOI: 10.1016/S0007-8506(07)61073-7.

[146] Walter, M.F. and Stahl, J.E. Connection between cutting and clamping forces in turning. International Journal of Machine Tools & Manufacture, Vol. 34, No. 7:991–1003, Oct 1994. DOI: 10.1016/0890-6955(94)90030-2.

[147] Thomas, W. Diniz, A. E., Suyama, D. I. and Magri, A. comparação entre a fixação convencional e a bucha *Easy Fix* para torneamento interno de aço endurecido com longos balanços da ferramenta (In Portuguese), (IX Cobef), Brazil, 2017.

[148] Rao, P.N., Rao, U.R.K. and Rao, J.S. Towards improved design of boring bars part 1: Dynamic cutting force model with continuous system analysis for the boring bar. Journal of Machine Tools Manufacture, 33–44, 1988. DOI: 10.1016/0890-6955(88)90005-3.

[149] Sortino, M., Totis, G. and Prosperi, F. Modeling the dynamic properties of conventional and high-damping boring bars. Mechanical Systems and Signal Processing, v. 34, p. 340-352, 2013. DOI: 1016/j.ymssp.2012.05.016.

[150] Popov, V. L., Heß, M. and Willert, E.Handbook of contact mechanics: exact solutions of axisymmetric contact problems. Springer Nature, 2019.

[151] Biot, M. A. Bending of an infinite beam on an elastic foundation. J. Appl. Mech., 59, A1–A7. [2] A.B. 1937.

[152] Vesic, A.B. Beams on Elastic Subgrade and the Winkler's Hypothesis. Proceedings, 5th International Conference of Soil Mechanics, pp. 845~ 850. 1963.

[153] Yan, L. Investigation on indentation rolling resistance of belt conveyor based on Hertz contact theory compared with one-dimensional Winkler foundation. Advances in Mechanical Engineering 10, no. 7. 2018. DOI: 10.1177/1687814018783938.

[154] Marto, A., Latifi, N., Janbaz, M., Kholghifard, M., Khari, M., Alimohammadi, P. and Banadaki, A. D. Foundation size effect on modulus of subgrade reaction on sandy soils. Electronic Journal of Geotechnical Engineering. 2012.

[155] Liang, R., Wu, W., Yu, F., Jiang, G. and Liu, J. Simplified method for evaluating shield tunnel deformation due to adjacent excavation. Tunnelling and Underground Space Technology 71. 2018. DOI: 10.1016/j.tust.2017.08.010.

[156] Qu, C. The improved foundation modulus for the use of Winkler foundation. In 2010 International Conference on Mechanic Automation and Control Engineering, pp. 1794-1797. IEEE, 2010.
[157] Sadrekarimi, J. and Akbarzad, M. Comparative study of methods of determination of coefficient of subgrade reaction. Electronic Journal of Geotechnical Engineering 14, no. 1. 2009.
[158] Winkler. Die Lehre von Elasticitaet und Festigkeit (in German). Prag 1867 (H. Dominicus), pp. 182-184.
[159] Cazzani, A. On the dynamics of a beam partially supported by an elastic foundation: an exact solution-set. International Journal of structural stability and dynamics 13, no. 08 2013. DOI: 10.1142/S0219455413500454.
[160] Hertz. H. Gesammelte Werke 1, 228. Uber das Gleichgewicht schwimmender elastischer Platten. 1895.
[161] Froio, D. and Rizzi, E. Analytical solution for the elastic bending of beams lying on a linearly variable Winkler support. International Journal of Mechanical Sciences. 2017. DOI: 10.1016/j.ijmecsci.2017.04.021.
[162] Wu, J-S. and H-M. Chou. A new approach for determining the natural frequencies and mode shapes of a uniform beam carrying any number of sprung masses. Journal of Sound and Vibration 220, no. 3. 1999. DOI: 10.1006/jsvi.1998.1958.
[163] Negri, D., Fiorentin, F. K. and Filho, J. M. C. A model updating method for plate elements using particle swarm optimization (PSO), modeling the boundary flexibility, including uncertainties on material and dimensional properties. Latin American Journal of Solids and Structures 15. 2018. DOI: 10.1590/1679-78254342.
[164] Neves, M.S., Skury, A.L.D., de Azevedo, M.G. and Bobrovnitchii, G.S. Cubic boron nitride competing with diamond as a superhard engineering material–an overview. J. Materials Research and. Technology. 2013, 2, 68–74. DOI: 10.1016/j.jmrt.2013.03.004.
[165] Walter, M.F. and Stahl, J.E. Connection between cutting and clamping forces in turning. International Journal of Machine Tools and Manufacture, Vol. 34, No. 7:991–1003, Oct 1994. DOI: 10.1016/0890-6955(94)90030-2.
[166] DIN 4768. Determination of Values of Surface Roughness Parameters Ra. Rz, Rmax Using Electrical Contact (Stylus) In-struments Concepts and Measuring Conditions. Berlin, Germany: Deutsches Institut für Norming, May, 1990.
[167] ISO 4288. Geometrical Product Specifications (GPS)—Surface Texture: Profile Method—Rules and Procedures for the As-sessment of Surface Texture. International Organization for Standardization (ISO), Geneva, Switzerland. Revised by ISO 21920-3:2021, 1996.
[168] Okubo, N., Yoshida, Y. and Hoshi, T. Application of Modal Analysis to Machine Tool Structures. CIRP Annals. 1982, 31, 243–246. DOI: 10.1016/S0007-8506(07)63306-X
[169] Inman, D. J., and Ramesh Chandra Singh. Engineering vibration. Vol. 3. Englewood Cliffs, NJ: Prentice Hall, 1994.
[170] Meirovitch, L. Fundamentals of vibrations. Waveland Press, 2010.
[171] Nguyen, A. R. Comparative Spectral Analysis of Flexible Structure Models: the Euler-Bernoulli Beam model, the Rayleigh Beam model, and the Timoshenko Beam Model. Master Thesis, University of New Hampshire. 2017.
[172] Rao, S. S. Vibration of continuous systems. John Wiley & Sons, 2019.

[173] Andrén, L. Håkansson, L. Brandt, A. and Claesson. I. Identification of dynamic properties of boring bar vibrations in a continuous boring operation. Mechanical systems and signal processing 18.4. 2004. DOI: 10.1016/S0888-3270(03)00093-1.

[174] Euler, L. De motu vibratorio laminarum elasticarum, ubi plures novae vibrationum species hactenus non pertractatae evolvuntur (In Latim). Novi Commentarii academiae scientiarum Petropolitanae, Vol. 17, pp. 449–487. 1773.

[175] Ren, Y., Feng, W. and Ma, B. Dynamic Modeling of Composite Boring Bars Considering Different Boundary Conditions. IOP Conference Series: Materials Science and Engineering. Vol. 382. No. 3. IOP Publishing, 2018. DOI: 10.1088/1757-899X/382/3/032026.

[176] da Silva, J. F., Nascimento, L. A. D. and Hoefel, S. S. Free vibration analysis of Euler-Bernoulli beams under non-classical boundary conditions. In IX Congresso Nacional de Engenharia Mecânica CONEM2016, Fortaleza-CE, Brasil. 2016.

[177] Doyle, P.F. and Pavlovic, M.N. Vibration of beams on partial elastic foundations. Earthquake Engineering and Structural Dynamics, 10(5), pp.663-674. 1982. DOI: 10.1002/eqe.4290100504.

[178] Motaghian, S. E., M. Mofid, and P. Alanjari. Exact solution to free vibration of beams partially supported by an elastic foundation. Scientia Iranica 18, no. 4. 2011. DOI: 10.1016/j.scient.2011.07.013.

[179] Blevins, R. D. Formulas for natural frequency and mode shape. 1979.

[180] Zhang, Y. and Liu, X. Response of an infinite beam resting on the tensionless Winkler foundation subjected to an axial and a transverse concentrated loads. European Journal of Mechanics-A/Solids 77. 2019. DOI: 10.1016/j.euromechsol.2019.103819.

[181] Kacar, A., Tan, H. T. and Metin, O. K. Free vibration analysis of beams on variable winkler elastic foundation by using the differential transform method. Mathematical and Computational Applications 16.3. 2011. DOI: 10.3390/mca16030773.

[182] Zhang, C., Ren, Y., Ji, S. and Zhang, J. Analysis of the composite boring bar dynamic characteristics considering shear deformation and rotational inertia. Applied Sciences 10, no. 4. 2020. DOI: 10.3390/app10041533.

[183] Hagedorn, P., DasGupta, A. Vibrations and waves in continuous mechanical systems. Wiley Online Library. 2007.

[184] Aenlle, M., Juul, M. and Brincker, R. Modal Mass and Length of Mode Shapes in Structural Dynamics, Shock and Vibration, vol. 2020, Article ID 8648769, 16 pages, 2020. DOI: 10.1155/2020/8648769.

[185] Chockalingam, S., Natarajan, U. and George, A. Damping investigation in boring bar using hybrid copper-zinc particles. Journal of Vibration and Control 23, no. 13. 2017. DOI: 10.1177/1077546315610946

[186] Kovacs, B. Free vibration of a laminated circular ring segment. Journal of sound and vibration 245, no. 4. 2001. DOI: 10.1006/jsvi.2000.3557.

[187] Kovács, B. Vibration analysis of layered curved arch. Journal of Sound and Vibration 332, no. 18. 2013. DOI: 10.1016/j.jsv.2013.03.011

[188] Liao, Y. and Wells, V. Modal parameter identification using the log decrement method and band-pass filters. Journal of Sound and Vibration, 330(21), 5014-5023. 2011. DOI: 10.1016/j.jsv.2011.05.017.

[189] Ge, C. and Sutherland, S. Application of experimental modal analysis to determine damping properties for stacked corrugated boxes. Mathematical Problems in Engineering. 2013. DOI: 10.1155/2013/651348.

[190] Gupta, P., Rajput, H.S. and Law, M. Vision-based modal analysis of cutting tools. CIRP Journal of Manufacturing Science and Technology, 32, pp.91-107. 2021. DOI: 10.1016/j.cirpj.2020.11.012.

[191] Gupta, P., Law, M. and Mukhopadhyay, S. Evaluating tool point dynamics using output-only modal analysis with mass-change methods. CIRP Journal of Manufacturing Science and Technology, 31, pp.251-264. 2020. DOI: 10.1016/j.cirpj.2020.06.001.

[192] Balden, V. The identification of structural modal parameters, as an alternative in-vivo diagnosis for osteoporosis. Master's thesis, University of Cape Town. 1997.

[193] Sun, R., Wong, W. and Cheng, L. Optimal design of a tunable electromagnetic shunt damper for dynamic vibration absorber. Mechatronics, 83, p.102763. 2022. DOI: 10.1016/j.mechatronics.2022.102763.

[194] Alammari, Y. Chatter Suppression in Boring Operations through Altering Tool Dynamics. Master's thesis, Graduate Studies, 2016.

[195] Song, Q., Shi, J., Liu, Z., Wan, Y. and Xia, F. Boring bar with constrained layer damper for improving process stability. The International Journal of Advanced Manufacturing Technology. 1951–1966. 2016. DOI: 10.1007/s00170-015-7670-5

[196] Pettersson, Linus. Vibration analysis of a boring bar. 2002.

[197] Andren, L., Håkansson, L., Brandt, A. and Claesson, I. Identification of dynamic properties of boring bar vibrations in a continuous boring operation. Mechanical systems and signal processing 18, no. 4. 2004. DOI: 10.1016/S0888-3270(03)00093-1.

[198] Yuvaraju, B. A. G., J. Srinivas, and B. K. Nanda. Nonlinear dynamics of friction-induced regenerative chatter in internal turning with process damping forces. Journal of Sound and Vibration. 2022. DOI: 10.1016/j.jsv.2022.117386.

[199] Fallah, M. and Moetakef-Imani, B. Investigation on nonlinear dynamics and active control of boring bar chatter. Journal of the Brazilian Society of Mechanical Sciences and Engineering 43, no. 3. 2021. DOI: 10.1007/s40430-021-02808-w.

[200] Rusinek, R., Wiercigroch, M. and Wahi, P. Modelling of frictional chatter in metal cutting. International Journal of Mechanical Sciences 89. 2014. DOI: 10.1016/j.ijmecsci.2014.08.020.

[201] Hendrowati, W., and Merdekawan, N. Modeling and analysis of boring bar vibration response in internal turning due to variation of the amount of DVA rubber in finish boring cut. Journal of Mechanical Science and Technology 35, no. 10. 2021. DOI: 10.1007/s12206-021-0907-3.

[202] Lankarani, H. and Nikravesh, P. Continuous contact force models for impact analysis in multibody systems. Nonlinear Dynamics, v. 5, n. 2, 193—207. 1994. DOI: 10.1007/BF00045676.

[203] Goldsmith,W. Impact: The theory and physical behavior of colliding solids. E. Arnold. 1960.

[204] Meirovitch, L. Fundamentals of Vibrations. McGraw-Hill higher education. 2001.

[205] Coromant, Sandvik. How to reduce vibration in metal cutting. SE-811 81. 2005.

LIST OF PUBLICATIONS RELATED TO THE TOPIC OF THE RESEARCH FIELD

(1) Wallyson Thomas Alves da Silva, Zsombor Fülöp, and Attila Szilágyi, Passive Damping Techniques for Vibration Suppression in Boring Operation with Long Overhangs, in Jármai K., Voith K. (eds) Vehicle and Automotive Engineering 3 (VAE 2020), 25 November, 2020, Miskolc, Lecture Notes in Mechanical Engineering. Springer, Singapore. DOI: 10.1007/978-981-15-9529-5_22.

(2) Wallyson Thomas Alves da Silva, Zsombor Fülöp, and Attila Szilágyi, Comparison between the performances of different boring bars in the internal turning of long overhangs, Nanomaterials Science & Engineering 2:3 pp. 124-134, 2020. DOI: 10.34624/nmse.v2i3.19533.

(3) Wallyson Thomas Alves da Silva, Zsombor Fülöp, and Attila Szilágyi, Comparison Between A Conventional and an Antivibrating Boring Bar in the Internal Turning of Long Overhangs, Design of Machines And Structures, 10:2 pp. 145-149, 2020. DOI: 10.32972/dms.2020.026.

(4) Wallyson Thomas Alves da Silva, Zsombor Fülöp, and Attila Szilágyi, Evaluating Cbn Tool Life in Hardened Boring Operations in Long Overhangs, Design of Machines and Structures, 10:2 pp. 150-154, 2020, DOI: 10.32972/dms.2020.026.

(5) Wallyson Thomas Alves da Silva, Zsombor Fülöp, and Attila Szilágyi, Köbös bórnitrid lapkás „hosszú" furat esztergakések élettartamának vizsgálata edzett acél megmunkálásának vonatkozásában, Multidiszciplináris Tudományok: A Miskolci Egyetem Közleménye, 10:4 pp. 31-35, 2020, DOI: 10.35925/j.multi.2020.4.5.

(6) Wallyson Thomas Alves da Silva, Zsombor Fülöp, and Attila Szilágyi, Hagyományos és rezgéscsillapított „hosszú" furat esztergakések viselkedéseinek összehasonlítása, Multidiszciplináris Tudományok: A Miskolci Egyetem Közleménye, 10 : 3 pp. 360-364, 2020, DOI: 10.35925/j.multi.2020.3.43.

(7) Wallyson Thomas Alves da Silva; Peterka, Jozef, Róbert Straka, Tomáš Vopát, Jakub Hrbál, and Michaela Kritikos. "Analysis of form Error and Roughness of Hardened Steel Workpieces Internally Turned with Different Tools in Long Overhangs." Research Papers Faculty of Materials Science and Technology Slovak University of Technology 30, no. 50: 21-29., DOI: 10.2478/rput-2022-0003.

(8) Wallyson Thomas Alves da Silva; Lucas Alexandre de Carvalho; Nobre; Filipe Ribeiro, and Silva Lima Matheus, Analysis of form errors and roughness of hardened steel workpieces internally turned with tool in long overhangs, Conference: Curitiba, Brazil 24.05.2021. - 26.05.2021, Conference proceedings Scientific, DOI: 10.26678/ABCM.COBEF2021.COB21-0123.

(9) Wallyson Thomas Alves da Silva, Anselmo Eduardo Diniz, and Attila Szilágyi, Performance Of CBN Insert Over Internal Turning Operation, Proceedings of the World Congress on Engineering 2021.

(10) Wallyson Thomas Alves da Silva, Rouben Rostamian, Attila Szilágyi, Dynamic Analysis of an Internal Turning Tool with Elastic Foundation (Winkler Model), Proceedings of the 10th ECCOMAS Thematic Conference on MULTIBODY DYNAMICS,

(11) Wallyson Thomas Alves da Silva, Dynamic Modeling of Internal Turning Tool Considering Different Spans and Boundary Conditions, Proceedings of the 24th Spring Wild Conference 2021.

(12) Glazyrin, Vladimir, Juraj Ruzbarsky, Yury Nikitin, Pavol Bozek, and Wallyson Thomas de Silva, Study of Dynamic Processes During the Finishing of Spherical Parts Made of Difficult-to-Machine Materials, MM Science Journal, 2022, DOI: 10.17973/MMSJ.2022_10_2022013.

(13) Wallyson Thomas Alves da Silva, Jozef Peterka, Tomas Vopat, Experimental Research on the Dynamic Stability of Internal Turning Tools for Long Overhangs, Journal of Manufacturing and Materials. Processing, 2023, 7, 61. DOI: 10.3390/jmmp7020061.

(14) Thomas, W., Jozef Peterka, Tamas Szabo, Marcos Vieira Albuquerque, Robson Pederiva, Laszlo Peter Kiss. Analytical and Experimental Investigation of the Dynamic Stability in Passive Damper Boring Bars. Procedia CIRP. 2023. (status: accepted).